

Durham E-Theses

A statistical model of large $P(_T)$ and large mass production

Reza Safari

How to cite:

Safari, Reza (1978) A statistical model of large $P(_T)$ and large mass production. Doctoral thesis, Durham University.

Use policy

The full-text may be used and/or reproduced, and given to third parties in any format or medium, without prior permission or charge, for personal research or study, educational, or not-for-profit purposes provided that:

- a full bibliographic reference is made to the original source
- a <https://etheses.durham.ac.uk/id/eprint/8417/> is made to the metadata record in Durham E-Theses
- the full-text is not changed in any way

The full-text must not be sold in any format or medium without the formal permission of the copyright holders.

Please consult the [full Durham E-Theses policy](#) for further details.

To my parents

✻

A STATISTICAL MODEL OF LARGE P_T

AND

LARGE MASS PRODUCTION

by

REZA SAFARI

A thesis presented for the degree of

Doctor of Philosophy

at the University of Durham

June 1978

The copyright of this thesis rests with the author.

No quotation from it should be published without
his prior written consent and information derived

from it should be acknowledged.

Mathematics Department
University of Durham

PREFACE

The work presented in this thesis was carried out at the University of Durham between October 1975 and June 1978 under the supervision of Professor Euan James Squires.

I am very pleased to express my sincere gratitude to Professor Squires. His patient help, guidance and encouragement have been invaluable throughout my studentship, and he has shown unfailing interest in the work presented in this thesis. I am also indebted to Professor Squires for his suggestion to the subject itself.

I would like to extend my thanks and indebtedness to the lecturers of theoretical physics for their stimulating talks and lectures from which I benefitted enormously.

I also wish to thank Pahlavi Foundation (Iran) for their financial support.

Finally I thank my parents and two of my brothers, Mr. Hossein Safari and Mr. Ali Safari and also my friend Mr. O.A. Zalishahier for all their help and support.

The material in this thesis is based essentially on two papers by Professor Squires and the author and some unpublished work carried out by them. No originality is made on Chapter 1, which is necessary only to explain the basic idea of the subject. The works and quotations from the other authors are explicitly indicated in the text, and some of the relevant experimental results are briefly described in Chapter 3.1. Chapter 2 and most of Chapters 3 and 4 are claimed to be original.

ABSTRACT

Generally this thesis deals with application of thermodynamical model to high energy interactions.

The first chapter is an introduction. We give the important definitions and also results needed in subsequent work. In chapter 2 a model incorporating various thermal components is proposed to discuss the production of secondaries having large transverse momentum component (i.e. $P_L \approx 0$). The model is compared to the ISR data of large P_T pions.

Chapter 3 gives a brief description of experimental situation about the azimuthal, rapidity and transverse momentum correlations. The general treatment of multi-temperature model (MTM) is expressed. Momentum recoil effect is included to fit the same/opposite side momentum correlations data. Some other relevant models are explained in this part for comparison. Finally calculations of average charged particles multiplicity accompanying the trigger particle is shown in this chapter.

Chapter 4 considers the transverse mass (m_T) universality and its agreement with MTM. Production of high mass particles and their correlation are investigated in the framework of MTM. Again some possible models of different authors are presented and referenced in here.

CONTENTS

	<u>Page No.</u>
CHAPTER I STATISTICAL THERMODYNAMICAL MODEL	1
1.1 Introduction	1
1.2 Introduction to the thermodynamical model	1
1.3 Formation of the thermodynamical system	5
1.4 Defects and successes of statistical thermodynamical model	13
CHAPTER II DEFINITION OF MULTITEMPERATURE MODEL	18
2.1 Single particle momentum distribution according to the multi-temperature model	19
2.2 Variation with energy of temperature distribution	22
CHAPTER III STUDY OF TWO PARTICLES CORRELATIONS AT LARGE TRANSVERSE MOMENTUM	25
3.1 Experimental evidences	25
3.2 The theoretical approach	35
3.3 Frogland's model	39
3.4 General treatment	43
3.5 Momentum Conservation effect	48
3.6 Charged particles multiplicity associated with the large P_T particle	51
CHAPTER IV PRODUCTION OF MASSIVE PARTICLES AND PHENOMENOLOGY OF m_T UNIVERSALITY	54
4.1 The universality of m_T	54
4.2 Michael's model	58
4.3 Effect of correlation on production of heavy particles.	62
REFERENCES	66
FIGURE CAPTIONS	68
TABLES	
FIGURES	

CHAPTER I

STATISTICAL THERMODYNAMICAL MODEL

1.1 Introduction

It is well known that at high energies, most collisions between elementary particles result in a large number of final state particles and that the simple two particle reaction is rare. This fact was being investigated in the domain of cosmic ray physics for a long time and has recently come to the forefront in accelerator experiments. There are many models used to explain these processes. Most of these, e.g. multi-peripheral and quark models are in some sense perturbative in that they involve a minimum number of specific couplings. This thesis deals with a model which begins from the opposite point of view, namely a thermodynamical model in which it is assumed that a very large number of basic interactions take place. So that thermodynamic equilibrium is reached. We shall see that some features of the data can be explained in a rather natural way using this model, although of course taken literally it predicts some things which are badly wrong. The correct features could be relevant to providing an understanding of and complement to the more detailed models. The plan of this chapter is as follows. We begin in Section 1 by giving an introduction to the thermodynamical model. In Section 2 the formation of thermodynamical systems is discussed. Finally in Section 3 we consider some defects and successes of the model.

1.2 Introduction to the thermodynamical model

The first suggestion that a collision of strongly interacting high energy particles could give rise to a system with many degrees of freedom



that reaches thermodynamical equilibrium is to be found in Heisenberg's paper (1) on collision of high energy weakly interacting particles. Later on statistical theory of multiple production was proposed by different authors (2-4). In 1953 Landu (5) completed the main hypothesis of the theory, namely the formation of the common system. This view was continued and completed by Hagdorn and other collaborators (6-7) with a series of papers.

From the thermodynamical point of view a high energy collision can be explained as follows. When two high energy particles collide, the energy available in their centre of mass system is realised in a small volume V_0 of order of nucleon volume. A thermodynamic equilibrium is established which is described by statistical thermodynamics of unlimited and undetermined number of more or less excited hadrons which then leave the region of interaction and decay strongly through a number of steps into stable forms.

The reason for formation of statistical systems can be explained by using the Mandalstman variables as follows. In a hadronic collision for a fixed collision energy when the multiplicity is low the incoming energy is shared among only a small number of S_{ij} 's, all of which will then have a good chance simultaneously to obtain large values. The particles are at high energy with respect to one another. We expect then the multiperipheral model to prevail. As the multiplicity is increased the same initial energy has to be shared between more and more S_{ij} 's, some of which are forced to be small. In the same way when the multiplicity is so high, none of the S_{ij} 's would have a chance to be large, all the final particles form a single fireball (statistical equilibrium) which is the characteristic process in high energy hadronic collisions. In the sense of this statement, one would expect a large number of possible

particle states and also continuous mass spectrum of hadrons. There would be no reason to distinguish between a resonance, fireball and the thermodynamical system, except that they differ in the degree of excitation. This would simply imply the self-consistency condition quoted by Hagedorn which requires $\rho(x)$ and $\sigma(x)$ to approach asymptotically to each other as $x \rightarrow \infty$.

Here we have $\rho(m)dm$ denoting the mass spectrum of hadrons (i.e. the number of excited hadrons with mass between m and $m + dm$) and $\sigma(E)dE$ denotes the number of states between E and $E + dE$ of the thermodynamical system where E is the total energy including the rest masses of the particles. For any given energy the system is described by a temperature $T(E)$, but certainly there is a highest temperature T_0 which governs all high energy phenomenon in which hadrons take part. This temperature is reached in all high energy events with sufficient total energy and momentum transfer. Here the reaction would be explained by the thermodynamics and conservation laws. Neither the details of interaction, nor the structure of the interacting hadrons will manifest themselves. Approach to the highest temperature T_0 can be explained as follows. We shall see that the density of states, i.e. $\sigma(E)$, grows already very fast if only one kind of particle is available. By increasing the kinetic energy we shall have increased energy levels inside the box or increased temperature. If there is the possibility of creating new kinds of particles, then the increase of energy shall be balanced by increasing both the kinetic energy (i.e. temperature) and the number of kinds of particles. The exponential growth of $\rho(m)$ (i.e. equation (11)) is consistent with this fact that the system uses up the energy to increase the temperature and the number of kinds of particles only until a certain temperature $\approx T_0$. When T_0 is approached creation of a new kind of particle would be easier than the increase of

the temperature so the process of creation of particles would continue with the constant temperature T_0 . This situation is comparable with the situation of a liquid at the boiling point in which the particles are emitted from the liquid into the vapour and thereby must overcome a large potential barrier which is to be replaced with potential wall of height m between non-existence and existence of a particle of mass m .

Accepting the existence of the highest temperature one would expect that this temperature must govern the transverse momentum distribution of outgoing particles. This distribution is not affected by any kinematical effect and from collision to collision enormously varying relative motions of different parts of the heated volume and any Lorentz transformation in the direction of the collision will leave p_T and its distribution invariant. Because of this invariance one can calculate the transverse momentum distribution for $T = T_0$.

The average number of particles in a quantum state E within the volume V is proportional (- for bosons, + for fermions)

$$\frac{1}{e^{E/kT} \pm 1} \quad (1)$$

Our units are: $h = c = k$ (Boltzman's constant) = 1. For collisions at high energies we shall make the usual assumption that all produced particles are relativistic. In such cases, the energy of the particle E in equation (1) can be approximated to the momentum

$$E^2 = (P_T^2 + P_L^2) + m^2 \approx P_T^2 + P_L^2 \quad (2)$$

where P_L and P_T stand for particles longitudinal and transverse part of momentum. So the number of particles having momentum with magnitude between p and $p + dp$ is proportional to

$$e^{\pm P/T} \quad (3)$$

Using this, the single particle's momentum distribution would be

$$E \frac{d^3\sigma}{dp^3} = \text{constant} (e^{\pm P/T} \pm 1) \approx \text{constant} e^{\pm P/T} \quad (4)$$

In the next section we would see that at the instant of decay of thermodynamical system the decay products no longer interact and their transverse momentum distribution is isotropic and determined by the Boltzman's type.

$$g_T(P_T) = C e^{-P_T/T} \quad (5)$$

To get this we have ignored the longitudinal part of the momentum in equation (4). C is a normalization constant. It contains the volume element V and possible dynamical factors.

1.3 Formation of the thermodynamical system

As we said, the characteristic process in hadronic collision is the formation of statistical systems usually made from the primary particles by losing their energy. It is widely admitted that the mechanism responsible for this are manifold. Many experimental data demonstrate the superposition of distribution of different types corresponding to collisions with different inelasticity coefficients.

According to definition the statistical system is that the particles contained in it exchange large 4-momentum. More accurately for the particles i and j, the Mandelstam variables $S_{ij} - t_{ij}$ are of the same order. Here the collision is called central where the system is at rest in common c.m.s. On the average the secondary particles have the same amount of kinetic energies. In central collision the multiplicity is larger. The

impact parameter is smaller and accordingly the angular momentum l is smaller, i.e. the expansion is isotropic. The energy transferred to new particles may be conveniently characterized by the inelastic coefficient K which is defined as the ratio of total energy of all newly produced particles to that of colliding particles. It is obvious that by this definition the inelasticity coefficient cannot be larger than unity. Of course the defined value corresponds to the annihilation of colliding particles and we do not have the particles of initial kind in the final state. As far as the energy transferred to the newly produced particles turn out to be somewhat different for each event of inelastic interaction, then it is convenient to introduce the mean inelasticity coefficient as

$$\langle k \rangle = \frac{\int_0^{\infty} K N(K) dK}{\int_0^{\infty} N(K) dK} \quad (6)$$

where $N(K)$ is the number of inelastic interactions with definite value of inelasticity coefficient. In reference (8) it is explained that the average inelasticity coefficient $\langle K \rangle$ is somewhat greater than .3 .

It is also discussed that the value of $\langle K \rangle$ determined in equation (6) can be approximately replaced by the product of the average number of produced particles and their average energy, i.e.

$$\langle K \rangle \approx \langle n \rangle \langle E \rangle$$

Experiments show that the average kinetic energy of secondary particles and also average multiplicity increases with energy. So one should expect the value of $\langle K \rangle$ to increase versus the energy of initial state.

The described central collision is not the only case, there is always an admixture of particles in the final state which are generated in the decay of primary particles which is excited during the collision

process and moves on ahead. This is the reason for inequality of kinetic energies of produced particles. As an example the kinetic energy of the secondary protons in N-N collision is noticeably higher than that of the pions. On the contrary, the average kinetic energy of pions produced in π -N collision essentially exceed that in N-N collision. At low multiplicities this leading effect would predominate. It should be borne in mind that even the central distribution can be broken into three parts, (a) isotropic part which can be ascribed to the decay of the statistical system at rest in the c.m.s., (b) a forward peak which can be ascribed to excitation and decay of incoming particle, (c) a backward peak which is similarly ascribed to the decay of target excited by collision. There are suggestions that if the excitation energy of the particles reaches several GeV, then their decay can also be considered statistically.

Peripheral or generally multiperipheral model is another mechanism responsible for inelastic collision processes, to which a lot of attention has been given to its development. Here one pion exchange connects the irreducible parts or if one speaks in the language of multiperipheral regge model, regions are the exchanged particles. Again the average multiplicity is growing with energy (i.e. the irreducible parts). In fact one can introduce clusters instead of the irreducible part, i.e. fireball-type accumulation of generated pions which cannot be reduced to a system of particles that exchange individual poles peripherally. The major difficulty of this scheme is that the final particles are collimated instead of being isotropic. The inelasticity coefficient for such processes is considerable. So if one wishes to describe the details, one is forced to introduce the effect of more fireballs and also leading effect. We referred to Hagdorn's work previously. Hagdorn (9) in his thermodynamical approach takes non-central and peripheral collisions into account

phenomenologically. In this theory particle generation is calculated statistically by means of statistical formulae for each given element of overlapping volumes of the colliding hadrons. The centre of mass system velocity of the entire system is described by a velocity distribution function chosen to agree with the experiment. The temperature of each element does not exceed a certain value T_0 and that the generated particles move apart without interacting.

In the following we shall discuss some aspects and relative consequences of statistical thermodynamical model (STM) of Hagedorn's to show that in spite of some defects to explain the entire phenomenon the S.T.M. turns out to be correct and fruitful.

Using quantum mechanics the probability of a collision process between two particles of four momentum p_1 and p_2 leading to a final state containing n particles with four momentum p_i ($i = 1, 2, \dots, n$) would be a function of matrix element and phase space volume, i.e. the density of available states in a normalization box. So

$$P(n) = \text{const} \int_0^\infty M_n^2 \delta(E - \sum_{i=1}^n E_i) \delta^3(\sum p_i) \prod_{i=1}^n d^3 p_i \quad (7)$$

Here we do not have an explicit form to the matrix element and the only way to describe the interaction between the particles might be the phase space explanation which one can evaluate. This shall be discussed in terms of statistical mechanics because of some relevant difficulties. In fact when one is talking about S.T.M. must remember two entirely different parts contained in it, namely kinematics and thermodynamics, where kinematics is related to the fireball model discussed before. However, a complete job would be done if all different sorts of fireballs be included, i.e. central, multiperipheral and even fireballs produced by excitation

of initial particles to take into account the through going particles. The thermodynamical part of S.T.M. is in fact the statistical model itself, but certainly there is inclusion of dynamics. The matrix element in equation (7) is the responsible element for dynamic or generally if one looks at equation (7) very carefully, one can realize the fact that the probability $P(n)$ is just the mixture of dynamics and phase space. Again what is the dynamic, and how to evaluate it. One really does not know. As Hagdorn realized, there is one clear way to get rid of dynamic. That is eliminating the dynamic by shifting the position of it as far as possible in favour of phase space. This would provide the chance of taking matrix element in equation (7) as a constant and so every thing shall be understood from phase space. Now let us concentrate on dynamic and try to eliminate it. This is well explained by Hagdorn (9). Hagdorn says dynamic has two certain aspects which eventually have to be connected. First of all it generates the resonance states, second it allows for carrying over much of the primary longitudinal momentum into the final particles. The author believes that if one can really include all resonance states the first part of dynamic could be shifted into the dynamics. For this one must pay attention to the fact that because of interaction the wave functions suffer a phase shift and the density of states inside the phase space volume is changed and so it must be readjusted to match the boundary condition. To produce a theoretical approach the integration in equation (7) is replaced by an integration over the total momentum and the relative momentum of particles 1 and 2 and also weighted by $(2\ell + 1)$ times of a form like

$$\frac{dn_{\ell}}{dp^{\prime}} dp^{\prime} = \left(\frac{R}{\pi} + \frac{1}{\pi} \frac{d\sigma_{\ell}}{dp^{\prime}} \right) dp^{\prime} \quad (8)$$

where $\frac{dn_{\ell}}{dp^{\prime}}$ is the available momentum states between the internal momentum

p' and $p' + dp'$. δ_{ℓ} is the phase shift and R is the radius of normalization volume. Here the first term is what would remain without interaction and the second is due to the two particle interaction of pair 1-2 in the ℓ th partial wave. By this means, if one takes a certain resonance one can reduce the matrix element in equation (7) in order not to take account twice for the same interaction. Including all the resonances due to the interaction of three-, four-, and also resonances produced by interaction of the last resonances with remaining particles possible cut on matrix element will have taken place which would leave it more and more constant. The second effect of dynamic responsible for longitudinal momentum of final particles is answered in terms of collective motion, which is in fact the explanation for the kinematic part of S.T.M. To be able to include all various fireballs, a continuum of fireballs is introduced. At a certain time Hagdorn describes a pp collision as illustrated in Figure (1). At the central part of the collision particles are at rest, but in the forward-backward direction there would be a collective motion. Going far from the centre the velocity of this collective motion would increase to almost the initial proton's velocity at the end. One knows that the local energy density is a function of local collective velocity. During the collision the incoming particle is decelerated. The lost of the kinetic energy is transformed into the heat and local excitation. When the process of deceleration and excitation terminated the particles start to emerge from the system. The particle production will be a function of local energy density, i.e. local collective velocity and it will be isotropic in the local rest frame. Then by Lorentz transformation of any local distribution one can get the required c.m.s. spectrum. The parameter used to describe the collective motion is a velocity factor λ , i.e. the ratio of actual local kinetic energy density to incoming energy density. To be

able to pick up all contribution to a given λ during the whole interaction over the whole interaction volume and for all impact parameters, a weight function $F(\lambda)$ is introduced which is a function of initial energy and normalized to 1 over half of the interval. This velocity weight function puts more weight for newly produced particles on low velocities (i.e. central part) and more weights for through going particles on high velocities (i.e. peripheral). As an example, if we take $f_m(p,E) d^3p$ to be the differential production spectrum of particles of mass m , then we have to Lorentz transform this isotropic spectrum from rest frame to the c.m. using the local weighted collective velocity $F(\lambda)$ and summing over all possible particular velocity to get the c.m. differential spectrum of particles of mass m . The author believes that by having $F(\lambda)$ the second feature of dynamic is understood by the same manner as the first aspect in the rest frame of the particles. To understand the discussion in detail the reader is requested to refer to Hagdor's published papers. So ultimately by accepting what we said, in fact we can ignore the dynamic and forget its more complications and take the matrix element constant and study the probability $P(n)$ just with phase space. As an example one particle momentum spectrum shall be

$$\begin{aligned}
 f_m(p,E) &= \sum_n f_m^n(p,E) \\
 &= \sum_n \sum_{\text{all resonances}}^{(n)} \int_{M_n}^{-2} \frac{dR}{dp} (E,p, \text{ masses}) \\
 &= \text{const} \sum_n \int \frac{dR}{dp} (E, p, \text{ masses})
 \end{aligned}
 \tag{9}$$

Here we have to know not just all resonances, but also must manage to compute a large number of phase integrals, which seems to be very difficult, especially for higher energies. This is the reason that why one must take

help from statistical mechanics which gives the same form as equation (7), provided that the energy and momentum conservation is ignored. Of course here in our statistical thermodynamic language there is a fixed temperature T for each energy E such that the expectation value of the energy is equal to the given energy E .

So from here a thermodynamical description for $f_m(p, E)$ would be as follows: it is one particle momentum spectra of a given sort (m) of particle participating in the equilibrium of a system comprising an indefinite number of all kinds of particles and resonances embodied in a heat bath of temperature $T(E)$, chosen such that $E = \langle E(T) \rangle$. This is the definition coming from Hagedorn and gives the Boltzman distribution of form (5) for the single particle spectra.

To introduce the whole resonance in equation (9) and all other similar equations, a function $\rho(m)dm$ is introduced which counts the number of the particles in the interval $\{m, m+dm\}$. So one can integrate over $\rho(m)$ instead of summing all resonances. Within the framework of strong interactions there is no obvious limit to a fireball mass so the mass spectrum $\rho(m)$ must be defined for all masses $0 \leq m < \infty$ using the self-consistency condition defined before, i.e.

$$\log \rho(m) \rightarrow \log \sigma(E=m) \quad \text{if } m \rightarrow \infty \quad (10)$$

It has been shown that (9)

$$\rho(m) \rightarrow cm^a \exp(-m/T_0) \quad (11)$$

where c is a constant and (9,12)

$$\begin{aligned} a &= -5/2 \quad \text{for weak bootstrap solution} \\ a &= -3 \quad \text{for strong bootstrap solution} \end{aligned} \quad (11^1)$$

The significant consequence of this exponential growth of mass spectrum is that T_0 is a universal highest temperature and

$$T_0 = 160 \text{ MeV} = 1.86 \times 10^{12} \text{ }^\circ\text{K} \quad (12)$$

This result is calculated by Hagdorn (9) by using the data for mass spectrum.

Using the transverse distribution, equation (5), it is also found that (9)

$$T_0 \approx m_\pi \quad (13)$$

So far we have understood what is the thermodynamical model and how the fireballs are made. In the following section we shall see some consequences of STM and also the possible defects of it at the end to complete this chapter.

1.4 Defects and successes of STM

According to what we said in previous sections, when a fireball is made it gives off its excitation energy in a sequence of particle emissions of the asymptotically bounded average energy which is equivalent to the existence of a highest temperature T_0 . As quoted in spite of having a single central decay of Figure(2a) allowing the unrestricted decay of the fireball into any number of fireballs and/or pions, the full bootstrap decay can be displayed as Figure (2b). The cascade decay of Figure(2c) is also the solution of bootstrap condition and we can show that the partition function coming both from bootstrap equation and from the cascade decay are the same. The linear decay is the dominant decay form in the full bootstrap decay. The average decay produces $\langle N \rangle = 2.4$ particles, one of them is heavy ($m_1, m_2 - m_i$) except that the end of the chain, while

the other 1.4 particles with average mass $\langle m \rangle = \text{some } m_\pi$ are light, most of them are pions, sometimes resonances or kaons, rarely baryons (10-12). The multiplicity distribution of $w(n)$ of fireballs in a biroball is a poisson distribut, i.e.

$$w(n,E) \approx \frac{\langle n \rangle^n}{n!} e^{-\langle n \rangle} \quad (14)$$

$$\text{where } \langle n(E) \rangle = \alpha \ln E + \text{constant} \quad (15)$$

Here α is a constant, reference (9).

Hagdorn has calculated the invariant cross-section, $E \frac{d^3\sigma}{dp^3}$ and the reason for logarithmic growth of average multiplicity, i.e. equation (15); turned out to be the central plateau which had energy independent light and elongated logarithmically. The fragmentation region appeared to have constant multiplicity. The calculated (Feynman variable) distribution agreed well with the data (9,13). Hatun Thun and Ranft (14) modified Hagdorn's work to describe the energy dependence of inclusive pion spectra in pion induced reactions. They showed strong deviation for

$$w(x) = \int \frac{2E}{\pi\sqrt{s}} \frac{d^3N}{dx dP_T^2} dP_T^2 \quad (16)$$

from scaling in the central region where it grows with primary energy, Figure (3). Except the region around the elastic peak at $x = 1$, good agreement of the model with experimental data has been reported. Inclusive π^0 spectrum has been compared with experimental data for reaction (15)



At small transverse momentum and outside the central region, the thermodynamic γ spectra scale in the range $6.3 \leq \sqrt{s} \leq 52.7$. But at large P_T the thermodynamic γ spectra deviated from scaling behaviour, Figure (4).

In the central region (i.e. $x = 0$), there is good agreement between inclusive spectra of the model and experimental results with respect to x in the region $0 \leq x \leq .15$.

Thermodynamical model was used to study the many particle distribution and correlations by Ranft and Ranft (16). They had two different choices for fireball mass M_F smaller than M_F^{\max} (the maximum kinematically allowed mass of fireball in the case of having a production of one fireball). The parameter w was used to show the energy and rapidity dependence of fireball mass. At $w = 0$ and $w = 1$ the model leads to the limiting case of multiperipheral and diffractive excitation model. By decreasing w from one the average number $\langle n_k \rangle$ of produced fireballs are to be increased.

The rapidity correlation function

$$\begin{aligned}
 c^{(2)}(y_1, y_2) &= \int dP_{T_1}^2 dP_{T_2}^2 \cdot \rho^2(p_1, p_2) \\
 &= \left(\frac{d^3 N}{dy_1 dy_2} \bigg/ \frac{dN}{dy_1} \cdot \frac{dN}{dy_2} \right)^{-1}
 \end{aligned}
 \tag{18}$$

was compared with experimental data at 12 GeV/c. The positive correlation was confirmed for all three charge states of pion at the point $y_1 = y_2 = 0$. At this point also

$$c^2(\pi^+ \pi^-) > c^2(\pi^+ \pi^+) > c^{(2)}(\pi^- \pi^-)
 \tag{19}$$

has resulted. Of course at rather low energies not much more than one fireball can be produced and so the contribution where both particles came from two different fireballs was ignored, and one fireball term was taken as the dominant one.

The function $C^2(y_1, y_2)$ has been studied for reaction



at 1500 GeV/c (16). The values of the function at large values of $|\Delta y|$ were reported to be mainly determined from two fireball terms and negative correlation has been shown.

Fireball model can also be used to discuss $e^+ e^-$ annihilation where it is assumed that an e^+ and e^- annihilate into a virtual photon which subsequently emits hadrons thermodynamically. In reference (17) the authors have used Hagdorn's multiperipheral fireball model in which fireballs are produced peripherally and uncorrelated. If the energy is increased more fireballs are produced as usual. The model fits the inclusive momentum distribution and the average charged multiplicity and also predicts the logarithmic rise of

$$R = \frac{e^+ e^- \rightarrow \text{hadrons}}{e^+ e^- \rightarrow \mu^+ \mu^-} \quad (22)$$

With respect to energy, Figures (5a, 5b and 5c). The longitudinal distribution is obtained from equation (4) by introducing the transverse component (P_T) and azimuthal angle ϕ and then integrating with respect to P_T and ϕ . The distribution of negative particles (π^-) with respect to P_L at c.m.s. in $\pi^- p$ collisions of $E_L = 25 \text{ GeV}/L$ is displayed in Figure 6. It seems that particles from statistical system predominate for very small values of P_L and the exponential picture resulted from Maxwell Boltzman distribution will not fit data except for a few MeV of P_L . So as we said in Section 1.2, a statistical thermodynamic picture fails to explain the longitudinal momentum distribution of secondaries in overall c.m.s. For this reason we shall take the zero longitudinal momentum and ignore the collective longitudinal motion of particles.

As a final remark we can stress that (SBM) is considered as one of the most consistent explanations of transverse motion of secondaries. As

mentioned before, the transverse motion has purely thermodynamical picture while the fireball system temperature does not exceed the ultimate value of $T_0 \approx m_\pi$, and we could get a good agreement with data until $P_T < 1.4 \text{ GeV}/c$ (Figure 7).

However the explanation of large P_T distribution encounters in this approach serious troubles and the known fact is not sufficient to explain it. The differences between large and small P_T interactions can be summarized as Table 1.

To incorporate the large P_T distribution we might assume that the fireball temperature at initial states of motion considerably exceed the ultimate temperature T_0 . It is just the presence of large initial temperatures that we relate to a possibility of large P_T secondaries.

It must be admitted that in any case, the character of transverse motion in large and small P_T process turns out to be similar and there must be a smooth joining between two parts. To describe the data we consider multi-temperature distribution which will be seen in the next chapter of this thesis.

CHAPTER II

DEFINITION OF MULTI TEMPERATURE MODEL

As we have seen in the previous chapter, the small P_T inclusive data around $y = 0$ is well explained by a thermodynamical model with $T \approx m_\pi$ MeV. This temperature is independent of initial energy and of the process considered. However at P_T larger than about 1.4 GeV/c the prediction is badly wrong. For example in Figure 7 we show that at $P_T = 5$ GeV/c the data exceeds the thermodynamical model by a factor of about 10^4 ! Various attitudes can be adopted at this point.

- (i) The model is wrong
- (ii) At large P_T a new phenomenon is occurring which dominates the extrapolated small P_T curve.
- (iii) The model requires some correction which is only significant for the large P_T .

It is of course conceivable that (i) is correct, but it is unwise to abandon too quickly such a very simple idea, especially when it appears to exhibit at least some approximation to the truth at low P_T . The second attitude is common and indeed an obvious candidate for the high P_T events are "hard" collision between postulated constituents of the nucleons. Whether the low P_T data are caused by a 'thermodynamical' process or also by direct constituent collision is still an open question here. However the smoothness of the curve between small and large P_T (and further evidence below) suggests that a common description of small and large P_T is likely. In this thesis we adopt the attitude in (iii) and try to see whether a reasonable modification of thermodynamic model can be made and whether it then gives prediction in accordance with

experiment. The simplest modification is to assume that we have thermodynamic equilibrium before particles emitted, but that for some reason the temperature of the emitted 'fireball' is not always the same, i.e. that there are distribution of temperatures. We refer to this model as the 'Multi-temperature' model (M.T.M.)

2.1 Single particle momentum distribution according to the M.T.M.

To answer some of the possible questions, we start with a single pion inclusive spectra which is generally defined as

$$\begin{aligned}
 F(P_T, Y, s) &= E \frac{d^3\sigma}{dp^3} = \frac{d^3\sigma}{P_T dP_T dy d\phi} \\
 &= \frac{1}{2\pi} \frac{d^2\sigma}{P_T dP_T dy}
 \end{aligned}
 \tag{23}$$

Where ϕ and y are azimuthal and rapidity variables respectively, and s defines the square of the centre of mass energy. Many theoretical models assume a factorized property for function $F(P_T, Y, s)$ of equation (23) and they (18) write the invariant x-section as a product of two independent functions of P_T and y_{Lab} as:

$$F(P_T, Y_{Lab}, s) = f(P_T) G(y_{Lab})
 \tag{24}$$

We shall be concerned with function $f(P_T)$. In fact since we compare with data at $y_{Lab} = 0$ the validity of equation (24) would not really concern us. So equation (23) could be transformed to

$$f(P_T) = \frac{d\sigma}{P_T dP_T} = \frac{\int_E \frac{d^3\sigma}{dp^3} dy d\phi}{\int dy d\phi}
 \tag{25}$$

We assume the inelastic cross-section (σ_{inel}) to be made up of (19) contributions from various temperature T , i.e.

$$\sigma_{inel} = \int_0^{\infty} \sigma(\lambda) d\lambda \quad (26)$$

Here λ is the inverse temperature and $\sigma(\lambda)$ is the cross-section for producing a temperature $T = \lambda^{-1}$. For each λ we expect a thermodynamical distribution of equation (5) i.e.

$$g_{\lambda}(P_T) = a(\lambda) e^{-\lambda P_T} \quad (27)$$

Using equation (27), the mean multiplicity per unit of azimuthal angle ϕ per unit of rapidity at fixed λ is given by

$$\begin{aligned} \bar{n}(\lambda) &= \int_0^{\infty} g_{\lambda}(P_T) \frac{dP_T^2}{2} = a(\lambda) \int_0^{\infty} e^{-\lambda P_T} P_T dP_T \\ &= a(\lambda) / 2 \end{aligned} \quad (28)$$

which gives the total mean multiplicity

$$\begin{aligned} \sigma \langle n \rangle &= \int_0^{\infty} P_T dP_T \int_0^{\infty} d\lambda e^{-\lambda P_T} a(\lambda) \sigma(\lambda) \\ &= \int_0^{\infty} d\lambda \sigma(\lambda) a(\lambda) / \lambda^2 \\ &= \int_0^{\infty} d\lambda \sigma(\lambda) \bar{n}(\lambda) \end{aligned} \quad (29)$$

If we wish to have a finite multiplicity even as $T \rightarrow \infty$, then we require $a(\lambda) \approx O(\lambda^2)$. An interesting possibility would be to have $a(\lambda) / \lambda^2 \approx \text{constant}$, i.e. a multiplicity independent of temperature. Finally we can make use

of our main assumption which requires the inclusive distribution $f(P_T)$ to be a sum of fixed temperature distributions and write it to be

$$f(P_T) = \int_0^{\infty} d\lambda \sigma(\lambda) g_{\lambda}(P_T) \quad (30)$$

Inserting (27) in equation (30) gives

$$f(P_T) = \int_0^{\infty} d\lambda \sigma(\lambda) a(\lambda) e^{-\lambda P_T} \quad (31)$$

This equation shows that $f(P_T)$ is the Laplace transform of the unknown function $\sigma(\lambda)a(\lambda)$. It is clear therefore that any reasonable data can be fitted by the model. Conversely a successful fit does not in any sense justify the model. For that we must consider other predictions (Correlations, see Chapter 3).

We have also to note that the data on $f(P_T)$ only determines the product $\sigma(\lambda)a(\lambda)$, not both of these quantities.

There are now several possible procedures. We can invert equation (31) to obtain $\sigma(\lambda)a(\lambda)$ as the inverse Laplace transform of the data. However this can only be evaluated if we have an explicit form for the data and even then it will not in general be simple to evaluate. In Chapter 3 (Section 4) we shall see that we can make use of the inverse Laplace transform for some purposes without actually evaluating it.

For our future calculations we shall consider a simple and useful fit to $f(P_T)$ which is given by Vanryckeghem (20), i.e.

$$f(P_T) = A \exp \left(-k(P_T^2 + v^2)^{1/4} \right) \quad (32)$$

This form produces $s^{-1/2}$ dependence for $A(s)$ and slow decrease of $k(s)$ with energy according to

$$A(s) = A' / \sqrt{s}$$

$$k(s) = k_0 - k_1(s) \ln \sqrt{s} \quad (33)$$

Here the parameters A' , k_0 , v and $k_1(s)$ have different values for various types of particles and they are displayed in Table 2. The corresponding multi-temperature single particle distribution is compared with $\theta = 90^\circ$ data of B.S. collaboration (40) at two different I.S.R. energies $\sqrt{s} = 23$ GeV and $\sqrt{s} = 45$ GeV. It is shown in Figure 8. The plot shows a good agreement of the model and data.

To discuss the energy and temperature relation and also the significance of the function $\sigma(\lambda)a(\lambda)$ in explaining the thermal condition of the so-called fireballs, we shall evaluate it by using a simple approach. This is to be seen below in the next section.

2.2 Variation with Energy of Temperature Distribution

As we saw in the previous section, there is a strong energy dependence of single particle spectra increasing with P_T , Figure 8. According to the multitemperature model, this fact must be explained by the function $\sigma(\lambda)a(\lambda)$ which is the inverse Laplace transform of $f(P_T)$, i.e.

$$\sigma(\lambda)a(\lambda) = \int_{-i\infty}^{i\infty} f(P_T) e^{\lambda P_T} dP_T \quad (34)$$

Ignoring the parameter v in equation (32), one can do this integration exactly. The result of that turns out to be

$$\sigma(\lambda)a(\lambda) = \frac{A K e^{-K^2/4\lambda}}{2\sqrt{\pi\lambda^3}} \quad (35)$$

which is a function of energy. To see the energy dependence of this form, the ratio

$$R = \frac{\sigma(\lambda)a(\lambda) \text{ at } \sqrt{s} = 53 \text{ GeV}}{\sigma(\lambda)a(\lambda) \text{ at } \sqrt{s} = 23 \text{ GeV}} \quad (36)$$

is plotted in Figure 9 versus temperature. But in fact we are interested in ν to be able to fit the low P_T data by the form (32). Certainly having kept it the integration in Equation (34) would be difficult and one might try a numerical approach to evaluate the inverse Laplace transform of $f(P_T)$. Our attempt to find an exact form for $\sigma(\lambda)a(\lambda)$ is described as follows.

Let us approximate the exact form of equation (32) as

$$f_\nu(P_T) = f_0(P_T) - \left(1 - e^{-k\sqrt{\nu}}\right) H(P_T) \quad (37)$$

where $f_0(P_T)$ is the deduced form from $f(P_T)$ of equation (32) by taking the parameter $\nu = 0$. Here we have represented a function H of P_T such that we can calculate its inverse Laplace transform and it confirms the constraints

$$H(P_T) = \begin{cases} 1 & \text{for } P_T = 0 \\ 0 & \text{for } P_T \gg \nu \end{cases} \quad (38)$$

Calculating the values of $H(P_T)$ in equation (37) one would expect a useful analytic form for it. Having this form there must be a good fit of the right hand side in equation (37) to the data, especially at lower P_T values. We have chosen this form to be

$$H(P_T) = e^{-a\sqrt{P_T}} \quad (39)$$

where a is a free parameter and a function of energy. Of course this form agrees with the requirements mentioned above. This form has been fitted to the corresponding values of $H(P_T)$ which gives

$$\begin{aligned}
 a &= 13.3 \text{ for } \sqrt{s} = 23 \text{ GeV} \\
 a &= 12.5 \text{ for } \sqrt{s} = 53 \text{ GeV}
 \end{aligned}
 \tag{40}$$

Inserting equation (39) into equation (37) our exact form for the single particle spectra would be

$$f(P_T) = A e^{-k\sqrt{P_T}} - A \left(1 - e^{-k\sqrt{v}}\right) e^{-a\sqrt{P_T}}
 \tag{41}$$

This form has been compared with the data at $\sqrt{s} = 23$ GeV. The result is plotted in Figure 10. It is obvious that this form can fit data very well indeed.

Inserting equation (41) into equation (34), one can get an exact form for the function $\sigma(\lambda)a(\lambda)$, i.e.

$$\sigma(\lambda)a(\lambda) = \frac{A k e^{-k^2/4\lambda}}{2\sqrt{\pi\lambda^3}} - A \left(1 - e^{-k\sqrt{v}}\right) \frac{a e^{-a^2/4\lambda}}{2\sqrt{\pi\lambda^3}}
 \tag{42}$$

Taking a from equation (40) we have presented the comparison of equations (42) and (35) in Figure 11 for two ISR energies, $\sqrt{s} = 23$ GeV, $\sqrt{s} = 53$ GeV. It is obvious that $\sigma(\lambda)a(\lambda)$ is increased versus the energy at high temperatures. At higher temperatures the curves go very rapidly towards the zero which is equivalent to the larger values of P_T in equation (32). So generally one would expect a high P_T particle at higher temperatures.

Finally we have compared the ratio R of equation (36) for the two cases using equations (35) and (41) which are displayed in Figure 8. The curves have generally the same shape and they indicate the discussed final result.

CHAPTER III

STUDY OF TWO PARTICLES CORRELATIONS AT LARGE P_T

We saw in Chapter II that the MTM can predict a fit to the data. However as we have noticed already the model has the freedom to fit any data, so in order to test it, we must see whether it gives any other predictions which are correct. Once the temperature distribution is given the model gives a definite prediction for any possible process, so in principle many tests are available. In this thesis we look at two particles correlations where one particle has a large transverse momentum. First we discuss the experiments.

3.1 Experimental Evidences

Generally the two particle correlation function depends on 4-momentum vectors P_1 and P_2 of two detected particles, namely (P_1, θ_1, ϕ_1) and (P_2, θ_2, ϕ_2) as well as s the centre of mass energy square. In this subsection we would describe the observation of hadron-hadron collisions in which the charged secondary hadrons are produced together with a large P_T (neutral or charged) hadron. An example of such a process could be the following double inclusive scheme.

$$P + P \longrightarrow h^{\pm}_0 + h^{\pm} + \text{anything} \quad (43)$$

A diagrammatic representation of this process is illustrated in Figure 12. Practically the large P_T particle is triggered ($P_T' > 2 \text{ GeV}/c$ in most of the experiments) in a fixed direction (y_0, ϕ_0) over a limited solid angle $(\Delta y_0, \Delta \phi_0)$ and the other products with transverse momentum \vec{P}_T^i are correlated to the large P_T particle. Depending on the sign of the scalar

products $(\vec{P}_T^i \cdot \vec{P}_T^j)$ they could be divided into two groups of "towards movers", i.e. when $\vec{P}_T^i \cdot \vec{P}_T^j > 0$, Figure 12b, and "away movers", i.e. $\vec{P}_T^i \cdot \vec{P}_T^j < 0$, Figure 12c. Mostly the emission of charged hadrons h^\pm in large P_T events is described by the double inclusive cross-section which is generally integrated over the acceptance Ω of the large P_T trigger h^\pm and normalized to the integrated single inclusive cross-section. Hence we define (29)

$$\frac{d^3 \langle N \rangle}{dy dP_T^2 d\phi} = \int_{\Omega'} \frac{d^3 p'}{E'} \cdot \frac{EE' d^6 \sigma_5}{d^3 p d^3 p'} \bigg/ \int_{\Omega} \frac{d^3 p'}{E'} \cdot \frac{E' d^3 \sigma}{d p'^3} \quad (44)$$

This formula is always compared with the equivalent one obtained for normal events, Figure 12a, i.e.

$$\frac{d^3 \langle N \rangle}{dy dP_T^2 d\phi} = \frac{1}{\sigma_{inel}} \cdot \frac{d^3 \sigma}{d p^3} \quad (45)$$

Here σ_{inel} is the hadron-hadron inelastic cross-section and represents the number of charged particles per GeV/c and per unit of rapidity and per radian of azimuthal produced in any elastic collision.

The ratio of the distributions (44) and (45) measure the strength of the correlation between h^\pm and h^\pm .

The apparent difference between normal and large P_T events could be realized from Figure 13 which displays the plots of the azimuthal angle " ϕ " against the rapidity " y " for all positive and negative tracks according to the integrated form of equations (44) and (45) over a possible range of P_T as,

$$\frac{d^3 \langle N \rangle}{dy d\phi} = \int_{P_T(\min)}^{P_T(\max)} d P_T^2 \frac{d^3 \langle N \rangle}{dy dP_T^2 d\phi} \quad (46)$$

In Figures 13b and 13c the trigger particle is taken with $y = -2$ and $\phi = 20^\circ$ and the accumulation in that region is due to it, and the density of the particles shows a maximum at $\phi = 200^\circ$ (which is 180° from the trigger) in a broad rapidity region of about four units and also a small second maximum is seen at the same y and ϕ as the trigger for negative particles. In Figure 14 the azimuthal distribution of reference (21) are shown for different charges in different rapidity intervals. It can be realized that for both negative and positive secondaries there is a strong correlation peaking at $\phi = 200^\circ$ (180° from the trigger) over a rapidity region $-4 < y < +2$. The lines shown for comparison are smoothed distributions obtained for normal events. Of course one can see that the peaks observed near $\phi = 200^\circ$ are stronger near the rapidity of the trigger and the strength of this correlation decreases as the distance in rapidity from the trigger increases. Figure 15 shows the azimuthal distributions of secondary charged particles for these different P_T intervals. It is clear that as the P_T of charged particles increases the structure in azimuthal distribution becomes narrower and more pronounced. Again the ϕ dependence of the particle density integrated over y from -2 to $+2$ for the π^0 , 90° data is shown in Figure 16. It is seen that the increase with P_T of the trigger particle is compatible with a linear increase up to the largest P_T of $5 \text{ GeV}/c$. This is displayed in Figure 17 also. These observations would be confirmed if one discusses them in the sense of rapidity and momentum distributions. As an example, for the 53° and 90° triggers (22), the rapidity distribution, formula (44) of the charged particles produced in both same/away side have been compared to the normal ones. For the same side movers an excess of particles density over a short range in rapidity (about $\Delta y = 1$ units) is seen centred at the same rapidity as the trigger, Figures 18 and 19, which

is supported by the measurements of M. Della Nega (23) done for $90^\circ \pi^0$ and 20° , 45° charged triggers. Of course the later data show slightly stronger correlations for 45° than 20° trigger.

For the away side movers we have presented the results coming from ACHM (22) data for the two triggers 53° and $90^\circ \pi^0$ and CCHK (23) data for four triggers (45°_{\pm} , 20°_{\pm}) with a covered rapidity range $|y| < 4$ in Figures 18, 19 and 20. The respective normal distributions are displayed just for comparison. All of the distributions agree with a broad-excess of particles above the normal distributions in the rapidity range about $-3 < y < 3$ which are centred at $y = 0$ as quoted before. This symmetry about $y = 0$ does not depend on the rapidity of the trigger. There is an asymmetry about zero in the rapidity distributions of secondaries for both charges shifted towards the rapidity of the trigger indicated for the lower P_T of trigger and higher multiplicities, Figures 21e, 21g. But this asymmetry has disappeared at higher P_T of the trigger. The effect of the asymmetry is reported to be more pronounced for negative particles than positive particles. In all other cases the distributions of different charges are the same for different triggers and resulting in a charge ratio depending on rapidity more positive than negative particles are produced in away side and the ratio of the positive to negative density rises with respect their transverse momentum and rapidities, Figure 22. We have already realised that there is a positive momentum correlation between the large P_T particle and charged secondaries. To show it explicitly the momentum correlations in both same side and opposite side is explained in terms of equation (44) integrated over rapidity and azimuthal variables, i.e.

$$F(h, P_T) = \frac{\frac{1}{\Delta y \Delta \phi} \int dy d\phi \int_{P_T' = h}^{\infty} dP_T' dy' d\phi' \frac{d^6 \sigma}{dP_T' dy' d\phi' dP_T dy d\phi}}{\int dy' d\phi' \int_{P_T' = h}^{\infty} dP_T' \frac{d^3 \sigma}{dP_T' dy' d\phi'}} \quad (47)$$

Which is the number of charged particles per GeV/c, per unit of the rapidity and per radiation of azimuthal observed together with a high P_T particle. For the same side movers the comparison of this equation with $h = 3$ GeV/c with equation (45) of normal events is done by some experimentalists (23-25) which are shown in Figures 23, 24 and 25. These results show the function F of (47) as a function of associated charged particle momentum at three different \sqrt{s} values. For all cases the distributions are above the normal ones and they indicate a positive momentum correlation. It is also clear that this correlation is independent of charge combination in pion pair, Figure 26.

The distribution for the same side movers increases slowly with energy and more the large P_T' , Figures 27 and 28. For the away side again data show a positive correlation in the central region and this correlation is even stronger than alongside correlation, Figures 23, 24 and 25. In contrast the alongside case the value of F of equation (47) at fixed value of P_T of associated particles appears to be independent of energy with some errors, Figures 29, 30 and 31. As the same side, the correlation in the opposite side is again independent of charge combination. Studying all these observations one could summarise the following features of the data:

- (i) At each certain energy all P_T distributions are well above the normal distributions, i.e. there is a positive correlation between the two large P_T particles. This means triggering on a large P_T

particle enhances the probability of finding another large P_T charged hadron.

- (ii) Azimuthal effect producing a peak at $\phi = 180^\circ$ from the trigger particle, i.e. the observation of a trigger calls for large P_T particles in the opposite hemisphere to balance its large value of P_T .
- (iii) Charged particle multiplicity accompanying the trigger depends on P_T of the trigger. A linear P_T dependence seems to be unavoidable. The increase with P_T is strongest in the neighbourhood of $\phi = 180^\circ$.
- (iv) Towards the trigger there is an enhancement of rapidity distribution of charged secondaries near the rapidity of trigger. The position of the distribution above the normal distribution grows with P_T of charged particles and the peak shrinks with them. But the away rapidity distribution is peaked at $y = 0$ being independent of the rapidity of trigger.

To describe all these features there are several types of models proposed. Unfortunately none of these models so far could explain all the data. In fact the observed positive correlation, i.e. feature (i) is well explained by MTM. This will be discussed in the next section. Using the energy and momentum conservation we have so far managed to fit the enhancement of positive correlation in away direction in comparison with the same direction, i.e. feature (ii). This will be seen in the 5th section of this chapter.

In the last section we shall try to explain the feature (iii) by using MTM. According to this model the charged particle multiplicity is increased with P_T of the trigger provided that the secondary particles have $P_T \gtrsim .5 \text{ GeV}/c$. The overall prediction of the model is not so bad, but in fact it is not a linear and good fit to the data also.

The case (iv) is not discussed by MTM. In fact we are dealing with $y = 0$ and ignoring any sort of rapidity correlations.

Other interesting models to discuss these features are the constituents interacting models. This is illustrated in Figure 33. Three kinds of processes occur here as follows:

- (a) The incident hadrons break up and each emits some constituents.
- (b) A constituent a of one incoming hadron undergoes a large angle scattering with a constituent b of another initial hadron and become as new particles c and d.
- (c) Now particles c and d each reforms into a jet (i.e. collection of particles in a certain phase space where the sum of their transverse momentum is large). Secondary charged particles and also the trigger particles are the fragments of these jets.

There are some reasons for validity of such models:

- (1) The single particle spectra at large P_T ($P_T \geq 1.5 \text{ GeV}/c$) turn out to fit the scaling form:

$$E \frac{d^3\sigma}{dp^3} = \frac{1}{P_T^{2n}} F(x_T, \theta_{c.m.}) \quad (48)$$

where

$$x_T = \frac{2P_T}{\sqrt{s}} \quad (49)$$

The parameter n represented in equation (48) is

$$n = N - 2 \quad (50)$$

where N is calculated by using the usual dimensional counting rule which is equal to the sum of elementary fields taken part in subprocesses.

$$a + b \longrightarrow c + d \quad (51)$$

(2) The shrinking of rapidity distributions peak with respect to the P_T of charged particles in towards side and resulting from it their transverse momentum with respect to the jet axis being limited is expected in a coplanar two jet structure also.

(3) Kinematic aspects of this coplanar two jet picture have been investigated by Ellis, Jacon, Lanshoff (26) which results in a good fit to the correlation data both in the same side and opposite side.

There are several types of hard scattering models being used to calculate the inclusive cross-section as an integral of the product of probabilities for three processes mentioned in a, b and c. These models differ one from another in the choice of the basic interaction (51) and corresponding to that in the form given to the $\frac{d\hat{\sigma}}{d\hat{t}}$ (\hat{s}, \hat{t}), where \hat{s} and \hat{t} are the s and t invariants for the hard scattering process. These models are as follows:

- (i) $q + q \rightarrow q + q$: quark-quark elastic scattering Model (27) (Q).
 - (ii) $q + \bar{q} \rightarrow m + m$: quark fusion model (28) (QF)
 - (iii) $q + m \rightarrow m + q$
 $\bar{q} + m \rightarrow m + \bar{q}$ } constituent interchange model (29) (CIM)
 - (iv) $q + q \rightarrow m + qq$
 $\bar{q} + \bar{q} \rightarrow m + \bar{q}\bar{q}$ } diquark model (30) (DQ) .
 - (v) Hard scattering types considering quantum chromodynamical processes (QCD)
- (52)

In this part we shall give a brief critical discussion of these models. Features (i) and (v) involve four elementary fields, i.e. $N = 4$ which results in P_T^{-4} dependence of inclusive spectra. This is not a good fit to the data because experimentally the behaviour of the spectra is closer to P_T^{-8} which involves 6 elementary fields, i.e.

Features (ii, iii, iv). Obviously these three models give at least one meson jet. There are evidences that the away side produced jet in large P_T events is similar to those in Lepton-Nucleon interactions. This means the jets in large P_T events must be quark jets. The important way to test this is to look at the cross-sections for different interactions and compare them. G. Donaldson, et al (32) have measured the cross-section for the processes:

$$\begin{aligned}
 (1) \quad & p + p \rightarrow \pi^0 x \\
 (2) \quad & \bar{p} + p \rightarrow \pi^0 x \\
 & \pi + p \rightarrow \pi^0 x \\
 & k + p \rightarrow \pi^0 x
 \end{aligned}
 \tag{53}$$

The result of measurements is equal for all these reactions. But certainly if one expects the process $q + \bar{q} \rightarrow M + M$ to take place, then there should be a difference of at least 40 times between the two processes (1) and (2). So one automatically would conclude that the feature (i) is the only correct process to be considered. At this stage one has two choices to discuss. Either the scattering probability for qq elastic scattering must be modified to produce P_T^{-8} dependence for inclusive spectra, or the scattering is assumed to be between two objects rather than single quarks, such as hadron-hadron scattering.

An example of such modification is the work done by Field and Feynman (27). The authors disregard the theoretical argument that the differential elastic cross-section of feature (i) must vary as $\hat{s}^2 f(\hat{t}/\hat{s})$ and try to fit a form:

$$\frac{d\hat{\sigma}}{d\hat{t}}(\hat{s}, \hat{t}) = \frac{A}{(-\hat{s}\hat{t})^3}
 \tag{54}$$

to the data. This form produces P_T^{-8} and good angular dependence of inclusive cross-section until $P_T = 5 \text{ GeV}/c$. The normalisation parameter is given:

$$A = 2.3 \times 10^3 \text{ mb GeV}^6 \quad (55)$$

It is well known that all partons are not quarks, that half of the momentum of nucleon is carried by another constituent, i.e. gluons. It is possible that some of the high P_T particles could result from gluon interactions, so to get a reasonable fit to the data one must include all contributions coming from gluon interactions. To the lowest order in perturbation theory, Culter and Sivers (31) have calculated the cross-section for all fundamental QCD processes (i.e. figure 5) as

$$qq \rightarrow qq, \quad \bar{q}\bar{q} \rightarrow \bar{q}\bar{q}, \quad q\bar{q} \rightarrow q\bar{q}, \quad qv \rightarrow qv, \quad \bar{q}v \rightarrow \bar{q}v, \\ \bar{q}q \rightarrow v\bar{v}, \quad v\bar{v} \rightarrow q\bar{q} \quad \text{and} \quad v\bar{v} \rightarrow v\bar{v} \quad (\text{where } v \text{ stands for a}$$

vector gluon). These processes contribute an approximately P_T^{-4} dependence to the invariant cross-section. Here the quark distributions are what Field and Fynman used in their calculations. Instead of parameter A they have introduced a form:

$$\alpha_s(Q^2) = \frac{.5}{(1 + .36 \ln(Q^2/4))} \quad (56)$$

for the quark-gluon coupling constant. Here Q^2 is the exchange momentum transfer. The calculated inclusive spectra of F.F. and C.S. models are exactly the same for $P_T \leq 5 \text{ GeV}/c$, but C.S. curves stand above F.F. curves for higher values of P_T . Both models work very well until $P_T \leq 5 \text{ GeV}/c$ but still there are some doubts for their correctness. Because A of equation (54) is too large and there is no theoretical argument to produce neither A nor $\alpha_s(Q^2)$ of equation (56). Both of

these models fail to fit very large P_T data. There is a recent data by Clerk et al (33) which show P_T^{-6} dependence for inclusive P_T spectra for $P_T \gg 5$. GeV/C. These facts indicate that all these models have their own theoretical defects and none of them has the ability to explain the entire data. They might be absolutely wrong or they still need very large corrections. So it is not just absurd, but also it is conceivable that one should assume a hadron-hadron scattering instead of constituent interacting models. We saw that the MTM could fit data very well and it would be unlikely to ignore it at this starting stage. It is worth pursuing it in the hope of obtaining the features which could be incorporated in a more elaborated theory to be able to answer all arising questions. In this thesis we will compare the predictions of MTM for different aspects to see whether some qualitative agreements are possible or not.

3.2 The Theoretical Approach

It was shown (Chapter 2) that the multi-temperature mode of particle production could fit the large P_T pion data and its energy dependence exactly. Our aim in this section is to compare the model with data in some aspects, e.g. correlations among the large P_T secondaries.

According to equation (43), the inclusive cross-section of two oppositely charged outgoing particles could be defined as:

$$f(P_T, P_T') = \frac{d^6 \sigma}{(P_T' dP_T' d\phi' dy') (P_T dP_T d\phi dy)} \quad (57)$$

Here we must remember the main assumption of the model, requiring the sum of different components for the observed particle spectra, which λ was the parameter characterizing each component and also the essential content

of the thermodynamical distribution (27) which implies the production of uncorrelated particles within each value of temperature (see Chapter I). So the overall inclusive spectrum (57) for the two particles is obtained:

$$f(P_T, P_T') = \int_0^{\infty} \sigma(\lambda) f_{\lambda}(P_T') f_{\lambda}(P_T) d\lambda \quad (58)$$

Inserting equation (27) would give

$$f(P_T, P_T') = \int_0^{\infty} a(\lambda)^2 \sigma(\lambda) e^{-\lambda(P_T' + P_T)} d\lambda \quad (59)$$

It is obvious that this equation has no dependence on azimuthal direction of the two particles and in fact ignores the momentum conservation. We have derived the consequence of this effect by introducing momentum recoil which shall be seen in the fifth part of this chapter. It is seen that $f(P_T, P_T')$ is a function of $(P_T' + P_T)$. This could be checked by using an appropriate experimental measurement, but suitable data is not yet available.

In order to exhibit the presented correlations we consider the normalized correlation function as

$$Z(P_T, P_T') = \frac{f(P_T, P_T') \sigma_{inel}}{f(P_T') f(P_T)} \quad (60)$$

which in our model is given by

$$Z(P_T, P_T') = \frac{\int_0^{\infty} d\lambda \sigma(\lambda) a^2(\lambda) e^{-\lambda(P_T' + P_T)} \int_0^{\infty} \sigma(\lambda) d\lambda}{\int_0^{\infty} d\lambda \sigma(\lambda) a(\lambda) e^{-\lambda P_T'} \int_0^{\infty} d\lambda \sigma(\lambda) a(\lambda) e^{-\lambda P_T}} \quad (61)$$

To get this equation we have used equations (26), (27) and (59).

Deviation of $Z(P_T', P_T)$ from unit would show that the correlation is attractive or repulsive. These correlations would be due to the fact

that more than one value of λ is contributing, which is the basic assumption of (M.T.M.). On the contrary if we choose a single value λ_0 for λ and replace $\sigma(\lambda)$ by $\sigma_{incl} \delta(\lambda - \lambda_0)$, we would obtain

$$Z(P_T, P'_T) = \frac{a^2(\lambda_0) e^{-\lambda_0(P'_T + P_T)}}{a(\lambda_0) e^{-\lambda_0 P'_T} a(\lambda_0) e^{-\lambda_0 P_T}} \equiv 1 \quad (62)$$

which indicates absence of correlation.

However since we know that $\sigma(\lambda)$ is a positive definite number, we can show that $Z(P'_T, P_T)$ is greater than or equal to unity for $P'_T = P_T$. To see that we can deal as follows:

Any integral of equation (61) can be written as scalar product of two ket or bra vectors, i.e.

$$\int \sigma(\lambda) d\lambda f(\lambda) g(\lambda) = \langle f | g \rangle \quad (63)$$

In Chapter 2 the functions in the left side are described. If we represent the function $e^{-\lambda P_T} a(\lambda)$ as a vector $|P_T\rangle$ then equation (61) would be

$$Z(P_T, P'_T) = \frac{\langle P_T | P'_T \rangle \langle 1 | 1 \rangle}{\langle P_T | 1 \rangle \langle 1 | P'_T \rangle} \quad (64)$$

If we take $P_T = P'_T$ then

$$Z(P_T, P'_T) = \frac{\langle P_T | P_T \rangle \langle 1 | 1 \rangle}{|\langle P_T | 1 \rangle|^2} \quad (65)$$

According to inequality

$$|\langle P_T | 1 \rangle|^2 \leq \langle P_T | P_T \rangle \langle 1 | 1 \rangle \quad (66)$$

Thus we have $Z(P'_T, P_T) > 1$ for $(P'_T = P_T)$ and we expect a positive correlation at least over some range in the neighbourhood of $P_T = P'_T$. One can understand the reason for the generally positive correlation in the following way. Observation of a high P_T particle is more likely if the event is highly temperature event, this then increases the probability of a second high P_T particle.

It will be noticed that the general form (61) is not the same as the measured quantity for correlations because all of the experiments are done with a trigger of momentum $(P'_T > h)$ and there is usually no fixed momentum selected for the trigger.

To get the desired expression and comparable with experimental data we should integrate both the denominator and numerator of equation (60) over acceptance of the triggering particle and redefine the correlation

function as

$$Z_h(P_T) = \frac{\int_{P'_T=h}^{\infty} P'_T dP'_T dy' d\phi' f(P'_T, P_T) \sigma_{inel}}{\int_{P'_T=h}^{\infty} P'_T dP'_T dy' d\phi' f(P'_T) f(P_T)} \quad (67)$$

This quantity is the same as function $F(h)$ of equation (47) divided by the normal single inclusive cross-section of equation (45).

So we would end with the relation

$$Z_h(P_T) = \frac{F(h) \text{ of equation (47)}}{F(\text{normal}) \text{ of equation (45)}} \quad (68)$$

In conclusion we can quote it again that the observed positive correlation is predicted by equation (67).

As we said, the single particle data uniquely gives $\sigma(\lambda) a(\lambda)$. To test our picture against the plots displayed for the content of section one and also justify the predictions, we require $\sigma(\lambda)$ and $a(\lambda)$ to be known.

So we have to choose a model for one of them. However we could in principle determine this form $Z(P'_T, P_T)$ for any P'_T , then $Z(P'_T, P_T)$ could be predicted for any other P'_T . But unfortunately there is no such data to follow the procedure. There is a certain model introduced by Fröyland which is to be seen in the next section. Then our continuation to calculate $\sigma(\lambda)$ $a(\lambda)$ directly from equation (31), at least for this aspect shall be seen in section four of this chapter.

3.3 Fröyland's Model

It is possible to transform the usual amplitude for high energy proton-proton scattering to a form as a function of impact parameter (34). This procedure would provide one with the necessary information about the inelastic overlap function, $G(b, S)$, which gives the probability of an inelastic interaction at a given impact parameter.

$$\frac{d \sigma_{inel}}{d^2 b} = G(b, S) \tag{69}$$

By using this fact and also assuming the incoherent production of particles, Froyland (35) presented the inclusive spectra as

$$E \frac{d^3 \sigma}{dp^3} = 2\pi \int b G(b, S) E \frac{d^4 \sigma}{d^3 p db} db \tag{70}$$

Here $\frac{d^4 \sigma}{d^3 p db}$ is the inclusive distribution for fixed impact parameter b . Fitting the data gives the expression for the $G(b, s)$ of the form (27)

$$G(b, s) = P \exp\left(-\frac{b^2}{4B}\right) + P_1 b^2 \exp\left(-\frac{b^2}{4B_1}\right) \tag{71}$$

Where P, B, P_1, B_1 are parameters independent of b , but they might depend on energy (36). The useful fit of these parameters with respect to energy is shown in figure (34).

Fröyland has ignored the collective motion of particles and has assumed the Maxwell-Boltzman distribution

$$E \frac{d^4 \sigma(s)}{d^3 p db} = N(b,s) e^{-E/kT(b,s)} \quad (72)$$

Here K is the Boltzman constant ($K = 1$ in the unit $h = G = 1$), $E = P_T^2 + m^2$ is the transverse energy and $T(b,s)$ is b and s dependent temperature.

The normalization function $N(b,s)$ has been described by two different models

$$\text{I} - N(b,s) = \frac{A}{\left[(kT)^2 + m(kT) \right]} \quad (73)$$

$$\text{II} - N(b,s) = V c^2 b^2$$

We have used the second model to fit the data in this section which leads to the following linear form of inverse temperature with respect to impact parameter

$$\lambda(b,s) = \frac{1}{T(b,s)} = cb + ds^{-1/4} \quad (74)$$

So the transverse momentum distribution equivalent to equation (30) could be written as

$$\begin{aligned} f(P_T) &= \int_0^\infty 2\pi b db f_b(P_T) = \frac{2\pi}{c} \int d\lambda f_\lambda(P_T) (\lambda - ds^{-1/4}) \\ &= \frac{2\pi}{c^2} \int_0^\infty G(\lambda) N(\lambda) (\lambda - ds^{-1/4}) e^{-E\lambda} d\lambda \\ &= \frac{2\pi V}{c^2} \int_0^\infty G(\lambda) (\lambda - ds^{-1/4})^3 e^{-E\lambda} d\lambda \\ &= \int_0^\infty \sigma(\lambda) a(\lambda) e^{-E\lambda} d\lambda \quad (75) \end{aligned}$$

This gives

$$\sigma(\lambda) a(\lambda) = \frac{2\pi}{c^2} v G(\lambda) \left(\lambda - ds^{-1/4} \right)^3 \quad (76)$$

and

$$f_\lambda(P_T) = v \left(\lambda - ds^{-1/4} \right)^2 G(\lambda) e^{-E\lambda} \quad (77)$$

Then the average multiplicity for a fixed value of impact parameter would be

$$\begin{aligned} \sigma(\lambda) \langle n(\lambda) \rangle &= 2\pi \int_0^\infty f_\lambda(P_T) P_T dP_T \\ &= 2\pi G(\lambda) v \left(\lambda - ds^{-1/4} \right) \int_0^\infty P_T dP_T e^{-\lambda E} \\ &= \pi v G(\lambda) \left(\lambda - ds^{-1/4} \right) \int_{m^2}^\infty d(P_T^2 + m^2) e^{-\lambda (P_T^2 + m^2)^{1/2}} \\ &= \pi v \left(\lambda - ds^{-1/4} \right) G(\lambda) \int_m^\infty t dt e^{-\lambda t} \\ &= 2\pi v \left(\lambda - ds^{-1/4} \right) G(\lambda) \left(-\frac{d}{d\lambda} \left[\frac{e^{-m\lambda}}{\lambda} \right] \right) \\ &= 2\pi v \left(\lambda - ds^{-1/4} \right) G(\lambda) \left[\frac{1}{\lambda^2} + \frac{m}{\lambda} \right] e^{-\lambda m} \end{aligned} \quad (78)$$

To find the expression corresponding to $\sigma(\lambda)$ and $a(\lambda)$ of multi-temperature model, we need to integrate equation (69) over impact parameter. This procedure would give the form comparable to equation (26).

$$\begin{aligned} \sigma_{inel} &= 2\pi \int G(b,s) b db = \frac{2\pi}{c^2} \int G(\lambda) \left(\lambda - ds^{-1/4} \right) d\lambda \\ &= \sigma(\lambda) d\lambda \end{aligned}$$

so

$$\sigma(\lambda) = \frac{2\pi}{c^2} \left(\lambda - ds^{-1/4} \right) G(\lambda) \quad (79)$$

Inserting into equation (76) would give

$$a(\lambda) = v \left(\lambda - ds^{-1/4} \right)^2 \quad (80)$$

Taking the inelastic overlap function as its scaled form with radius

$R(s)$, (35), equation (75) for single particle inclusive spectra would be

written as

$$f(P_T) = \frac{2\pi RV^4}{c^2} \int_{\frac{ds}{R}^{-1/4}}^{\infty} \left(t - \frac{ds}{R}^{-1/4} \right)^3 e^{-Ert} \left(P e^{-\frac{R^2 t^2}{4B}} + P_1 R^2 t^2 e^{-\frac{R^2 t^2}{4B_1}} \right) dt \quad (81)$$

Here the variable λ is changed to $T = \frac{\lambda}{R}$.

Using equations (79) and (80), the two particle spectra of equation (59)

could be expressed as

$$f(P_T', P_T) = \frac{2\pi V^2 R^6}{c^2} \int_{\frac{ds}{R}^{-1/4}}^{\infty} \left(t - \frac{ds}{R}^{-1/4} \right)^5 e^{-Rt(E' + E)} G(Rt) dt \quad (82)$$

Then the momentum correlation function corresponding to equation (47)

could be described as

$$F(P, \lambda) = \frac{\frac{2\pi}{c^2} V^2 R^6 \int_{\frac{ds}{R}^{-1/4}}^{\infty} dt \left(t - \frac{ds}{R}^{-1/4} \right)^5 G(Rt) e^{-RtE} x}{\frac{2\pi}{c^2} VR^4 \int_{\frac{ds}{R}^{-1/4}}^{\infty} dt \left(t - \frac{ds}{R}^{-1/4} \right)^3 G(Rt) x \int_{P_T' = h}^{\infty} dP_T' P_T' e^{-Rt(P_T'^2 + m^2)^{1/2}} \int_{P_T' = h}^{\infty} dP_T' P_T' e^{-Rt(P_T'^2 + m^2)^{1/2}}}$$

$$= \frac{VR^2 \int_{\frac{ds}{R}^{-1/4}}^{\infty} dt \left(t - \frac{ds}{R}^{-1/4} \right)^5 G(Rt) e^{-RtE} \left(\frac{1}{R^2 t^2} + \frac{h+m}{Rt} \right) e^{-(m+h)Rt}}{\int_{\frac{ds}{R}^{-1/4}}^{\infty} dt \left(t - \frac{ds}{R}^{-1/4} \right)^3 G(Rt) \left(\frac{1}{R^2 t^2} + \frac{h+m}{Rt} \right) e^{-(m+h)Rt}} \quad (83)$$

Division of this equation to $f(P_T)$ of equation (81) represents the usual correlation function $Z_h(P_T)$ of equation (67).

The parameter C in the previous equations appears to be as a function of $(b\sqrt{s})$, but it has been chosen as a constant of order One as Fröyland (35).

Using the result of reference (36), the parameters were calculated as

$$\begin{aligned}
 R^2(s) &= 1. + 0.05 \ln s \\
 v &= .56 \\
 C &= 1. \\
 d &= 10.1 \text{ GeV}^{-1/2}
 \end{aligned}
 \tag{84}$$

Putting these values into equations (81) and (83), we have evaluated $Z_h(P_T)$ at $\sqrt{s} = 52.7 \text{ GeV}$ and $h = 3. \text{ GeV}/c$. It is plotted as a dashed curve in figure 35 and we see that the correlation effect is too small or there is no correlation at all to explain the observations. So the linear form of inverse temperature as a function of impact parameter is inconsistent with experimental results.

3.4 General Treatment

As we predicted the (M.T.M.) can fit the two particle inclusive data. Our aim in this section is to evaluate $Z_h(P_T)$ of equation (67). Here we will present a particular parametrized for $a(\lambda)$ which is quite satisfactory to show the plausible correlations. The momentum conservation will be excluded until the next section and so we shall "average" the same/opposite correlations. To start with, we can calculate $\sigma(\lambda) a(\lambda)$ from equation (31), which is the inverse laplace transform of $f(P_T)$.

$$\sigma(\lambda) a(\lambda) = \frac{1}{2\pi i} \int_{C-i\infty}^{C+i\infty} f(P_T) e^{\lambda P_T} dP_T \tag{85}$$

Our prediction and its consequence is consistent with $\sigma(\lambda)$ $a(\lambda)$ tends to zero as $\lambda \rightarrow \infty$. Considering this fact the contour in equation (85) has been chosen to go along the imaginary axis. So the two particle momentum spectra of equation (59) could be expressed

$$f(P_T, P_T') = \int_0^\infty d\lambda a(\lambda) e^{-\lambda(P_T' + P_T)} \int_{-i\infty}^{i\infty} \frac{dq}{2\pi i} f(q) e^{\lambda q} \quad (86)$$

For P_T and P_T' positive we could reverse the orders of integration to obtain

$$f(P_T, P_T') = \int_{-i\infty}^{i\infty} \frac{dq}{2\pi i} f(q) \int_0^\infty d\lambda a(\lambda) e^{-\lambda(P_T' + P_T - q)} \quad (87)$$

Here we would parametrize $a(\lambda)$ as a polynomial of degree $n > 1$ with $a_0 = 0$

$$a(\lambda) = \sum_1^n a_n \lambda^n \quad (88)$$

Then

$$\begin{aligned} f(P_T, P_T') &= \int_{-i\infty}^{i\infty} \frac{dq}{2\pi i} f(q) \sum_1^n \int_0^\infty d\lambda a_n \lambda^n e^{-\lambda(P_T' + P_T - q)} \\ &= \int_{-i\infty}^{i\infty} \frac{dq}{2\pi i} dq \sum_1^n \frac{a_n n!}{(P_T' + P_T - q)^{n+1}} \\ &= \sum_1^n (-1)^n a_n \frac{n!}{2\pi i} \int_{-i\infty}^{i\infty} \frac{f(q)}{(q - P_T' - P_T)^{n+1}} dq \quad (89) \end{aligned}$$

Using Cauchy's integral formula we can get a simple relation between

$f(P_T', P_T)$ and n th order derivatives $f^{(n)}$ of the two particle inclusive cross-section as

$$f(P_T', P_T) = \sum_1^n (-1)^n a_n f^{(n)}(P_T' + P_T) \quad (90)$$

To evaluate $Z_h(P_T)$ of equation (62) we need also

$$\int_h^\infty P_T' dP_T' f(P_T', P_T) = \sum a_n (-1)^{n-1} \left[h f^{(n-1)}(h+P_T) - f^{(n-2)}(h+P_T) \right] \quad (91)$$

and

$$\begin{aligned} \int_h^\infty P_T' dP_T' f(P_T') &= P_T' f^{(-1)}(h) - \int_h^\infty f^{(-1)}(P_T') dP_T' = \\ &= P_T' f^{(-1)}(h) - f^{(-2)}(h) \end{aligned} \quad (92)$$

Here we have used the relation

$$f^{(-1)}(h) = - \int_h^\infty dP_T' f(P_T') \quad (93)$$

Inserting equations (91) and (92) into equation (62) we can get

$$Z_h(P_T) = \frac{\sigma^{inel} \sum_n a_n (-1)^n \left[h f^{(n-1)}(h+P_T) - f^{(n-2)}(h+P_T) \right]}{f(P_T) \left[h f^{(-1)}(h) - f^{(-2)}(h) \right]} \quad (94)$$

We shall take use of Vanryckeghem (20) fit, i.e. $f(P_T) = A e^{-k(P_T^2 + v^2)^{1/4}}$, to the single particle spectra as before. Then some simple approximation would give

$$f^{(n)}(h) = \left[\frac{-k}{2^4 \sqrt{h^2 + v^2}} \right]^n f(h) \quad (95)$$

To evaluate $Z_h(P_T)$, we insert equation (95) into equation (94), then

$$Z_h(P_T) = \frac{\sigma^{\text{inel}}}{A} \sum_n a_n \left(\frac{K}{2^4 \sqrt{(h+P_T)^2 + v^2}} \right)^n \left(\frac{(h+P_T)^2 + v^2}{h^2 + v^2} \right)^{1/4} \\ \times \exp \left\{ K \left[4\sqrt{h^2 + v^2} + 4\sqrt{P_T^2 + v^2} - 4\sqrt{(h+P_T)^2 + v^2} \right] \right\} \quad (96)$$

This form can be simplified still further if we try a fit involving only one non-zero value a_n . Then the cross-section constraint can easily be incorporated. First we use equations (31) and (32) to write

$$A e^{-K\sqrt{P_T^2 + v^2}} = \int_0^\infty \sigma(\lambda) a(\lambda) e^{-\lambda P_T} d\lambda \\ = \int_0^\infty \sigma(\lambda) a_n \lambda^n e^{-\lambda P_T} d\lambda \quad (97)$$

The assumption $a_n \lambda^n = a(\lambda)$ is used to derive this form. We multiply both sides by P_T^{n-1} and integrate from zero to infinity, thereby obtaining

$$A \int_0^\infty P_T^{n-1} e^{-K\sqrt{P_T^2 + v^2}} dP_T = a_n \int_0^\infty \lambda^n a(\lambda) d\lambda \int_0^\infty e^{-\lambda P_T} P_T^{n-1} dP_T \\ = a_n \int (n-1)! \sigma(\lambda) d\lambda = a_n (n-1)! \sigma^{\text{inel}} \quad (98)$$

or

$$\frac{a_n \sigma^{\text{inel}}}{A} = \frac{1}{(n-1)!} \int_0^\infty P_T^{n-1} e^{-K\sqrt{P_T^2 + v^2}} dP_T \quad (99)$$

Inserting into equation (96) would give our final expression for correlation function $Z_h(P_T)$ as

$$\begin{aligned}
 Z_h(P_T) &= \frac{1}{(n-1)!} \left(\frac{K}{2\sqrt{(h+P_T)^2 + v^2}} \right) \left(\frac{(h+P_T)^2 + v^2}{h^2 + v^2} \right)^{1/4} \\
 &\times e^{K \left[\sqrt{(h^2 + v^2)} + \sqrt{P_T^2 + v^2} - \sqrt{(h+P_T)^2 + v^2} \right]} \\
 &\times \int_0^\infty P_T^{n-1} e^{-K\sqrt{P_T^2 + v^2}} dP_T \quad (100)
 \end{aligned}$$

This form has one free parameter, n . It can be an integer or non-integer. We expect no difference for both cases. For even values of n the integral can be evaluated easily. As an example if we consider the case when n equal 2., we would get a constant average multiplicity (e.g. see equation (28)). The procedure for this would be

$$\frac{a_n \sigma_{inel}}{A} = \int_0^\infty P_T dP_T e^{-K\sqrt{P_T^2 + v^2}} = \int_{\sqrt{v}}^\infty y^3 dy e^{-ky}$$

Here we have introduced y according to

$$P_T^2 + v^2 = y^4$$

So we can obtain

$$\begin{aligned}
 a(\lambda) &= a_2 \lambda^2 = \frac{A \lambda^2}{\sigma_{inel}} \left[\frac{3}{K^4} + \frac{3\sqrt{v}}{K^3} + \frac{3v}{2K^2} + \frac{v^{3/2}}{2K} \right] \\
 &= \frac{A \lambda^2 G(K, \lambda)}{\sigma_{inel}} \quad (101)
 \end{aligned}$$

Inserting into equation (28) would give

$$\bar{n}(\lambda) = \frac{a(\lambda)}{\lambda^2} = \frac{AG(k,v)}{\sigma_{inel}} = \text{constant} \quad (102)$$

Then

$$z_h(P_T) = \left[\frac{3}{K^2} + \frac{3\sqrt{v}}{K} + \frac{3v}{2} + \frac{kv^{3/2}}{2} \right] \frac{1}{4 \sqrt{(h^2 + v^2) ((h + P_T)^2 + v^2)}} \quad (103)$$

$$e^K \left[4\sqrt{h^2 + v^2} + 4\sqrt{P_T^2 + v^2} - 4\sqrt{(h + P_T)^2 + v^2} - 4\sqrt{v^2} \right]$$

This is plotted in figure 35 and also to see the difference made by changing the form of $a(\lambda)$, we have also calculated equation (100) with other values of n . The plot with $n = 2.5$ seems to give a reasonable fit to the data. Of course we have not taken into account the momentum conservation effect in this calculation yet. In the following section we will show the most detailed fits, using the recoil effect in our calculation.

3.5 Momentum Conservation Effect

In the previous sections we discussed the observed azimuthal distributions indicating a strong peak at $\phi = 180^\circ$ from the trigger and also presented some data, supporting a strong momentum correlation for the away side movers than the same side movers as triggering particle. These features are mostly due to momentum recoil effect which has not been included in the M.T.M's. calculations yet. Our final attempt to complete the model and obtain a good comparison of equation (100) with the data is proceeded as follows.

According to the definition of the thermodynamical model (see Chapter 1) and also improvements done to it (M.T.M.), when two protons collide they liberate all their energy in a volume V and form a compound system of mass m in their own centre of mass system. The system endures certain dynamic and subsequent expansions. The production of particles takes place at various temperatures. At an explicit and probably higher temperature we expect at least a pion with negligible longitudinal motion to trigger the apparatus. The rest of the system will be a cluster of mass M_C . The transverse motion of this cluster must balance the large P_T of emitted trigger. In the rest frame of the system the momentum four vectors could be defined as

$$P'_T = \left[(m^2 + P_T'^2)^{1/2}, 0, 0, P'_T \right] \quad (104)$$

$$P_C = \left[(M_C^2 + P_T'^2)^{1/2}, 0, 0, -P'_T \right] \quad (105)$$

To explain the double inclusive form (43) we would also have the second pion to emerge with momentum four factor

$$P_\pi = \left[(m_\pi^2 + P_T^2)^{1/2}, 0, 0, P_T \right] \quad (106)$$

Now consider a Lorentz transformation of the c.m.s. and the laboratory system. So the last two momentum four vectors could be expressed in the lab system as

$$P_C = \left[M_C, 0, 0, 0 \right] \quad (107)$$

$$P_{\pi_2} = \left[(m_\pi^2 + P_{T_2}^2)^{1/2}, 0, 0, P_{T_2} \right] \quad (108)$$

According to the definition, the scalar product of momentum four vectors is invariant under the transformation, so we can stress

$$(M_C^2 + P_T'^2)^{1/2} (m_\pi^2 + P_T^2) \pm P_T' P_T = M_C (m_\pi^2 + P_{T_2}^2)^{1/2} \quad (109)$$

We can ignore the pions mass to rewrite it

$$P_T \left[(M_C^2 + P_T'^2)^{1/2} \pm P_T' \right] = M_C P_{T_2}$$

or

$$P_{T_2} = \frac{P_T}{M_C} \left[(M_C^2 + P_T'^2)^{1/2} \pm P_T' \right] \quad (110)$$

Experiments always take $P_T' = h = 3. \text{ GeV}/c$. If we expect $M_C \gg h$, which we do, the expansion of the content of the bracket in equation (110) would result

$$P_{T_2} = P_T \left[1 \pm \frac{P_T' = h}{M_C} \right] \quad (111)$$

The \pm signs are respectively for the same and away side movers.

Putting $(h + P_{T_2}) = \left\{ h + P_T \left[1 \pm \frac{h}{M_C} \right] \right\}$ instead of $(h + P_T)$ in equation (100) we can get our final expression for the same side and away side correlation functions $Z_h(P_T)$ as:

$$\begin{aligned} Z_h(P_T) &= \frac{1}{\Gamma(n)} \left(\frac{K}{2 \sqrt{(h + P_{T_2})^2 + v^2}} \right) \left(\frac{(h + P_{T_2})^2 + v^2}{h^2 + v^2} \right)^{1/4} \\ &\times e^{K \left[4\sqrt{h^2 + v^2} + 4\sqrt{P_T^2 + v^2} - 4\sqrt{(h + P_{T_2})^2 + v^2} \right]} \\ &\times \int_0^\infty P_T^{n-1} e^{-K \sqrt{P_T^2 + v^2}} dP_T \quad (112) \end{aligned}$$

Here as we said, the parameter n can be an integer or non-integer number and $\Gamma(n)$ is the usual gamma function for the case n being a real number.

We have taken the maximum value of \sqrt{s} to M_C and calculated equation (112) for three values of $n = 2, 2.5, 3$. These plots are displayed in

figures 36, 37 and 38. It seems that the case $n = 2.5$ is much more plausible and the recoil effect is much more acceptable. Of course the whole centre of mass energy cannot be taken away by the recoil system. To check this fact we have used $M_C = (.2 - .4 - .6 - .8)\sqrt{s}$. The result with $M_C = .8\sqrt{s}$ gives the best fit which is seen in figure 36. So as a general summary of the results we can confirm the fact that the M.T.M. does give a reasonably good description of the correlations and the variations between the towards side and away side.

3.6 Charged particles multiplicity associated with the large P_T particle

There is evidence shown in figure 16 that the peak centred at $\phi = 180^\circ$ of azimuthal dependence of the mean charged multiplicity $\langle n \rangle$ becomes much more pronounced at large P_T values of trigger particle. To clarify this fact we have represented the P_T variation of $\langle n \rangle$ in three different azimuthal regions for three different triggers (π^+ , k^- , p) in figure 40. There is also the s dependence of $\langle n \rangle$ displayed in figure 41 at $P_T = 1$ GeV/C and $P_T = 2.5$ GeV/C for triggers (π, p, \bar{p}). As the result of this picture (37) an approximate linear P_T and $\ln(s)$ parametrization has been suggested to fit the data.

$$\begin{aligned} \langle n(s, P_T) \rangle &= A + B P_T + C \ln(s) \\ &= A' + B (P_T - 1) + C \ln (s/s_0) \end{aligned} \quad (113)$$

with $\sqrt{s_0} = 44.7$ GeV

The measured average multiplicity seems to depend on the quantum numbers of the triggers, i.e. the parameters A', B, C have the following relations:

A' is ϕ dependent and $A'(P) > A'(\bar{P}) \approx A'(K^-) > A'(k^+) = A'(\pi^\pm)$

B is ϕ (very small) dependent and $B(\bar{P}) > B(P) \approx B(K^-) > B(k^+) = B(\pi^\pm)$

As ϕ increases, there is a tendency for $C(\bar{P})$ to increase, for $C(P)$ to remain constant and for $C(\pi)$ and $C(K)$ to decrease.

To explain some features of this data we can define the average multiplicity of pion type P_T accompanied by the trigger pion of type P'_T

by

$$\langle n(R) \rangle_{P'_T} = \frac{\int_R f(P_T, P'_T) P_T dP_T d\phi dy}{f(P'_T)} \quad (114)$$

where R represents a region of P_T, y, ϕ which in practice shall be the acceptance region of the apparatus.

Using equation (90) we can write this as

$$\langle n(R) \rangle_{P'_T} = \frac{\sum_n (-1)^n a_n \int_R f^{(n)}(P_T + P'_T) P_T dP_T dy d\phi}{f(P'_T)} \quad (115)$$

Suppose the apparatus measures all particles with a certain region of ϕ, y with $P_T > P$ then equation (115) becomes

$$\begin{aligned} \langle n(>P_T) \rangle_{P'_T} &= \frac{\sum_n (-1)^{n-1} a_n \left[P_T^{(n-1)}(P_T + P'_T) - f^{(n-2)}(P_T + P'_T) \right]}{f(P'_T)} \\ &= \frac{\sum_n a_n \left[P_T \left(\frac{K}{2\sqrt{(P_T + P'_T)^2 + v^2}} \right)^{n-1} + \left(\frac{K}{2\sqrt{(P_T + P'_T)^2 + v^2}} \right)^{n-2} \right]}{e^K \left\{ \left[(P_T + P'_T)^2 + v^2 \right]^{1/4} - (P_T^2 + v^2)^{1/4} \right\}} \end{aligned} \quad (116)$$

This is a complicated expression and comparison with experiment requires care. Especially the range for P is a very fundamental important necessity. For example if we take the case with $P_T = 0$, we cannot include the effect of momentum conservation and again we must accept the average of

the same/opposite distributions; so equation (116) would be:

$$\langle n(>0) \rangle_{P'_T} = a_n \left(\frac{K}{2^4 \sqrt{P'^2_T + v^2}} \right)^{n-2} \quad (117)$$

If we take the case with $n = 2$, then

$$\langle n(>0) \rangle_{P'_T} = a_2 = \frac{A}{\sigma_{inel}} \left(\frac{3}{K^4} + \frac{3\sqrt{v}}{K^3} + \frac{3v}{2K^2} + \frac{v^{3/2}}{2K} \right) \quad (118)$$

which is just energy dependent and cannot fit the data. Here we have used equation (101).

For the case $n = 2.5$ which produces the best fit for the correlation function

$$\langle n(>0) \rangle_{P'_T} = \frac{A}{\sigma_{inel}} \int_0^\infty P_T^{1.5} dP_T e^{-K^4 \sqrt{P_T^2 + v^2}} \times \left(\frac{K}{2^4 \sqrt{P_T^2 + v^2}} \right)^{1.5} \quad (119)$$

which might increase with respect to energy but unfortunately it decreases with P'_T of the trigger and cannot agree with the data.

As a general comment if P is such that

$$\frac{P_T K}{\left((P_T + P'_T)^2 + v^2 \right)^{1/4}} \gg 1 \quad (120)$$

Then for two different triggers P'_T value, we can have (for $n = 2.5$)

$$\frac{\langle n(>P_T) \rangle_{P'_{T1}}}{\langle n(>P_T) \rangle_{P'_{T2}}} = \left(\frac{P'_{T2} + P_T}{P'_{T1} + P_T} \right)^{3/4} \frac{e^{K \left[(P_T + P'_{T2})^{1/2} - P'_{T2} \right]}}{e^{K \left[(P_T + P'_{T1})^{1/2} - P'_{T1} \right]}} \quad (121)$$

For P'_{T2} fixed, this expression decreases with P'_{T1} for small P_T ($< .5$ GeV/C) and increases with P'_{T1} for large P_T ($P_T \geq .5$)

CHAPTER IV

PRODUCTION OF MASSIVE PARTICLES AND PHENOMENOLOGY OF m_T UNIVERSALITY

4.1 The Universality of m_T

Following the observation of production of ψ and other massive particles there has been a great deal of interest in the mechanism for production. Many models use a single, "hard", collision between constituents to produce the ψ 's, in which case the rate depends upon a coupling constant. However it is of interest to see whether the multi-temperature thermodynamical model can be applied to these processes. A crucial feature of all such models is that particle production rates are determined by the particle energy, or, since we work at $y \approx 0$, by the transverse mass $m_T = (m^2 + p_T^2)^{1/2}$. As we shall see this feature is well supported by the data, in particular it explains the observed suppression of production of heavy particles. A theoretical reason for m_T dependence of production rate would be as follows.

The inclusive production cross-section of a hadronic system C in reaction $a + b \rightarrow c + \text{anything}$ is a function of three invariants named s, t and u, and can be described by a covariant amplitude as

$$F_{ab}^C(s, t, u) = E_c \frac{d^3 \sigma_{ab}^c}{d^3 p_c} \quad (122)$$

where $s = (P_a \cdot P_b)$, $t = (P_a \cdot P_c)$, $u = (P_b \cdot P_c)$; P_a, P_b, P_c are the four momentum of a, b and c and $E_c = P_c^0$.

These invariants could be replaced by a set of defined variables:

$$\begin{aligned} m_T &= (P_{cT}^2 + m_c^2)^{1/2} \\ x_T &= m_T / \sqrt{s} \\ x_L &= \frac{P_{cZ}}{\sqrt{s}} \end{aligned} \quad (123)$$

If we consider only frames which differ from ab centre of mass system by a boost along the transverse (T) direction to the beam. As we said in the previous chapter, the majority of experiments are done in the central rapidity region, i.e. $X_L = 0$, which dominates the production multiplicities at higher energies. This fact is true not just for light particles, but also is true for massive particles productions. So if one accepts the dominant central region of whole particle production and takes the quoted 3 invariants large enough, then we could find the relation:

$$\frac{ut}{s} \approx m_T^2 \quad (124)$$

This gives the universality hypothesis, i.e. the inclusive cross-section of equation (122) depends on m_T rather than m and P_T of produced particles separately. Accepting the naive thermodynamical model (see Chapter 1). This statement would be supported by Plank's formula of equation (5), i.e.

$$E \frac{d^3\sigma}{d^3p} \approx g e^{-\frac{1}{T} \sqrt{m^2 + P_T^2}} \approx g e^{-m_T/T} \quad (125)$$

For a single production of massive particle m with ordinary spin J_M and Isospin I_M the factor g is given by

$$g = (2I_M + 1) (2J_M + 1) \quad (126)$$

If we generalize equation (125) to the multi-temperature model then the corresponding assumption would be that a universal function of m_T should fit the P_T , m and s dependence of production of all particles. A possible form for this is that given by Vanryckeghem(20) which is designed to fit the data for light particles and which we have used earlier, namely:

$$E \frac{d^3\sigma}{dp^3} \approx A e^{-K\sqrt{m^2 + P_T^2 + v^2}} = A e^{-K\sqrt{m_T^2 + v^2}} = f(m_T) \quad (127)$$

Note that we ignore the small variation of k and v with the type of produced particle which is a "non-thermodynamical" effect. If full thermodynamical equilibrium were not attained in high energy collisions another reason for smallness of production rates for high mass particles could be Zweig rule. This nonachievement of thermal equilibrium might be from the collision time which is expected to be very short. If we express all these dynamical factors together with factor g of equation (126) within a factor λ the exact inclusive production cross-section should be

$$E \frac{d^3\sigma}{dp^3} = \lambda f(m_T) \quad (128)$$

We would discuss the validity of the factor (λ) later in this section, but it has turned out to be equal to 1 (38,39). This indicates that such dynamical factors are either absent or surprisingly close to unity. So at this stage we would take $\lambda = 1$ to continue our discussion.

Taking the P_T dependence of π , ρ , ϕ and ψ from references 40, 41 and 42; and using equation (123) Michael (38) has demonstrated the m_T dependence of inclusive cross-section which is displayed in figure 42. Here the curves for ρ , ϕ and ψ are normalized to $\frac{d\sigma}{dy} = 2 \text{ mb}$, 0.1 mb and $0.1 \mu\text{b}$ respectively.

We have compared equation (128) with this data for ρ and ψ particles at $P_{\text{Lab}} = 200 \text{ GeV}/c$ (corresponding to $\sqrt{s} = 20 \text{ GeV}$) in figures 43, 44. Qualitative agreement of data and multi-temperature prediction is obvious. By this consideration it is clear that taking λ equal to unity is the best feature. It suggests the approach to the thermodynamical equilibrium before the observed hadrons are emitted. This confirms the fact that the

small production rate of massive particles is mainly due to the large value of m_T and related to the rapid exponential decrease of $f(m_T)$ versus m_T . One can realize that even if we include the factor g of equation (126) the production will not be large enough to describe the possible dynamical factors as Zweig's suppression factor. However the parameter A of equation (127) seems to be taken too large. If we expect the thermodynamical model to explain directly emitted particles and ignore the contribution of resonance decay outside the interaction region, A might be smaller. This would provide the inclusion of some factors as g into equation (128). Having accepted m_T universality one can predict the increase of σ with energy for a fixed (large mass) from the consequence of corresponding behaviour of π -meson cross-section at fixed (large P_T). This can be calculated as

$$\int_0^{\sqrt{s}/2} P_T dP_T E_C \frac{d^3\sigma}{dp^3} = \int_0^{\sqrt{s}/2} P_T dP_T E_\pi \frac{d^3\sigma_\pi}{dp^3} \quad (129)$$

So we can guess the same energy dependence for pions and massive particles. This is well supported by experimental measurements. For comparison see figure (44). Comparison of data with equation (129) is displayed in figure 45 for various particles.

Integrating the MTM expression (i.e. equation (127)) over P_T one can also show the energy dependence of production cross-section. For particle of mass m and per unit of rapidity the result would be (43)

$$\frac{d\sigma}{dy} = 2\pi A G(k, a) \quad (130)$$

where

$$G(k, a) = \dots \left(\frac{\sqrt{a}}{k} + \frac{3a}{k^2} + \frac{6\sqrt{a}}{k^3} + \frac{6}{k^4} \right) \quad (131)$$

and

$$a = (m_C^2 + v^2)^{1/2} \quad (132)$$

Reasonable approximation would give

$$\left. \frac{d\sigma}{dy} \right|_{y=0} \approx \frac{4\pi A m^{3/2}}{K} \exp(-k\sqrt{m}) \quad (133)$$

We have displayed the comparison of this formula with data in figure 46 for ψ (3.1). Except the low energy region the formula can fit the data very well. Doing the same calculation for ψ' (3.7) would give

$$\begin{aligned} \left. \frac{d\sigma_{\psi'}}{dy} \right|_{y=0} &\approx 0.027 \mu\text{b} (= .0036 \mu\text{b exp}) \text{ at } \sqrt{s} = 19 \text{ GeV} \\ &\approx 0.05 \mu\text{b} (= .03 \mu\text{b exp}) \text{ at } \sqrt{s} = 30 \text{ GeV} \\ &\approx 0.218 \mu\text{b} \text{ at } \sqrt{s} = 63 \text{ GeV} . \end{aligned} \quad (134)$$

which are slightly higher than observed values. But the difference is decreasing by increasing of energy. We do not have data for considerably higher ISR energies and those who are measured indicates large errors. Roughly saying we hope the model to fit any accurate data.

4.2 Michael's Model

In this section we want to consider an alternative approach due to Michael to the apparent m_T universality discussed in the previous section. This begins by postulating that the rise of large P_T pion data with energy is due to the necessity of having to satisfy momentum conservation. Thus when one large P_T particle is observed the other particles must have, on average, a higher P_T than in a usual event. Due to the suppression of high P_T this then further reduces the large P_T cross-section. The reduction factor increases to unity as the energy increases, because then the recoil momentum can be shared among a large number of

particles. Hence the rise of large P_T pion data with energy is explained.

Note that if this picture is valid, then there should not be a corresponding effect for large m , small P_T , particles, so observed universality would be an accident. Indeed the large m cross-section should be independent of energy and should be compared to the large P_T cross-section at infinite energy. For fixed m_T this would then require a significant (Zweig-rule) suppression for ψ , etc. (i.e. the factor λ would be $\ll 1$). It is possible to argue with the above picture on the grounds that 'thermodynamics' should apply in the centre-of-mass system of the decaying 'fireball' rather than in the centre-of-mass of the original collision. In this case the above recoil suppression effect should not occur. As we shall see below the data suggests that the large m processes have the same energy dependence as large P_T (at fixed m_T), so they confirm that Michael's model is incorrect.

An independent emission type of model is a possible mechanism to explain the idea. Here each cluster decays isotropically into pions having the Gaussian distribution for the transverse momentum. The general case of Gaussian class of models define (46)

$$\frac{1}{\sigma_n} \frac{d\sigma_n}{dq_{T_1} \dots dq_{T_n}} = \exp \left[-A(q_{T_1} \dots q_{T_n}) \right] \delta(\sum q_{Ti}) \quad (135)$$

Expanding this in a Taylor series about $q_{T_i} = 0$, keeping only the lowest order term and insisting on rotational and parity invariance would give the ansatz

$$\frac{1}{\sigma_n} \frac{d\sigma_n}{dq_{T_1} \dots dq_{T_n}} = C \exp \left(- \sum_{i,j=1}^n M_{ij} q_{T_i} q_{T_j} \right) \delta(\sum q_{T_i}) \quad (136)$$

where M is a real symmetric matrix and c is a normalization constant.

It is a simple consequence of equation (136) that the transverse momentum distribution of any one of n particles has a Gaussian form (45)

$$f(q_T) = \exp(-\beta q_T^2) \quad (137)$$

Here we have

$$\beta^{-1} = \langle p_T^2 \rangle \quad (138)$$

In large P_T events if we consider the P_T of the trigger to be shared equally among the other particles, the transverse momentum of the balancing particles shall be changed from q_{T_i} to

$$q_T = P_T / \langle n \rangle \quad (139)$$

Inserting this into equation (137) we would have the expression

$$e^{-\beta \sum_i (q_{T_i} - P_T / \langle n \rangle)^2} = e^{-\beta \sum_i q_{T_i}^2 - \beta \sum P_T / \langle n \rangle} \quad (140)$$

instead $e^{-\beta \sum_i q_{T_i}^2}$ in matrix element of equation (136)

To get the form (140) the momentum constraint $\sum_i q_{T_i} = 0$ has been used. So having a large P_T particle would require a momentum suppression

$$MS = e^{-\beta \sum P_T^2 / \langle n \rangle} \quad (141)$$

It is obvious that the large P_T particle with energy E would reduce the energy available for other particles to

$$Q^2 = (\sqrt{s} - E)^2 - q_T^2 \quad (142)$$

Using this the full suppression factor coming from energy and momentum

conservation (46) would be

$$D(Q^2, q_T) = \left(\frac{Q^2}{s}\right)^{g^2-1} \frac{\ln s}{\ln Q^2} \exp \left[-\frac{P_T^2}{\langle n \rangle \langle P_T^2 \rangle} \right] \quad (143)$$

Taking an asymptotic P_T distribution of single particle spectra, Michael has included this suppression factor which gives reasonable fit to the large P_T pion data. For production of a particle of momentum q^μ this spectra is

$$\frac{1}{\sigma} E \frac{d^3\sigma}{dq^3} = g^2 f(q_T) D(Q^2, q_T) \quad (144)$$

As we said asymptotically the factor D in equation (144) tends to 1, (Figure 4) and the single particle spectra is given by $f(q_T)$ with a rapidity density of g^2 . The parameter g^2 is related to the average multiplicity as

$$\langle n \rangle = g^2 \ln \langle n \rangle \quad (146)$$

Because of substantial rise of inclusive spectra from ISR to asymptotic energies a flatter P_T dependence for $f(q_T)$ is chosen (46), i.e.

$$f(q_T) = \frac{1}{\pi a^2} \left(1 + \frac{q_T^2}{a^2}\right)^{-2} \quad (146)$$

Inserting this into equation (144) and taking

$$\begin{aligned} \langle n \rangle &= -3.8 + 1.88 \ln s + \frac{1}{\sqrt{s}} \\ \frac{1}{a^2} &= 13 \text{ GeV}^2 \\ g^2 &= 2.3 \\ \sigma_{\text{tot}} &= 40 \text{ mb} \end{aligned} \quad (147)$$

We have repeated Michael's (46) calculation of pion spectra and compared

it with MTM fit to the data. There is a very good agreement of two distributions both for small and large P_T region. The result of suppression factor $D(Q^2, q_T)$ calculated from equation (143) is displayed in figure 47. The curves are the distributions of $D(Q^2, q_T)$ with respect to energy for different fixed q_T 's. The agreement with data is quite satisfactory.

To explain the m_T universality and production of massive particles a dependence on the type of the produced particle is suggested. The author expects the form

$$\left. \frac{d\sigma}{dy dP_T^2} \right|_{y=0} \sim \sigma_{TOT}^2 (cp) f(m_T) \quad (148)$$

for inclusive spectra of pp scattering at asymptotic energies. Here $\sigma_{TOT}^2 (cp)$ gives an asymptotic reduction in production cross-section of particles at different quark content.

Inserting $m_T^2 = m^2 + q_T^2$ instead of q_T^2 in equation (144) we have repeated the calculation for ψ as pion. The factor $\sigma_{TOT}^2 (cp)$ turns out to be approximately 65 in order to produce equal cross-section for pion and ψ at fixed $m_T = 3.1$ GeV. Unfortunately this model does not show the rise of cross-section for massive particles, e.g. ψ , at existing energies. The inclusive ψ production cross-section is illustrated in figure 48 for two ISR energies, $\sqrt{s} = 23$ GeV, $\sqrt{s} = 63$ GeV. There is no increase of the spectra at small q_T 's at all, which is the reason why the model is not adequate.

4.3 Effect of correlation on production of heavy particles

In Chapter 3 we saw how the multi-temperature description of large P_T pion production automatically gave positive correlation for production

of two large P_T particles and that the predicted correlation agreed well with the data. If our explanation of this correlation and of m_T universality have any claim to reality then the same type of correlation should be observed among production of two large mass particles. Here we calculate the effect of this correlation on production of two heavy particles by using MTM. A crucial result of this procedure is that the correlations are calculable versus the particles mass. For production of two heavy particles one might suggest that the probability of obtaining particles 1 and 2 together can be explained by the product of the probabilities of obtaining them separately, i.e.

$$\frac{1}{\sigma_{inel}} E_1 E_2 \frac{d^6\sigma}{d^3P_1 d^3P_2} = \lambda_1 \lambda_2 \frac{f(m_{T1}) f(m_{T2})}{\sigma_{inel} \sigma_{inel}} \quad (149)$$

This equation ignores any sort of correlation among the products. It has been used by Fratschi (39) to describe the two heavy particles production by applying the pure thermodynamical model. To explain the small production rates of massive particles the Zweig's suppression factor and some other dynamical factors have been taken into account. To get this equation, equations (128) and (123) have been used. As we know this equation is not true for production of large P_T pions, where there are substantial momentum correlations. Our aim in this section is to show the strength of this correlation. Again here we have difficulty with factor λ of equation (128), which must be obtained from data as explained before. It would be cancelled in the correlation effect otherwise we shall take it equal to 1. Using the definitions of chapter 3, the cross-section for producing particles 1 and 2 is

$$\frac{d^2 \sigma^{(1,2)}}{dy_1 dy_2} = (2\pi)^2 \int_{P_{T_1}} dP_{T_1} \int_{P_{T_2}} dP_{T_2} f(m_{T_1}, m_{T_2}) \quad (150)$$

here $f(m_{T_1}, m_{T_2})$ is the inclusive cross-section for producing a particle of momentum P_{T_1} and mass m_1 together with a particle of momentum P_{T_2} and mass m_2 . It is given by

$$f(m_{T_1}, m_{T_2}) = \frac{f(m_{T_1}) f(m_{T_2})}{\sigma_{inel}} \quad (151)$$

when correlations are ignored as in the work of Fratschi, Hammer (39) and MTM predicts instead.

$$f(m_{T_1}, m_{T_2}) = a_n f^{(n)}(m_{T_1}, m_{T_2}) = \frac{AG(k, v)}{\sigma_{inel}} f^{(n)}(m_{T_1} + m_{T_2}) \quad (152)$$

To get this relation we have used equations (90) and (99), where

$$f^{(n)}(z) = \frac{d^n f(z)}{dz^n} = \left(\frac{-k}{2^4 \sqrt{z^2 + v^2}} \right)^n f(z) \Big|_{z=m_{T_1} + m_{T_2}} \quad (153)$$

Using equations (150) and (151) the uncorrelated two particles cross-section would be:

$$\begin{aligned} \frac{d^2 \sigma_{uncorr}^{(1,2)}}{dy_1 dy_2} &= \frac{(2\pi)^2 A^2}{\sigma_{inel}} G(km_1) G(km_2) \\ &= \frac{1}{\sigma_{inel}} \left(\frac{d\sigma^1}{dy_1} \right) \left(\frac{d\sigma^2}{dy_2} \right) \end{aligned} \quad (154)$$

where

$$\begin{aligned} G(km_i) &= \int_{P_{T_i}} dP_{T_i} f(m_{T_i}) = \int_{m_i}^{m_{T_i}} dm_{T_i} f(m_{T_i}) \\ &= m_i f^{(-1)}(m_i) - f^{(-2)}(m_i) \\ &\approx m_i \frac{2\sqrt{m_i}}{k} f(m_i) \end{aligned} \quad (155)$$

For the case $n = 2$, inserting equations (162) and (153) into equation (150) the correlated two particle cross-section is:

$$\begin{aligned} \frac{d^2\sigma_{\text{corr}}^{(1,2)}}{dy_1 dy_2} &= \frac{(2\pi)^2 A G(\kappa, \nu)}{\sigma_{\text{inel}}} \int_0^\infty P_{T_1} dP_{T_1} \int_0^\infty P_{T_2} dP_{T_2} \frac{d^2 f(z)}{dz^2} \\ &= \frac{(2\pi)^2 A^2 G(\kappa, \nu)}{\sigma_{\text{inel}}} m_1 m_2 \exp \left[-k (m_1 + m_2)^{1/2} \right] \end{aligned} \quad (156)$$

Comparison of equations (154) and (156) gives:

$$\begin{aligned} \frac{d^2\sigma_{\text{corr}}^{(1,2)}}{dy_1 dy_2} &= \frac{1}{2} k \sqrt{\nu} \left(\frac{\nu^2}{m_1 m_2} \right)^{1/2} \exp \left[-K (m_1 + m_2)^{1/2} \right. \\ &\quad \left. - m_1^{1/2} - m_2^{1/2} + \nu^{1/2} \right] \frac{d^2\sigma_{\text{uncorr}}^{(1,2)}}{dy_1 dy_2} \end{aligned} \quad (157)$$

Equations (154) and (157) lead to the cross-section for $\psi\psi$, $\psi\psi'$, $\psi'\psi'$, DD^- and ψDD^- given in table 3. There is large correlation effect increasing by the mass of doubly produced particles which is not obtained on the pure thermodynamical model. As we said, we predict the thermodynamic equilibrium to reach i.e. $\lambda = 1$. Of course this is not a very encouraging prediction since it limits the amount of measured dynamical information. However the accurate measurement of ψ cross-section might produce a value for λ in favour of these dynamical effects.

REFERENCES

1. W. Heisenberg, Z Phys. 101 (1936) 533
2. G. Wataghin, Phys. Rev. 63 (1943) 137 66 (1944) 149
3. E. Fermi, Progr. Theor. Phys. 5 (1950) 570
4. I. Ya Pomeranchuk, Dokl Akad. Nauk. SSSR 79 (1951) 88
5. L.D. Landau, IZV. AN SSSR, Scr. fiz. 17 (1953) 51
6. R. Haydorn, Nuovo Cimento Supp. 3 (1965) 147
7. R. Haydorn, J. Ranft. Nuovo Cimento Supp. 6 (1968) 169
8. V.S. Barashenkov, V.M. Maltsev, Fortschritte der Phys. 15 (1967) 435
9. R. Haydorn, Nucl. Phys. B24 (1970) 93
10. E.L. Feinberg, Soviet Phys. Uspekhi, 14 (1972) 405
11. S.J. Frautschi, Phys. Rev. D3 (1971) 281
12. C.J. Hamer and S.J. Fr tschi, Phys. Rev. D4 (1971) 2125
13. J. Engels, H. Satz, K. Schilling, Phys. Letters 49B (1974) 171
14. Hutan Than and J. Ranft, Nuovc Cimento Letters, 5 (1972) 655
15. Hutan Than et al. Nuovo Cimento Letters 5 (1972) 537
16. J. Ranft, G. Ranft, Nucl. Phys. B53 (1973) 217
17. S. Kayigama et al. Prog. Theor. Phys. 57 (1977) 1647
18. F. Elvekgaet et al. Phys. Letters, 60B (1976) 456
19. R. Safari, E.J. Squires, Acta Physi Pholonica B8 (1977) 253
20. L.G.F. Vanryckeghem, A new parametrization for single particle inclusive distribution. Department of Applied Maths. Liverpool University, Liverpool.
21. M. Della Negra et al. Nucl. Phys. B104 (1976) 365
22. K. Egger† et al. Nucl. Phys. B98 (1975) 73
23. M. Della Negra, Review talk given at the VII International Colloquium on multi-particle reactions, CERN published 76-52 on large transverse momentum phenomenon.

24. ISR Discussion meeting between experimentalists and theoreticians, CERN, on correlations among large P_T particles
25. F.W. Busser et al. CERN Preprint, A study of inclusive spectra and two particles correlations at large transverse momentum.
26. S.D. Ellis, M. Jacob and P.V. Landshoff, Nucl. Phys. B108 (1976) 93
27. R.A. Field and R.P. Feynman, Phys. Rev. D15 (1977) 2590
28. P.V. Landshoff and J.C. Polkinghorne, Phys. Rev. D8 (1973) 4197
29. D. Sivers, S.J. Brodsky and R. Blankenbecler, Phys. Reports 23 (1976) 1
30. M.K. Chase and W.J. Stirling, Nucl. Phys. B133 (1978) 157
31. R. Culter and D. Sivers, Phys. Rev. D17 (1978) 196
32. G. Donaldson et al. Physical Rev. Letters 40 (1978) 917
33. A.G. Clark et al. Phys. Letters, 74B (1978) 167
34. Frantz Henrey et al. Nucl. Phys. 370 (1974) 445
35. J. Frøyland, A connection between inelastic overlap function and inclusive pion production at ISR energies. Oslo, preprint.
36. R. Henzi and P. Valin, Phys. Letters 48B (1974) 119
37. B. Alper et al. Nucl. Phys. B114 (1976) 1
38. C. Michael, Phys. Letters 63B (1976) 301
39. S.C. Frantschi et al. 1976a Caltech preprint CALT 68-562 submitted to the Nucl. Phys.
40. B. Alper et al. Nucl. Phys. B100 (1975) 237
41. R. Singer et al. Phys. Letters 60B (1976) 389
42. K.J. Anderson et al. Phys. Rev. Lett. (1976) 237
43. R. Safari, Euan J. Squires, Nucl. Phys. G3 (1977) 45
44. C. Kourkoumelis, A study of J/ψ production in proton-proton collisions, CERN 77-06.
45. L.M. Saundress, D.E. Soper, Phys. Rev. Letters D7 (1973) 133
46. C. Michael, L. Vanryckeghem, Consequences of momentum conservation for particles production at large P_T , University of Liverpool's preprint on November 1976.

FIGURE CAPTIONS

- Figure 1 Proton-proton collision at a certain time according to Hagedorn's interpretation. λ is a velocity factor (see the text).
- Figure 2a Statistical decay
2b Full bootstrap decay
2c Linear cascade decay
- Figure 3 Comparison of the inclusive pion spectra, (a) $\pi^+ P \rightarrow \pi^+ + X$ and (b) $\pi^+ P \rightarrow \pi^- + X$ at 8 and 16 GeV according to the thermodynamical model with the experimental data. Thermodynamical model: — 16 GeV/C, - - - - - 8 GeV/C, Beaupre et al: 0 16 GeV/C, . 8 GeV/C.
- Figure 4 Comparison of the inclusive spectra $pp \rightarrow \gamma + \text{anything}$ at ISR energies with the data, according to the thermodynamical model. The spectra are plotted in the c.m.s. in the form $E \frac{d^3 N}{d^3 P} = F(X, P_T^2, S)$ for $0 \leq X \leq .15$ and different values of P_T^2 for $\sqrt{s} = 44.7$ GeV: $\blacksquare \sqrt{s} = 30.20$ GeV, $\bullet \sqrt{s} = 47.7$ GeV, $\blacktriangle \sqrt{s} = 52.7$ GeV.
- Figure 5a Invariant cross-section for inclusive charged particle production. The solid lines present the fits of the model. See text.
- 5b Charged multiplicity as a function of \sqrt{s} . The solid line represents the fits of the model. See text.
- 5c $R = \frac{\sigma_h}{\sigma_{\mu\mu}}$ as a function of \sqrt{s} . The solid line represents the fits of the model. See text.
- Figure 6 Centre of mass longitudinal momentum distribution for all negative particles and all multiplicities in 25 GeV/C $\pi^- P$ collisions.

- Figure 7 Pion transverse momentum distribution. Dashed line denotes the thermodynamical result.
- Figure 8 Plot of single particle inclusive spectra for π^+ at two different ISR energies and $\theta = 90^\circ$. The curves are the fits using the parametrization of reference (20) to the multitemperature model.
- Figure 9 The ratio R of equation (36) versus temperature. The solid and dashed curves are corresponding curves belonging to equations (35) and (42) respectively.
- Figure 10 The inclusive single particle spectra with respect to P_T . The solid curve represents the data of reference (40) and the circles correspond to equation (41) of MTM.
- Figure 11 $\sigma(\lambda)$ $a(\lambda)$ versus the temperature at two ISR energies $\sqrt{s} = 23$ GeV (i.e. Solide Curves), $\sqrt{s} = 53$ GeV (i.e. dashed curves).
- Figure 12a The inclusive emission of charged hadron h in a minimum bias event $pp \rightarrow h^{\pm} h^{\pm} x$
- 12b The inclusive emission of a charged hadron h^{\pm} in a large P_T event, triggered on a charged or neutral large P_T' hadron h^{\pm} at fixed c.m. angle θ , in the ϕ hemisphere towards the trigger, $pp \rightarrow h^{\pm} h^{\pm} x$
- 12c In the ϕ hemisphere away from the trigger
- Figure 13 Plots of azimuthal angle ϕ versus rapidity y for (a) all charged particles observed in normal inelastic pp collisions, (b) all positive particles with $P_T > .5$ GeV/C observed in large P_T events. The triggering particles can be seen clustered around $y = -2$, $\phi = 20^\circ$, (c) all negative particles with $P_T > 0.5$ GeV/C observed in large P_T events.

Figure 14 Azimuthal distributions of positive and negative particles with $P_T > 0.5$ GeV/C in large P_T events. The lines indicate the azimuthal distributions observed in normal events. The trigger is centred at $\phi = 20^\circ$ and $y = -2$.

Figure 15 Azimuthal distribution of charged particles in the rapidity interval $-3 < y < 2$ for different P_T intervals of secondaries. The trigger is centred at $\phi = 20^\circ$.

Figure 16 Azimuthal distribution of charged particle densities integrated over $|y| < 2$ as a function of P_T of the π^0 for the 90° data. The lines are hand-drawn curves through the data. The data are symmetrized around $\phi = 180^\circ$ to reduce the statistical errors (22). A typical error bar is shown for the $P_T = 5$ GeV/C data.

Figure 17 Charged particle densities integrated over $|180^\circ - \phi| < 30^\circ$, $|y| < 1$ as a function of P_T' (right hand scale). For a comparison with the data of reference (12) of reference (22), the ratio to the normal events also have been given (left-hand scale). In the CCR experiment the charged particle ratios are given for the interval $|130 - \phi| < 23^\circ$, $|y| < 0.8$. The definition of minimum bias triggers is not exactly the same in the two experiments.

Figure 18 Charged particle densities for the 53° data. The solid lines give charged particle densities in normal events.

Figure 19 Charged particles densities for the 90° data, averaged over events with P_T of the $\pi^0 > 2$ GeV/C. The solid lines give charged particle densities in normal events.

Figure 20 Rapidity distributions of charged particles produced away from the $20^\circ \pm$ and $45^\circ \pm$ large P_T triggers for three P_T intervals. The vertical scale is the charged multiplicity, times 100, per interval of $\Delta\phi$ and Δy (in radian⁻¹). Normal distributions are shown as solid lines.

Figure 21 Rapidity distributions of positive and negative particles with $P_T > 0.25$ GeV/C in away region. Two samples of large P_T events are distinguished: Lower P_T events $1.5 < P_T' < 1.7$ GeV/C, Higher P_T events $P_T' > 2.5$ GeV/C. Inside each sample a cut is made on the observed charged multiplicity: Low multiplicity $N < 7$. High multiplicity $N \geq 7$. The trigger is at $y = -2$.

Figure 22 Charged ratios. The ratio of positive to negative particles in the ϕ region opposite to the trigger is plotted as a function of their transverse momentum for different y intervals. Lines are drawn to guide the eye.

Figure 23 Function F of equation (47) versus associated charged particles momentum (P_{T2}) at $\sqrt{s} = 44.8$ GeV. The open squares show the normal distribution of equation (45) at the same energy.

Figure 24 As picture 23, but this one is displayed at $\sqrt{s} = 52.7$ GeV.

Figure 25 As plot (23), but this is displayed at $\sqrt{s} = 62.4$ GeV.

Figure 26 Plot of F of equation (47) versus P_T of various opposite side associated charged particles.

Figure 27 Plot of equation (47) versus P_T of associated charged particles at different ISR energies for the π^0 trigger.

Figure 28 Plot of F of equation (47) with respect to energy at different associated charged particles momentum region shown above.

Figure 29 Away side distribution of F of equation (47) versus P_T of associated charged particles at different ISR energies.

Figure 30 The same as Figure 29, but this is displayed by π^0 triggering particle.

Figure 31 Energy dependence of F of equation (47) for different momentum region of associated charged particles.

Figure 32 Rapidity distributions of charged particles emitted towards the 90° large P_T π^0 trigger for four P_T intervals of associated particles.

(a) $.4 < P_T < .6$ GeV/C

(b) $.6 < P_T < .8$ GeV/C

(c) $.8 < P_T < 1.1$ GeV/C

(d) $1.1 < P_T < 1.7$ GeV/C

Figure 33 The hard scattering model for the large transverse momentum process $A + B \rightarrow C + X$

Figure 34 Results of fits to data: (a), (b), (c) and (d) represent the parameters, P , P_1 , B and B_1 respectively. Solid and dashed lines are visual fits linear and quadratic in $\ln P_L$ respectively.

Figure 35 Showing $Z_h(P_T)$ the ratio between the conditional inclusive cross-section and the inclusive cross-section. A value of unity means there is no correlation effect. The dotted line represents the experimental value of the same side and the upper limit is the experimental value on the opposite side. The dashed curve is the prediction of the Froyland model and the curves called by values of n are the predictions of MTM.

Figure 36 Plot of $Z_h(P_T)$ versus P_T of the charged particle accompanying the trigger at $\sqrt{s} = 52.7$ GeV. The upper and lower dotted curves are the experimental values on the opposite and same side respectively. The solid curves are the calculated value using MTM and also including the recoild effect with $n = 2$ and $M_c = \sqrt{s} = 52.7$ GeV.

Figure 37 Plot of $Z_h(P_T)$ versus P_T of the charged particle accompanying the trigger at $\sqrt{s} = 52.7$ GeV. The upper and lower dashed curves are the experimental values on the opposite side and same side respectively. The solid curves belong to MTM after including the momentum recoild effect for the case with $n = 2.5$ and $M_c = \sqrt{s} = 52.7$ GeV.

Figure 38 Plot of $Z_h(P_T)$ versus P_T of the charged particle accompanying the trigger at $\sqrt{s} = 52.7$ GeV. The upper and lower dashed curves are the experimental values on the opposite side and same side respectively. The solid curves belong to MTM after including the momentum recoil effect for the case $n = 3$ and $M_c = \sqrt{s} = 52.7$ GeV.

Figure 39 Plot of $Z_h(P_T)$ of equation (112) versus P_T with $n = 2.5$ and $M_c = .8 \sqrt{s}$. The dashed limits show the opposite/same side correlations at $\sqrt{s} = 52.7$ GeV.

Figure 40 The P_T dependence of average charged multiplicity of π^+ , k^- , P in three ϕ regions. Linear curves are superimposed curves resulting from a fit to equation (113) of the text.

Figure 41 The $\ln S$ dependence of average charged particles multiplicity (integrated over ϕ) for π^+ , P and \bar{P} triggers at $P_T = 1.0$ and 2.0 GeV/C. The curves result from a fit to equation (113) of the text.

- Figure 42 Experimental invariant single particle production cross-section as a function of the transverse mass for different types of particles. See the text for references.
- Figure 43 Invariant single particle spectra (for ρ particles) versus the transverse momentum. Triangles are the data taken from reference (38) for $\sqrt{s} = 20$, GeV and the curve belongs to MTM at the same energy.
- Figure 44 The ψ production cross-section predicted from equation (127) for $\sqrt{s} = 20$ GeV (lower curve) and $\sqrt{s} = 52.7$ GeV (upper curve). The data points are from reference (38).
- Figure 45 Data on total inclusive cross-sections in pp interactions for different particle types are shown as a function of particle mass at energies around $\sqrt{s} = 24$ GeV along with the prediction of m_T universality, calculated from the π transverse momentum spectra at the different energies labelled on the graph.
- Figure 46 Plot of $d\sigma/dy|_{y=0}$ for J/ψ production as a function of \sqrt{s} coming from equation (133). The data points are from reference (44).
- Figure 47 The suppression fact, D , defined in equation (143) as a function of energy at fixed q_T values. The curves are just eye line to make the picture clear.
- Figure 48 The inclusive ψ production cross-section by using equation (148): $\Delta\sqrt{s} = 63$ GeV , $\circ\sqrt{s} = 23$ GeV.

QUANTITIES	SMALL P_T	LARGE P_T
P_T dependence of inclusive single particle cross section at $\sigma = 90^\circ$	Exponential decrease as e^{-6P_T}	The observed decrease is much slower
Energy dependence of cross section at $\sigma = 90^\circ$	At large collision energies the cross section is just a function of P_T and scaling behavior is obvious	Scaling is not reached and for fixed P_T the cross section varies with energy
Composition of produced particles	Mostly π -mesons	Heavy particles appear and take part
Dependence of P_T distribution on Feynman variable	No dependence is clear	A rapid decrease for $X = \frac{2P_T}{\sqrt{s}} \neq 0$ is shown
Charge effect ($pp \rightarrow \pi + X$)	Equal π^+ and π^- has been reported	More π^- than π^+ mesons has been observed

Table 1: The difference between large P_T and small P_T events

TYPE OF PARTICLE	PARAMETERS				
	$A \times 10^{-4} \frac{\text{mb}}{\text{GeV}^2}$	$K_0 (\text{GeV})^{1/2}$	$v \text{ GeV}$	$K_1 (s) (\text{GeV})^{-1/2}$	χ^2_{NDF}
π^+	186 ± 69	$16.50 \pm .15$	$0.29 \pm .04$	$1.37 \pm .04$	11.3
π^-	192 ± 71	$16.63 \pm .12$	$0.29 \pm .04$	$1.37 \pm .04$	14.2
K^+	14 ± 13	$14.95 \pm .27$	$.38 \pm 0.12$	1.29 ± 0.08	5.0
K^-	22 ± 18	$16.69 \pm .32$	$.42 \pm .15$	1.54 ± 0.1	6.4
p	372 ± 252	16.8 ± 0.45	$0.73 \pm .09$	1.01 ± 0.19	2.56
\bar{p}	1125 ± 712	$18.4 \pm .75$	$.86 \pm .04$	$1.38 \pm .08$	6.20

Table 2: Best values from a fit to the $y = 0$ data
of reference (40) taken from reference (20).

\sqrt{s} (GeV)	UNCORRELATED					CORRELATED					RATIO				
	$\psi\psi$	$\psi\psi'$	$\psi'\psi'$	$D\bar{D}$	$\psi D\bar{D}$	$\psi\psi$	$\psi\psi'$	$\psi'\psi'$	$D\bar{D}$	$\psi D\bar{D}$	$\psi\psi$	$\psi\psi'$	$\psi'\psi'$	$D\bar{D}$	$\psi D\bar{D}$
23.8	18×10^{-6}	31×10^{-7}	60×10^{-8}	22×10^{-7}	15×10^{-7}	28×10^{-6}	4×10^{-5}	2.6×10^{-5}	4.8×10^{-4}	4.6×10^{-5}	180	270	430	22	306
48	10×10^{-5}	22×10^{-6}	48×10^{-7}	89×10^{-7}	44×10^{-6}	12×10^{-3}	4.1×10^{-4}	1.4×10^{-4}	1.5×10^{-1}	27×10^{-4}	120	180	280	17	188

Table 3: $\frac{d^2\sigma}{dy_1 dy_2}$ in $\mu\text{b.}$

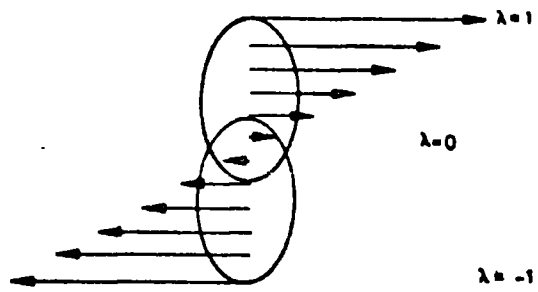


Figure 1

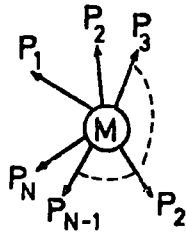


Figure 2a.

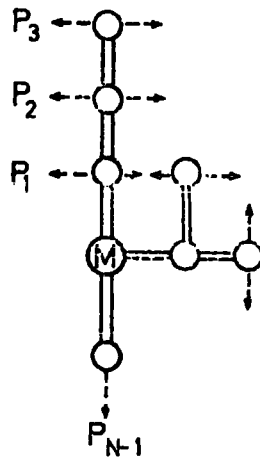


Figure 2b.

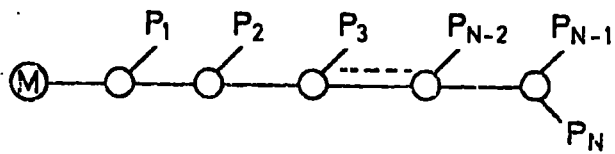


Figure 2c

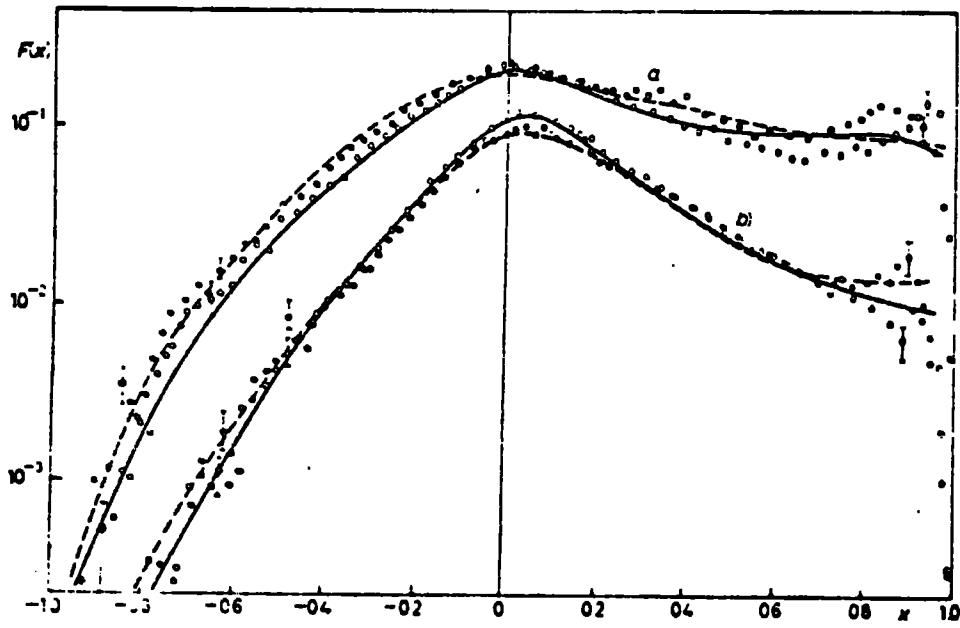


Figure 3

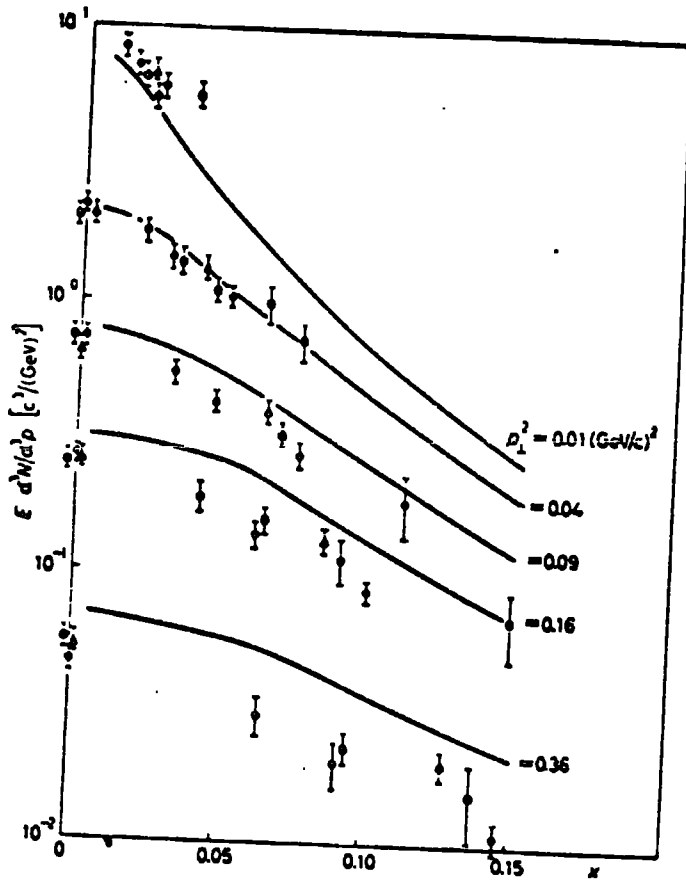


Figure 4

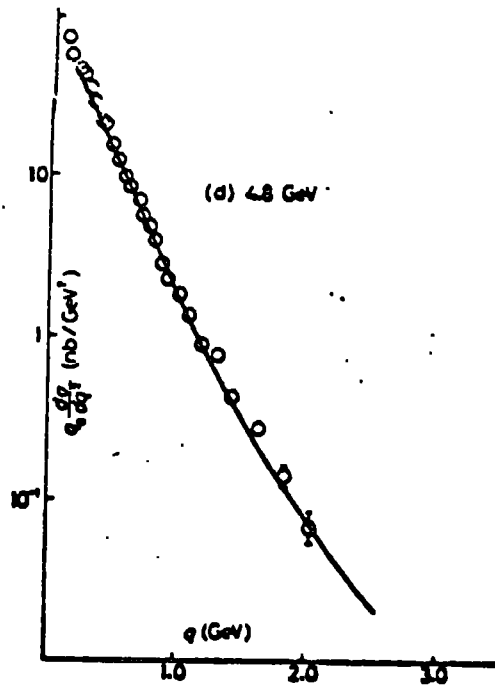
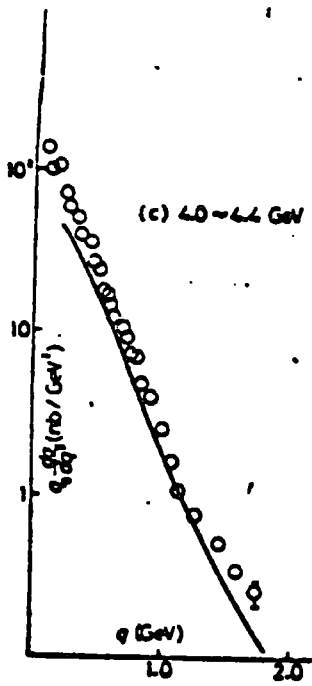
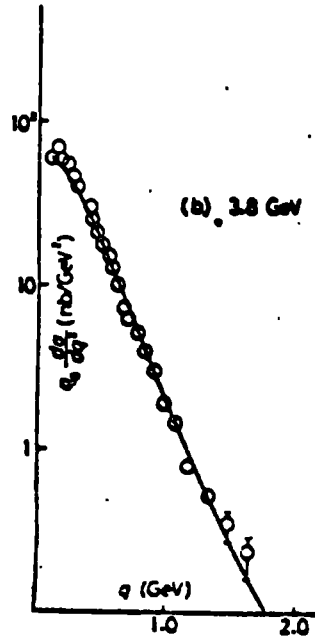
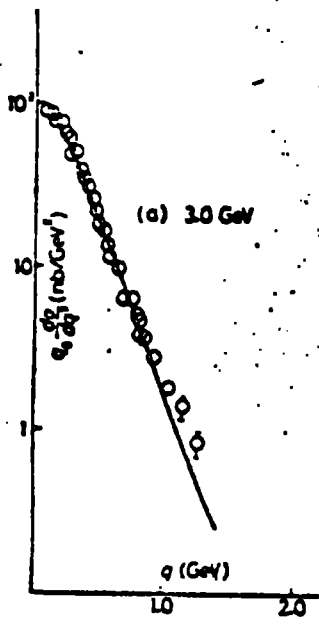


Figure 5a

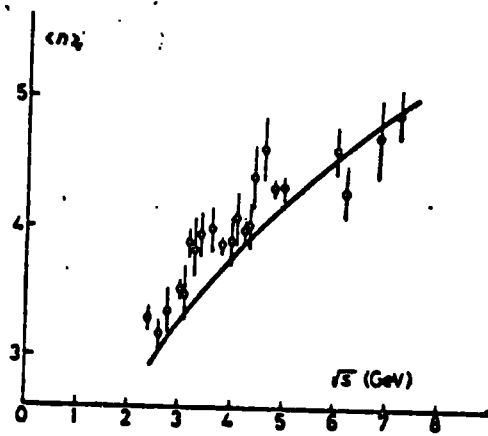
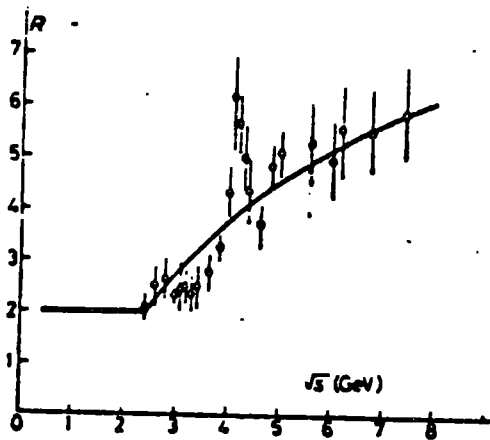
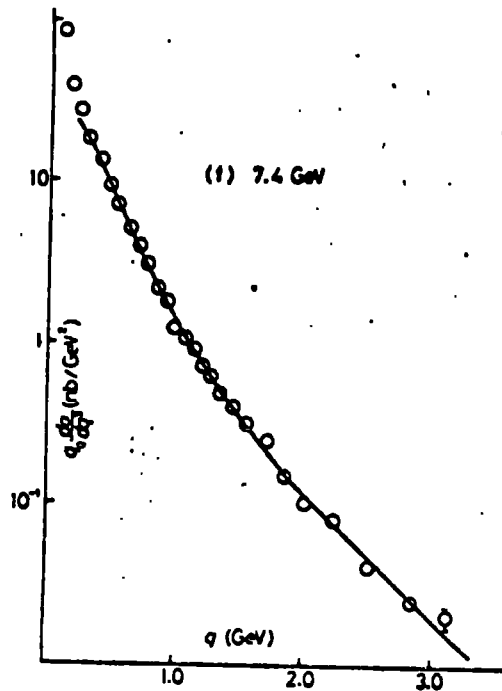
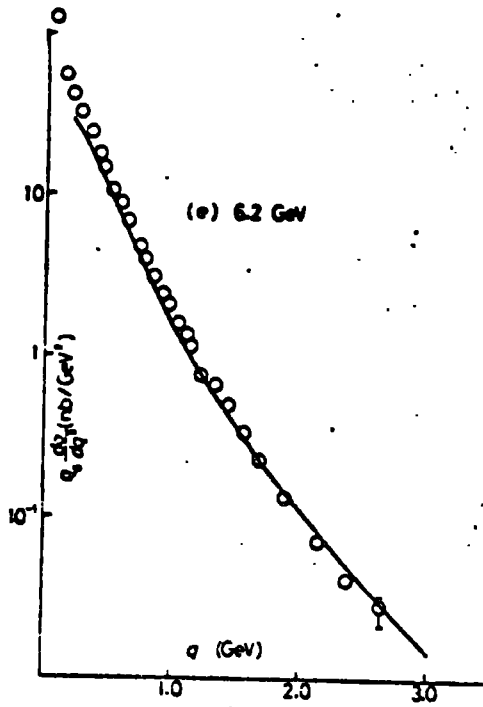


Figure 5c

Figure 5b

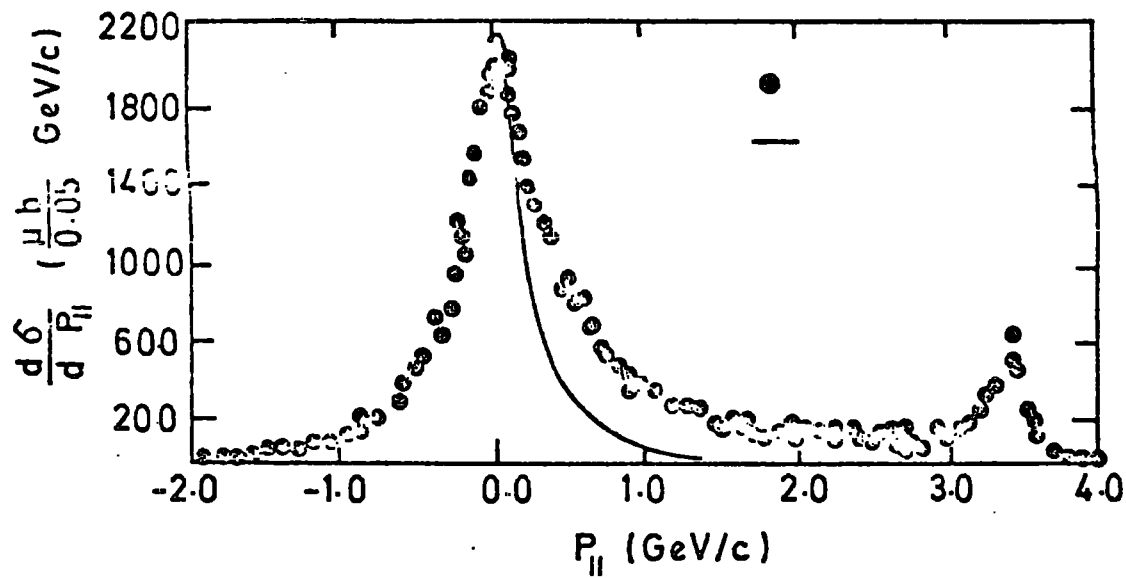


Figure 6

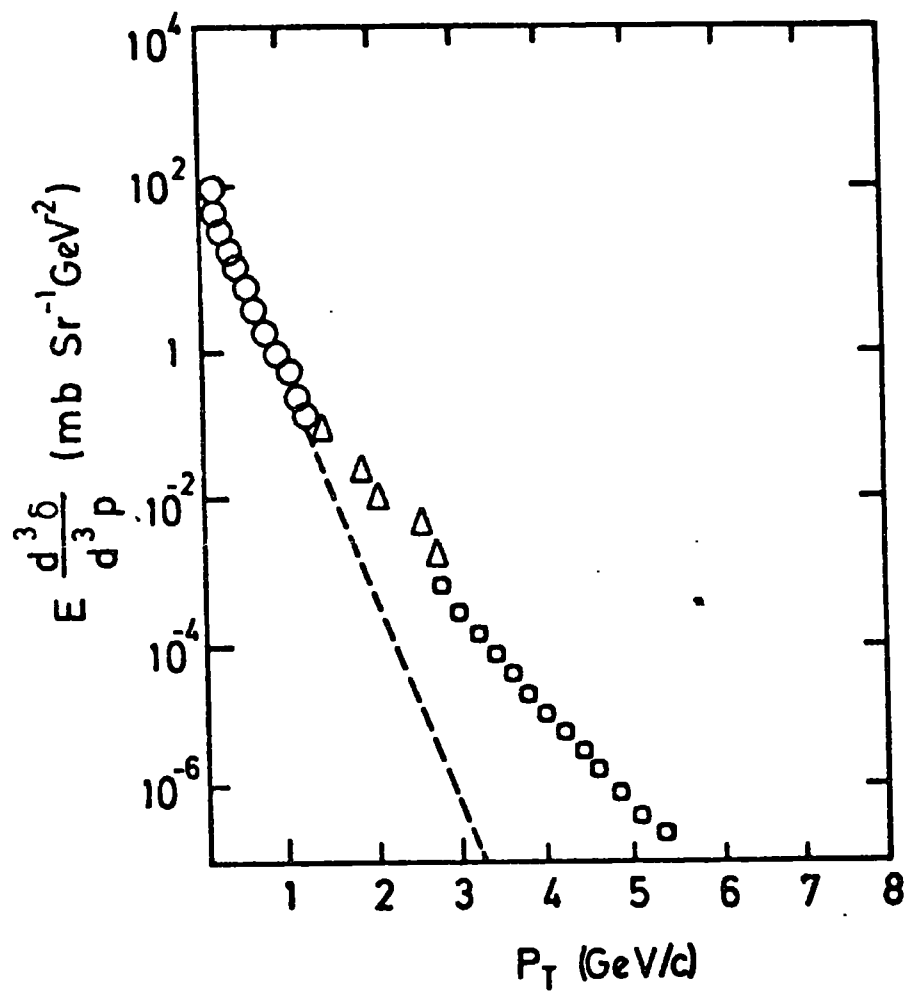


Figure 7

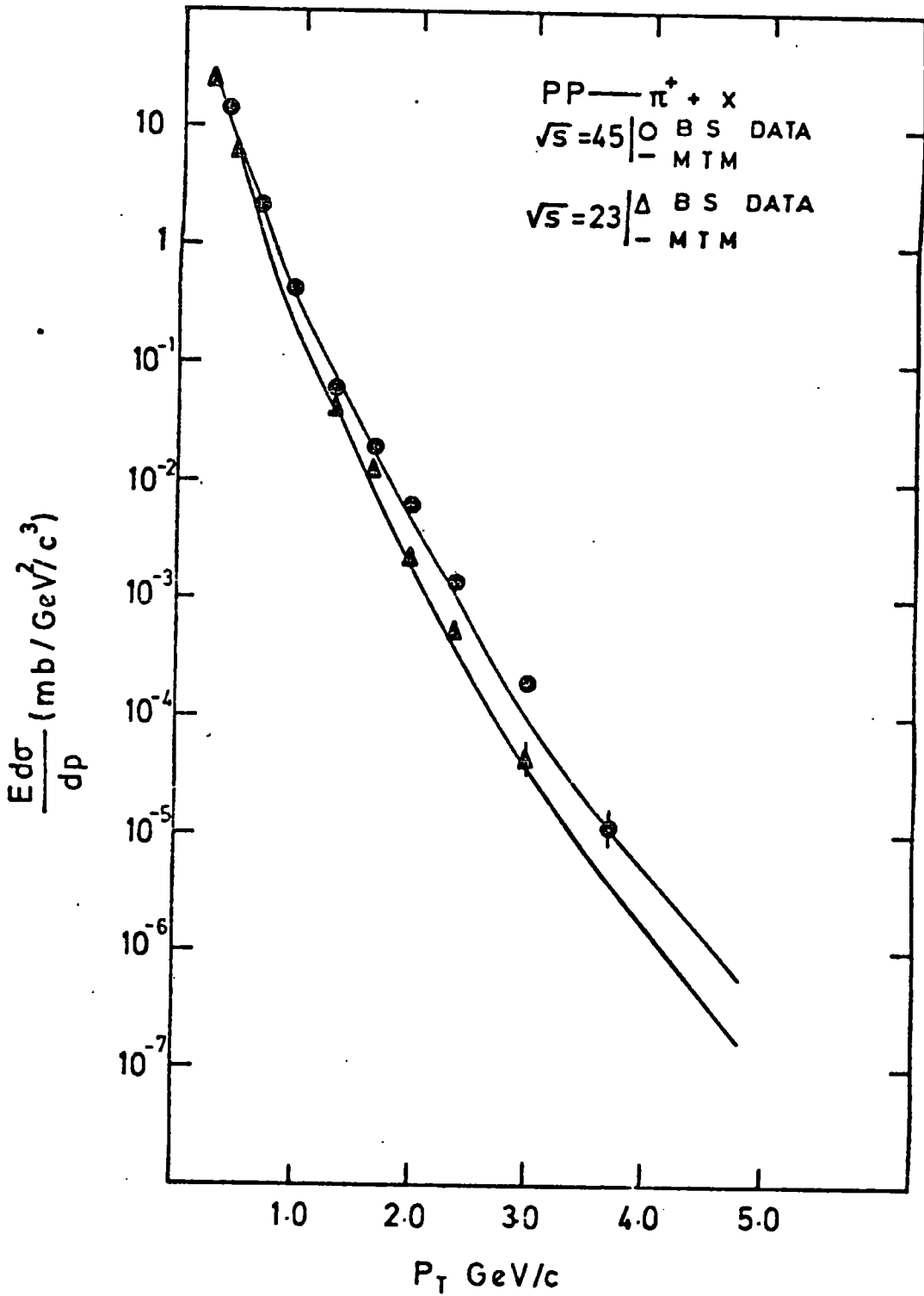


Figure 8

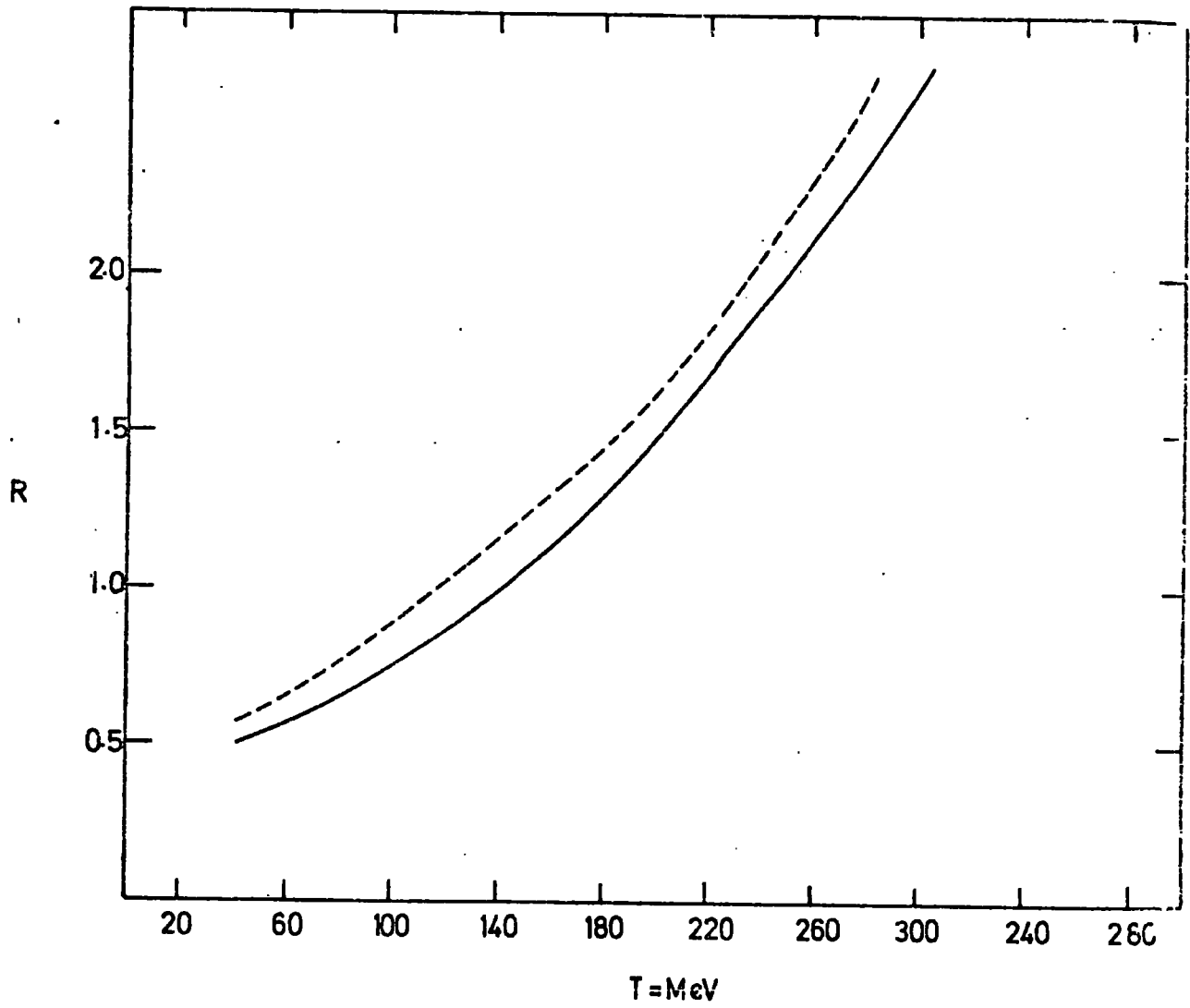


Figure 9

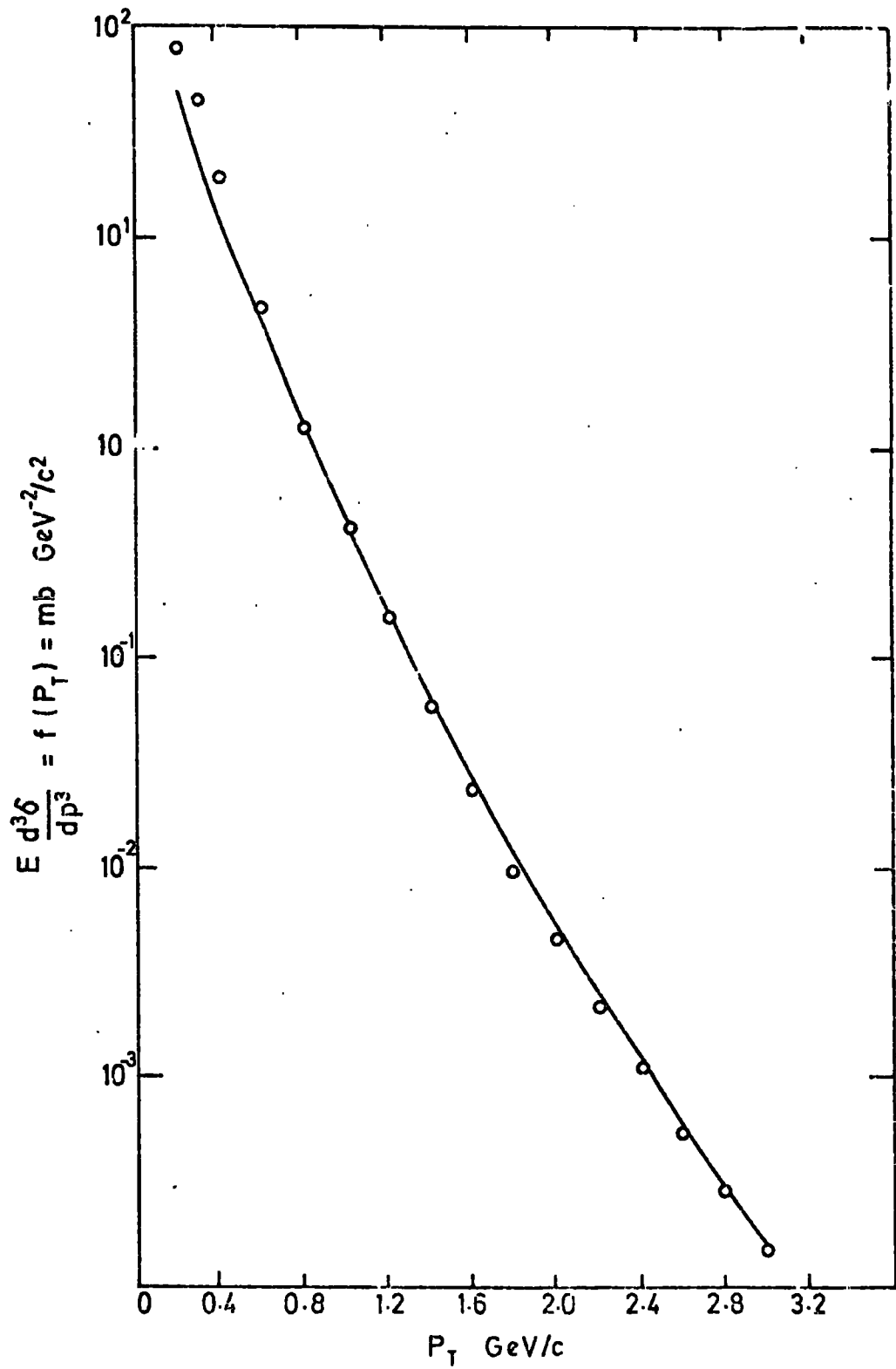


Figure 10

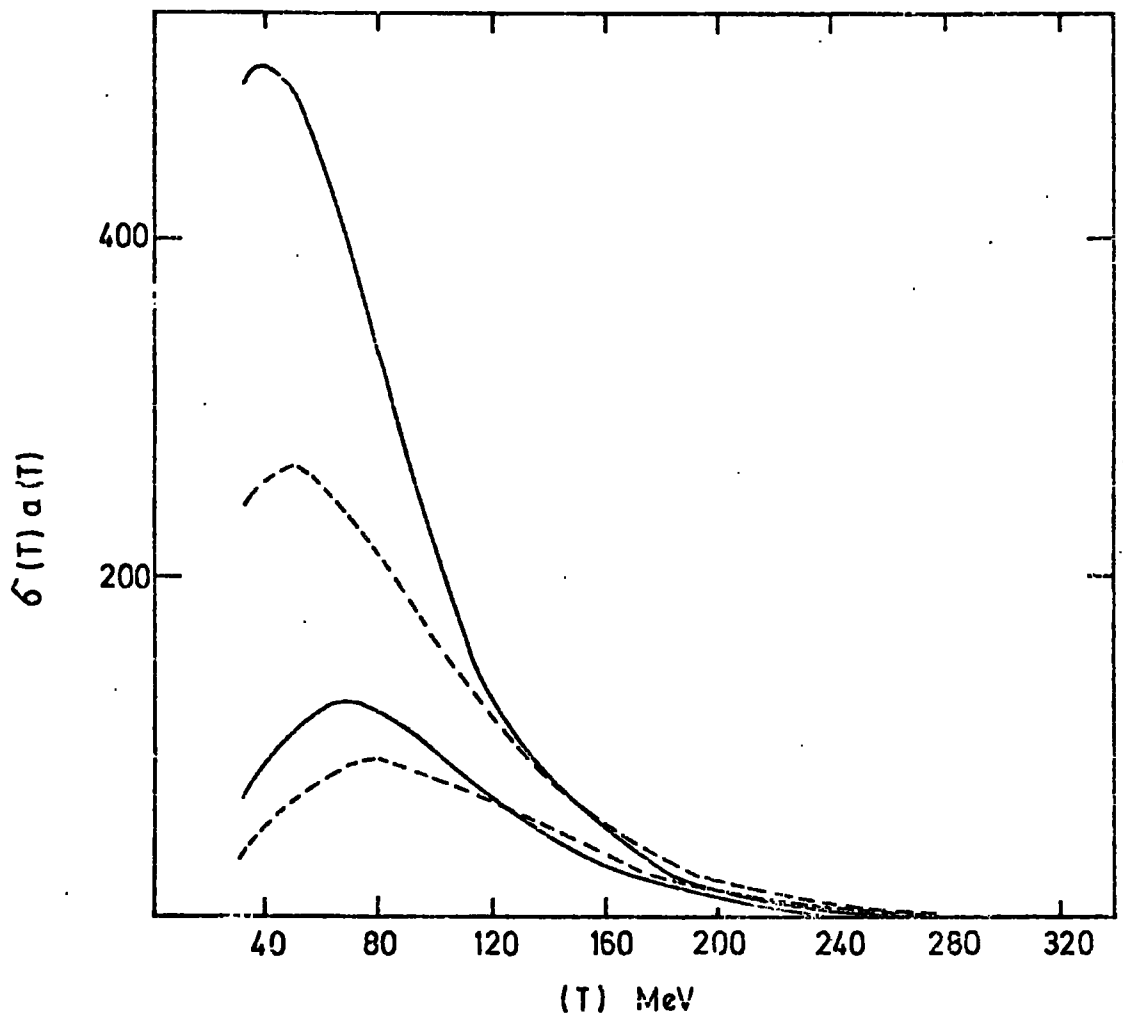
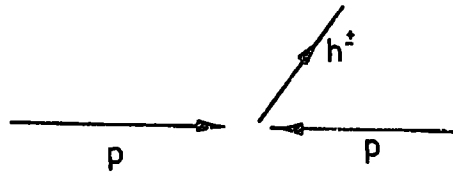
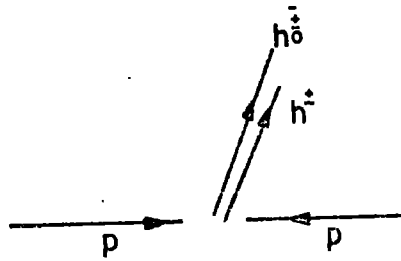


Figure 11

(a)



(b)



(c)

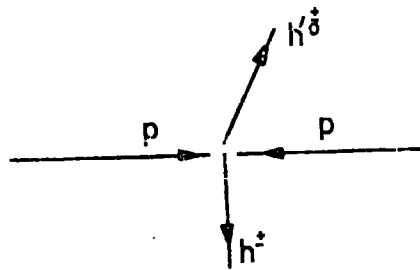


Figure 12

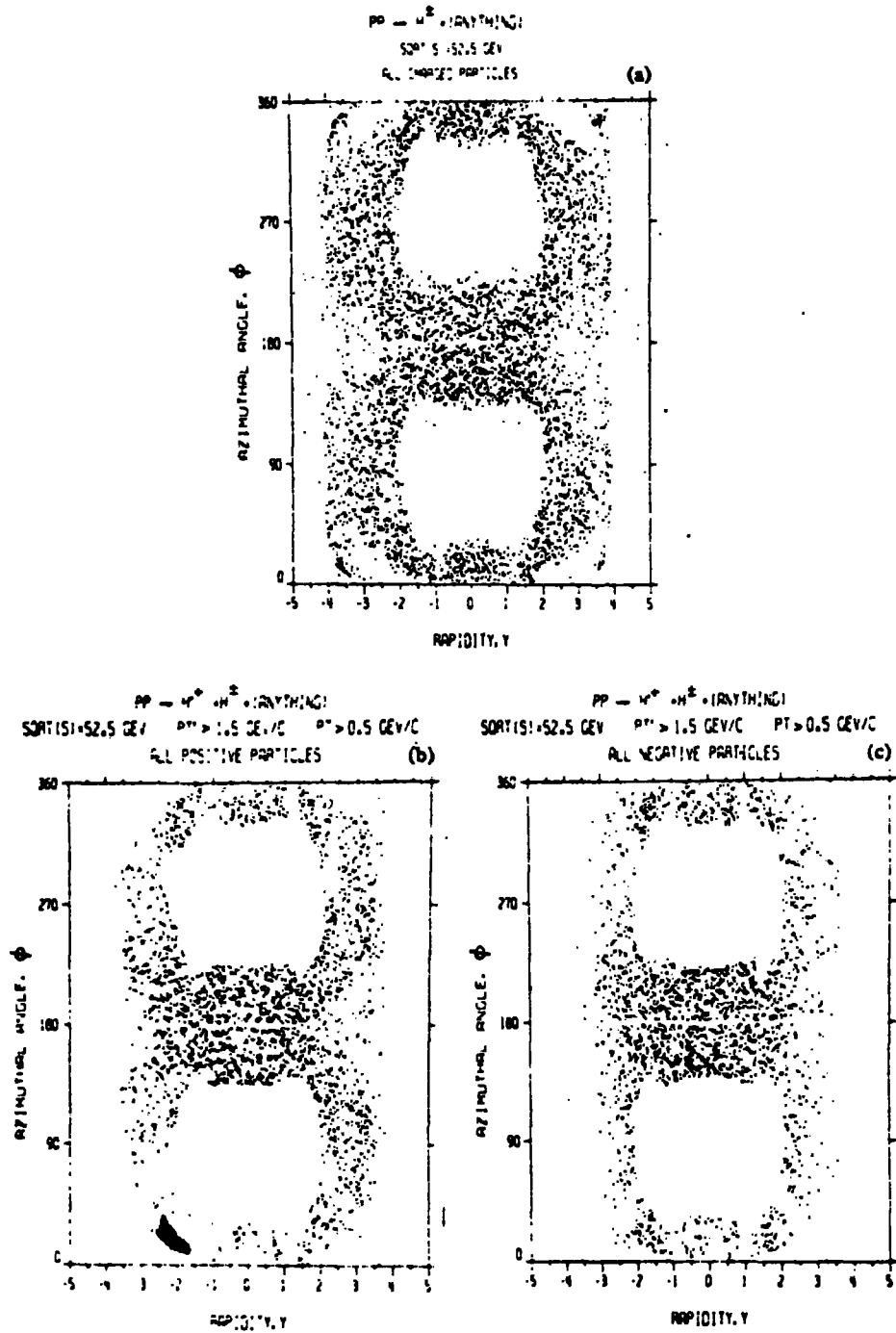


Figure 13

$PP \rightarrow H^+ \cdot H^\pm \cdot (\text{ANYTHING})$
 $\text{SQRT}(S) = 52.5 \text{ GEV} \quad PT > 0.5 \text{ GEV}/C \quad PT' > 1.5 \text{ GEV}/C$

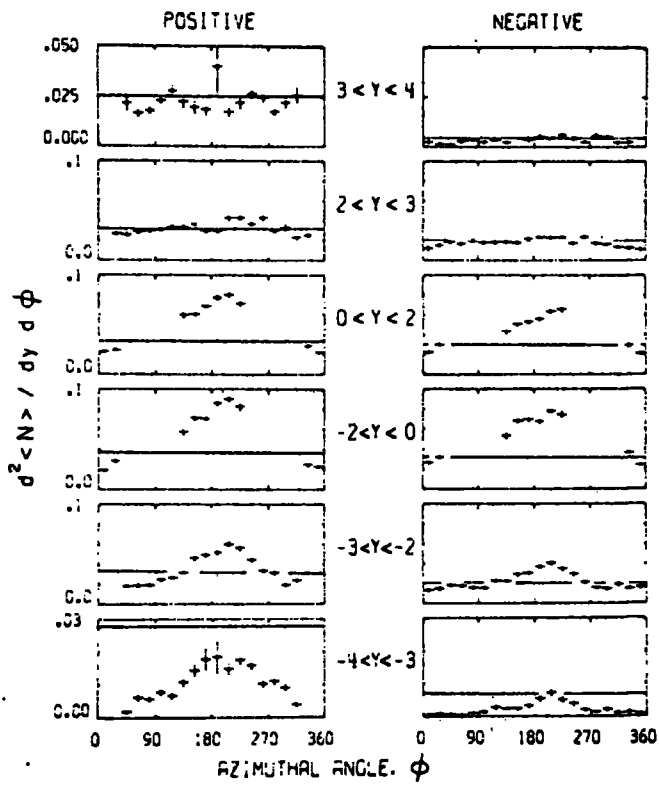


Figure 14

$PP \rightarrow H^+ + H^- \text{ (ANYTHING)}$
 $\sqrt{S} = 52.5 \text{ GEV}$ $PT > 1.5 \text{ GEV}/C$ $-3 < Y < -2$

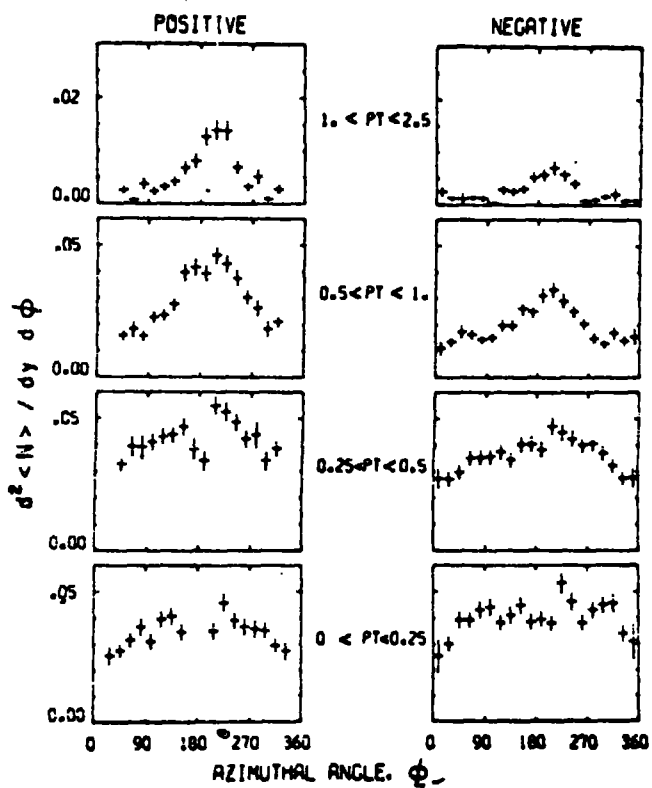


Figure 15

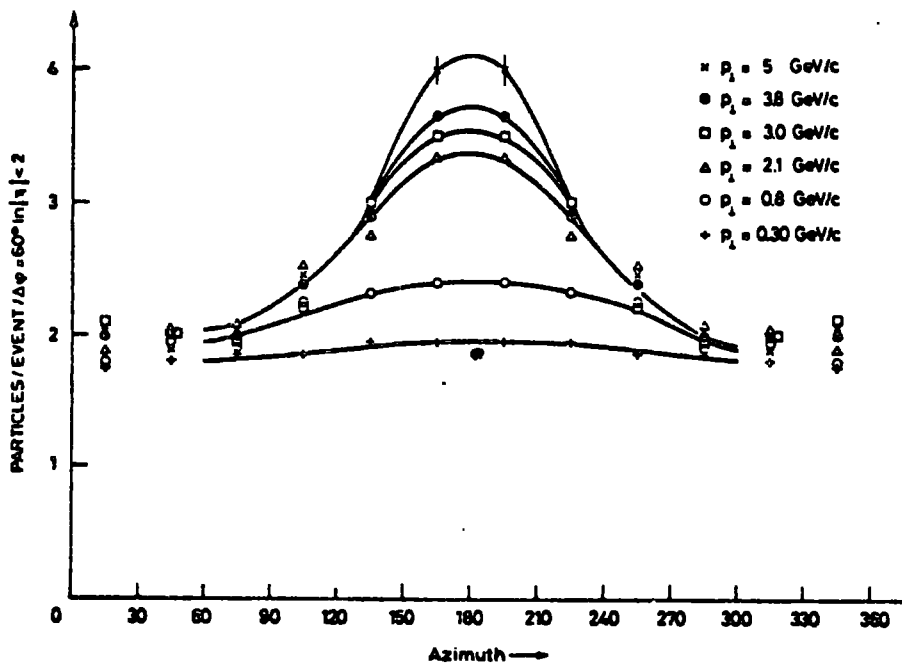


Figure 16

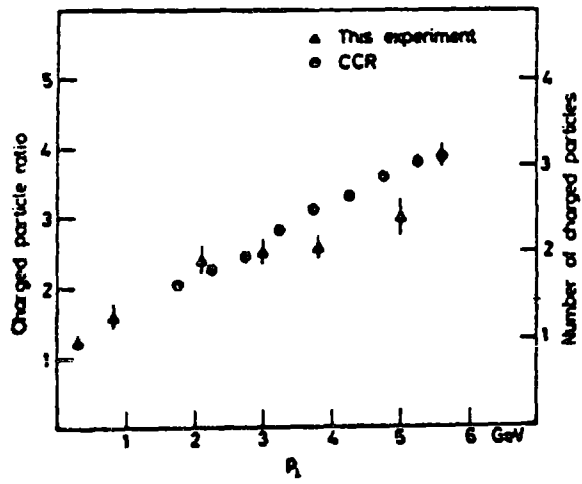


Figure 17

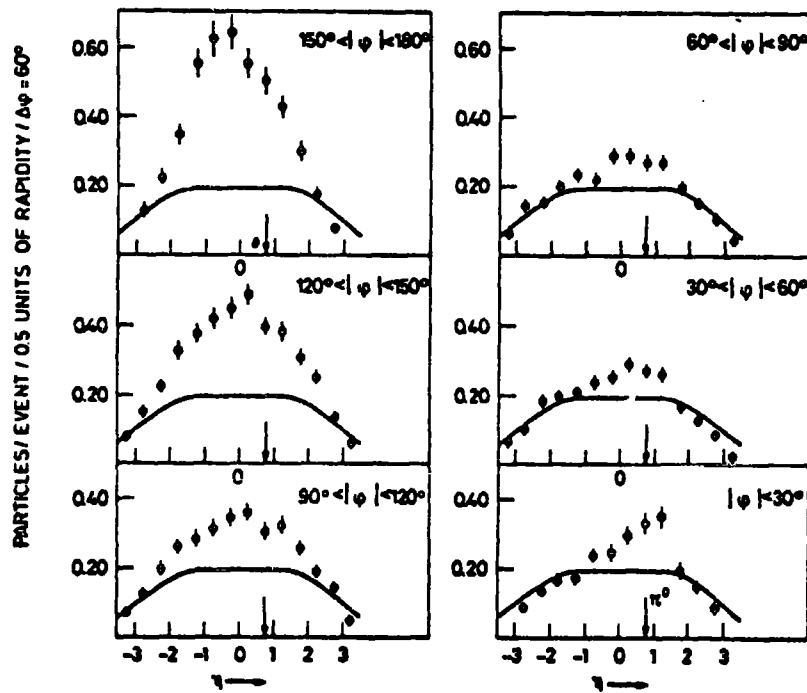


Figure 18

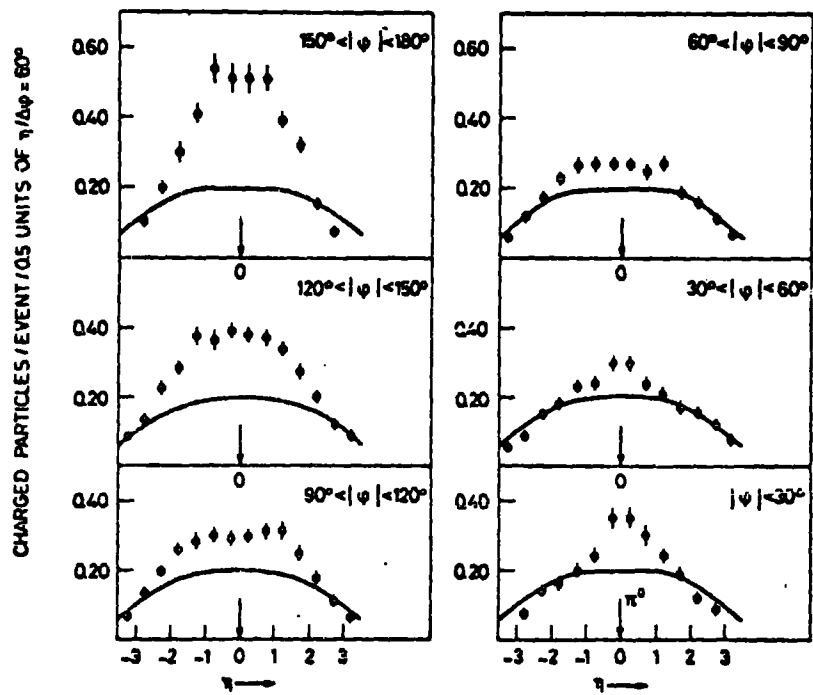


Figure 19

RAPIDITY DISTRIBUTIONS AWAY THE TRIGGER

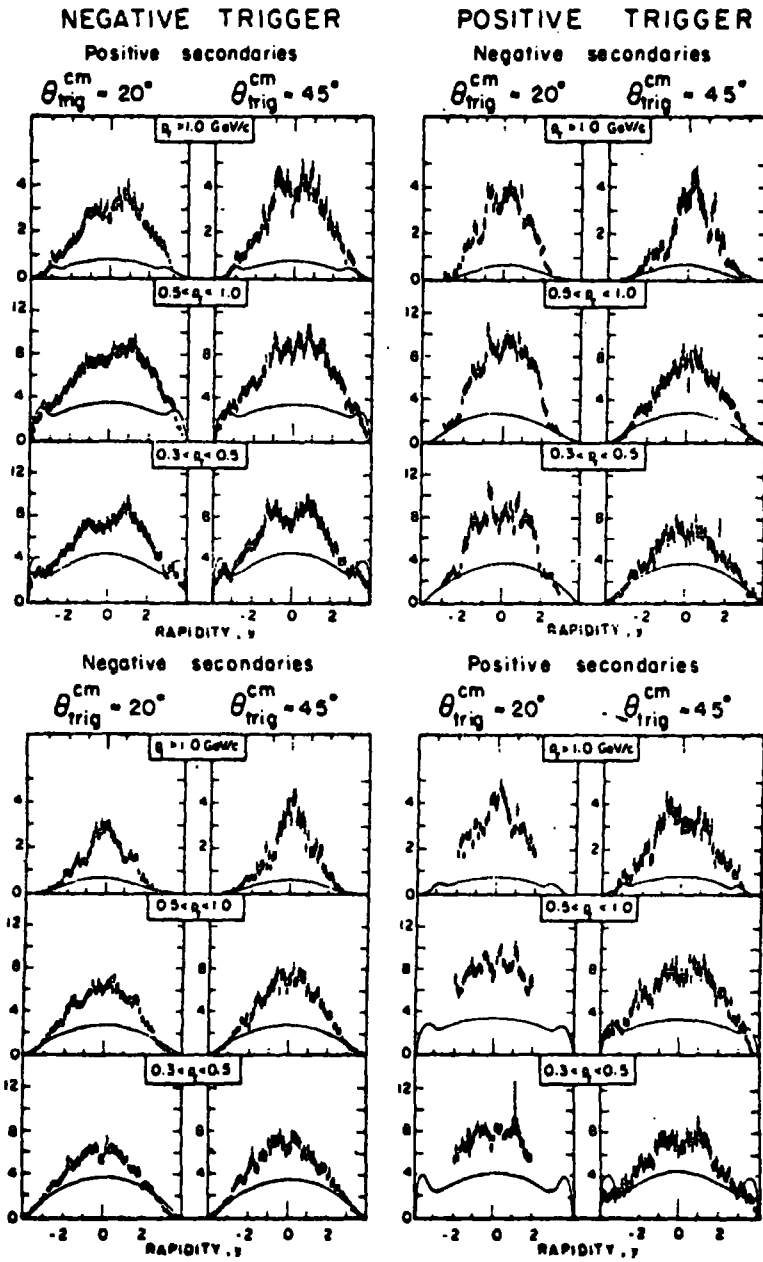


Figure 20

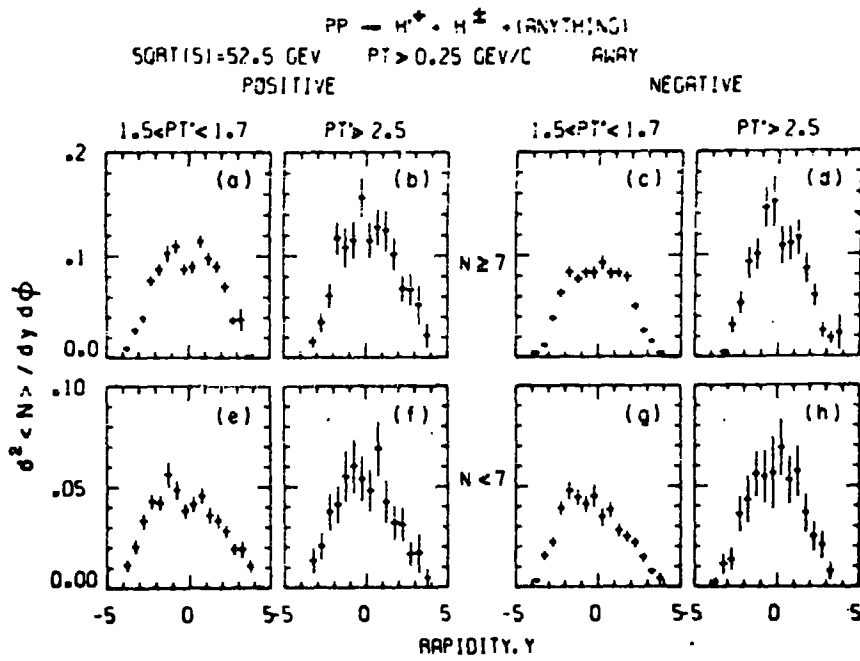


Figure 21

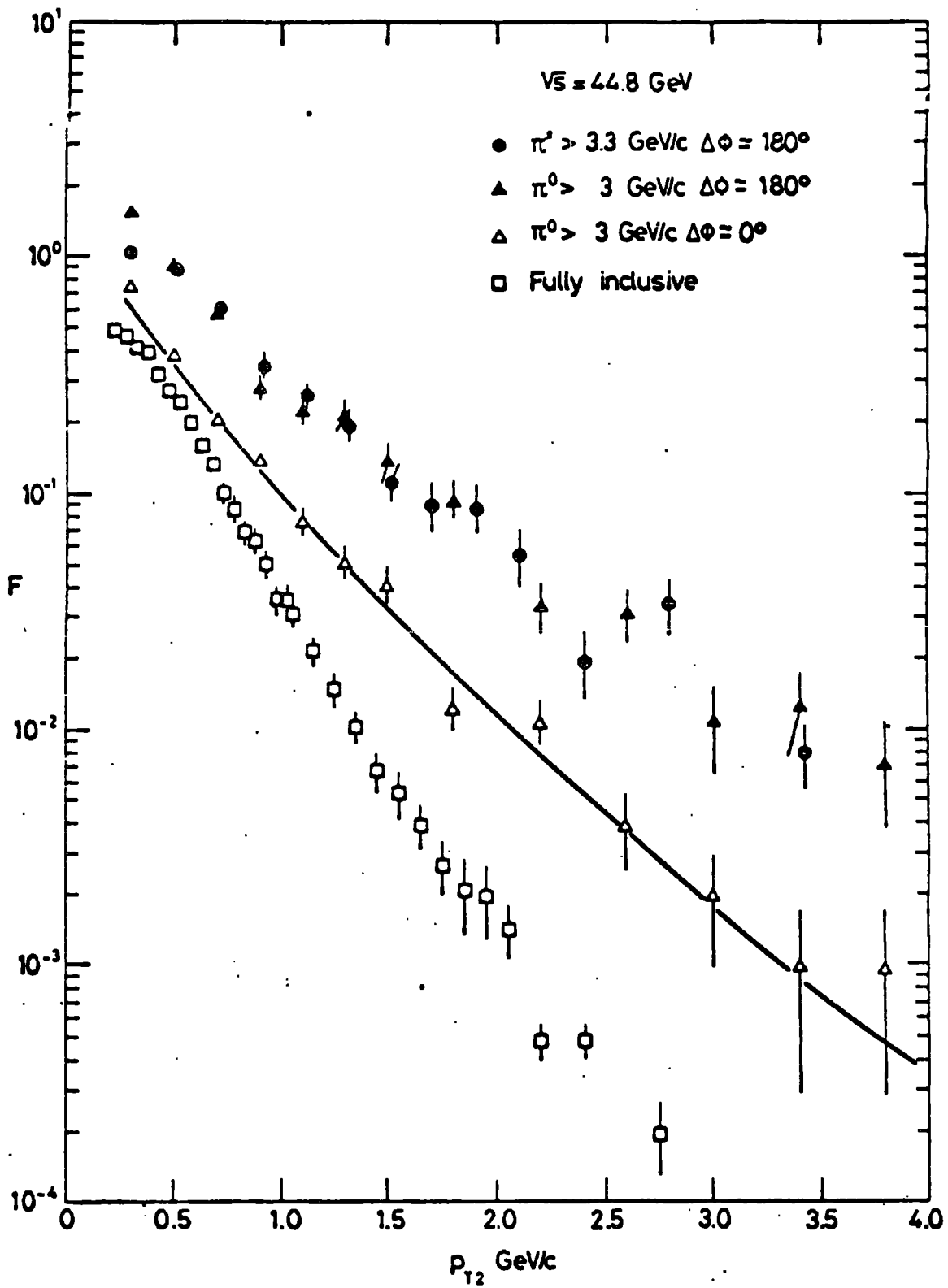


Figure 23

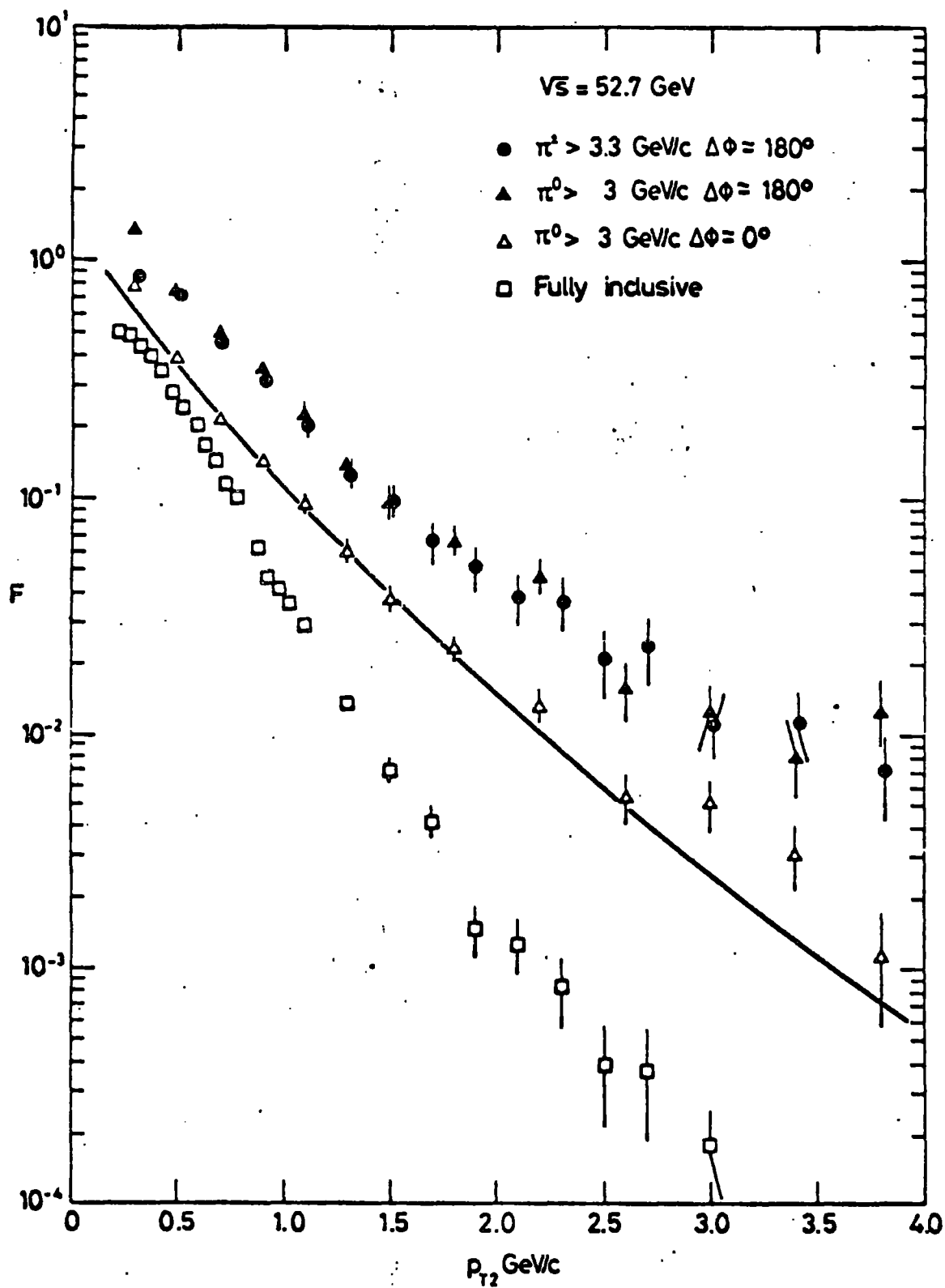


Figure 24

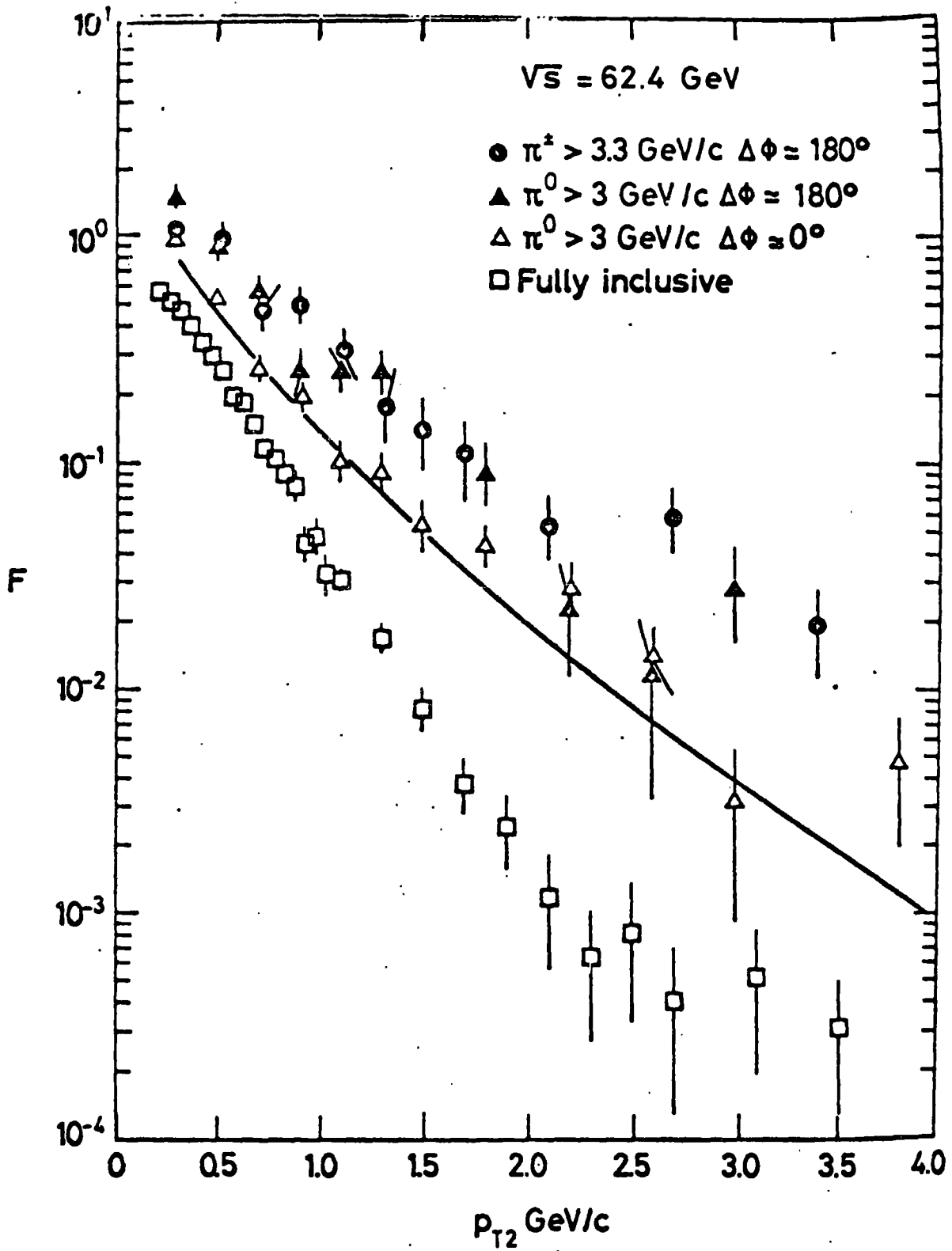


Figure 25

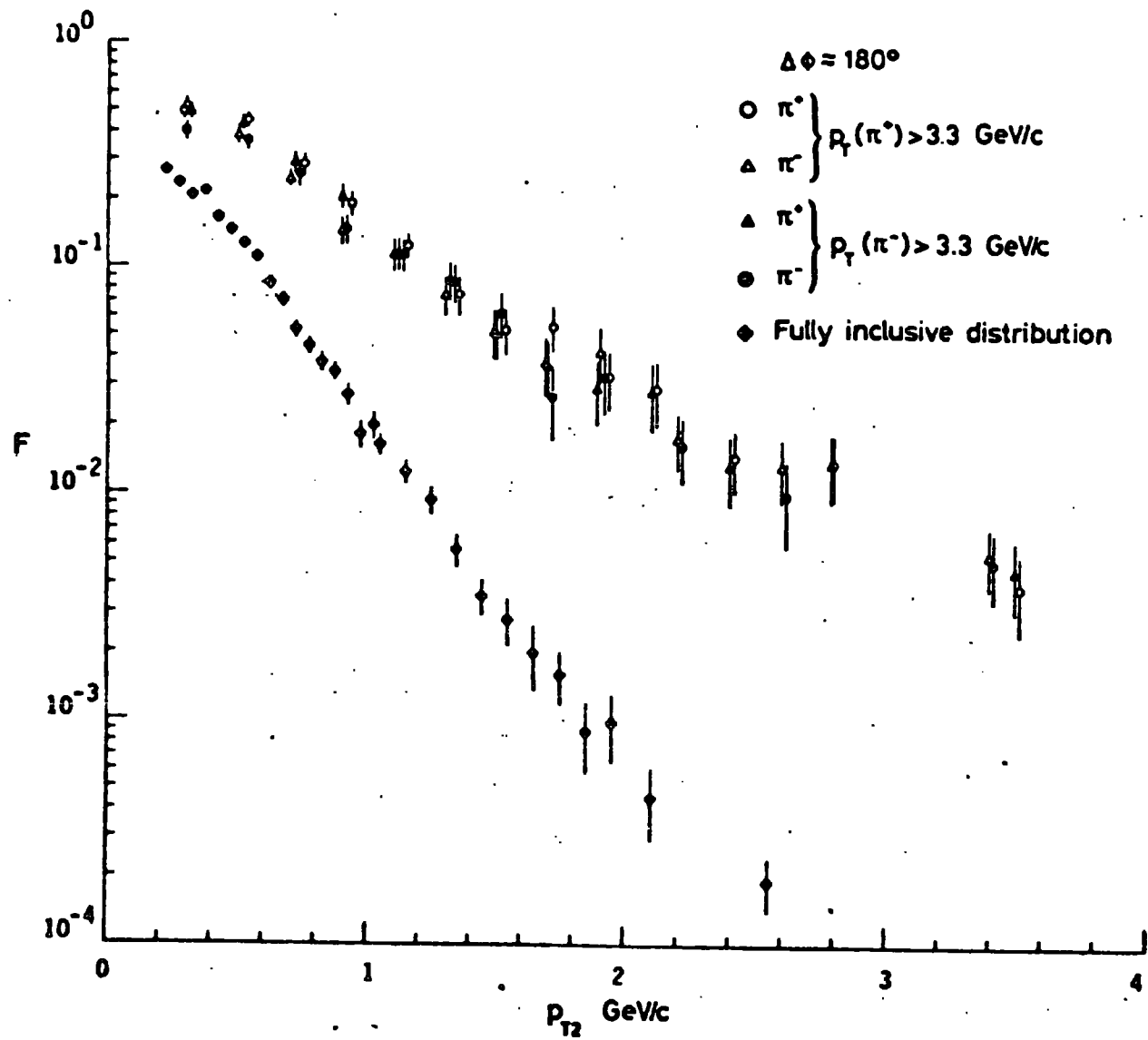


Figure 26

"SAME SIDE" CHARGED PARTICLES

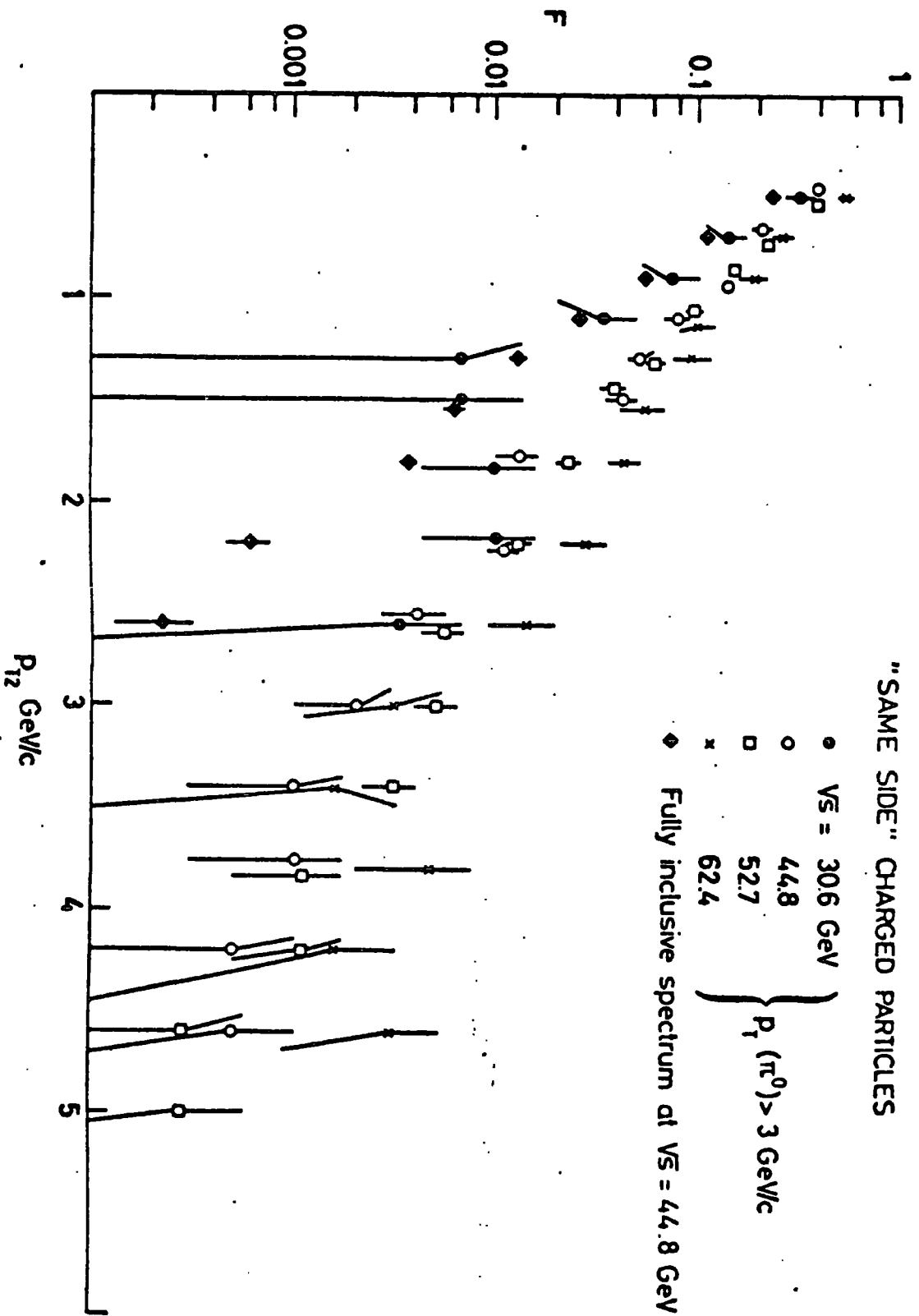


Figure 27

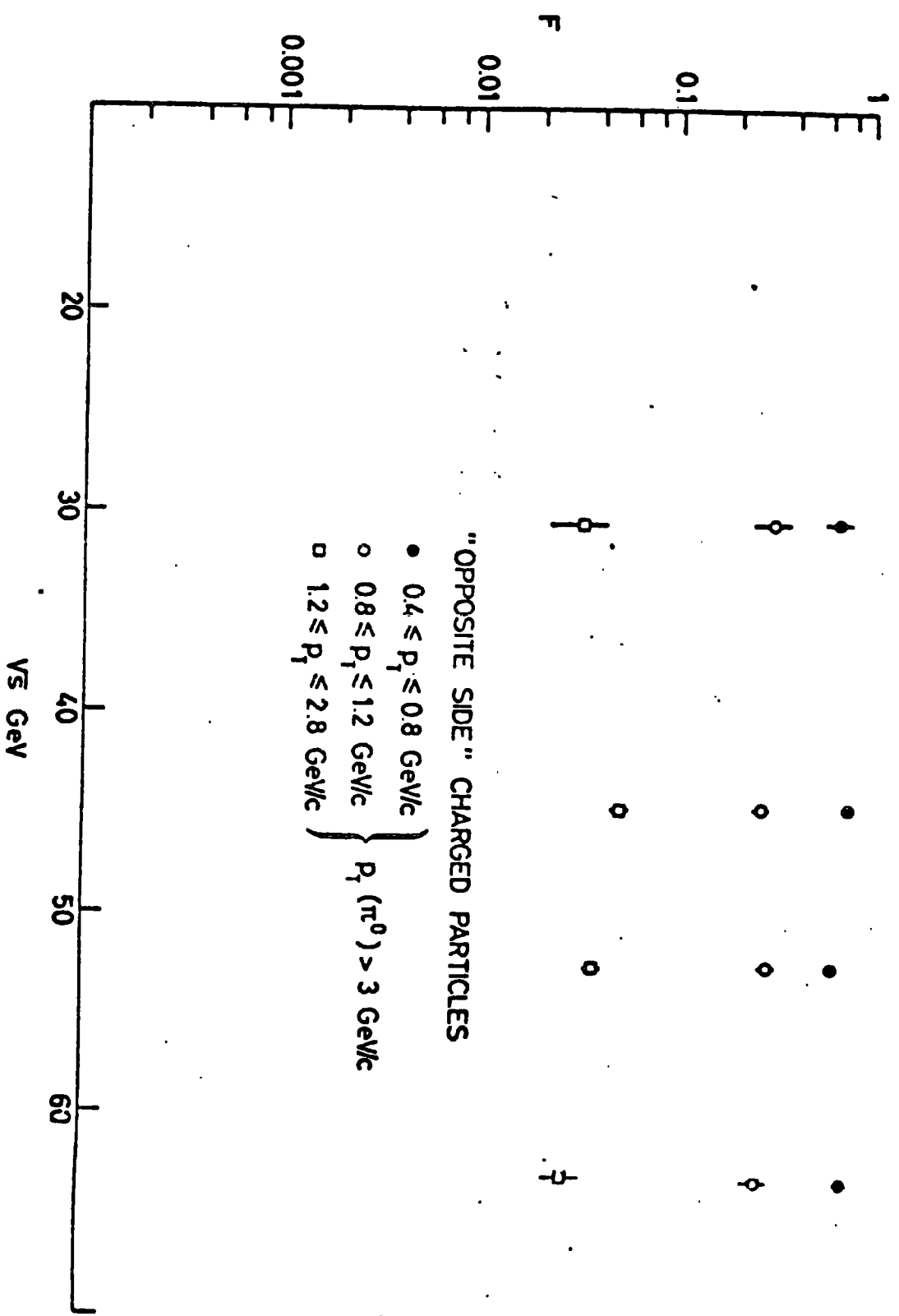


Figure 28

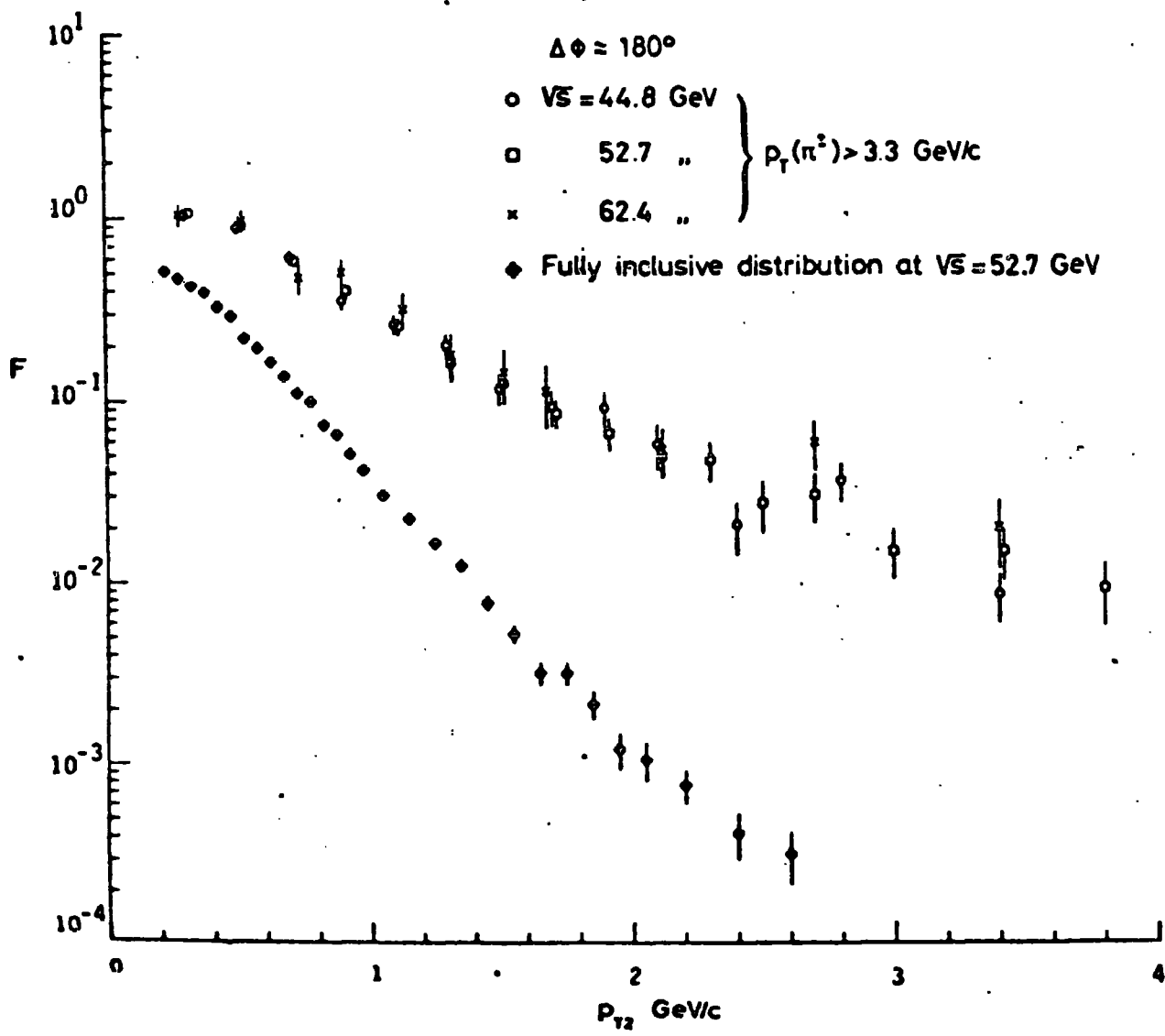


Figure 29

"OPPOSITE SIDE" CHARGED PARTICLES

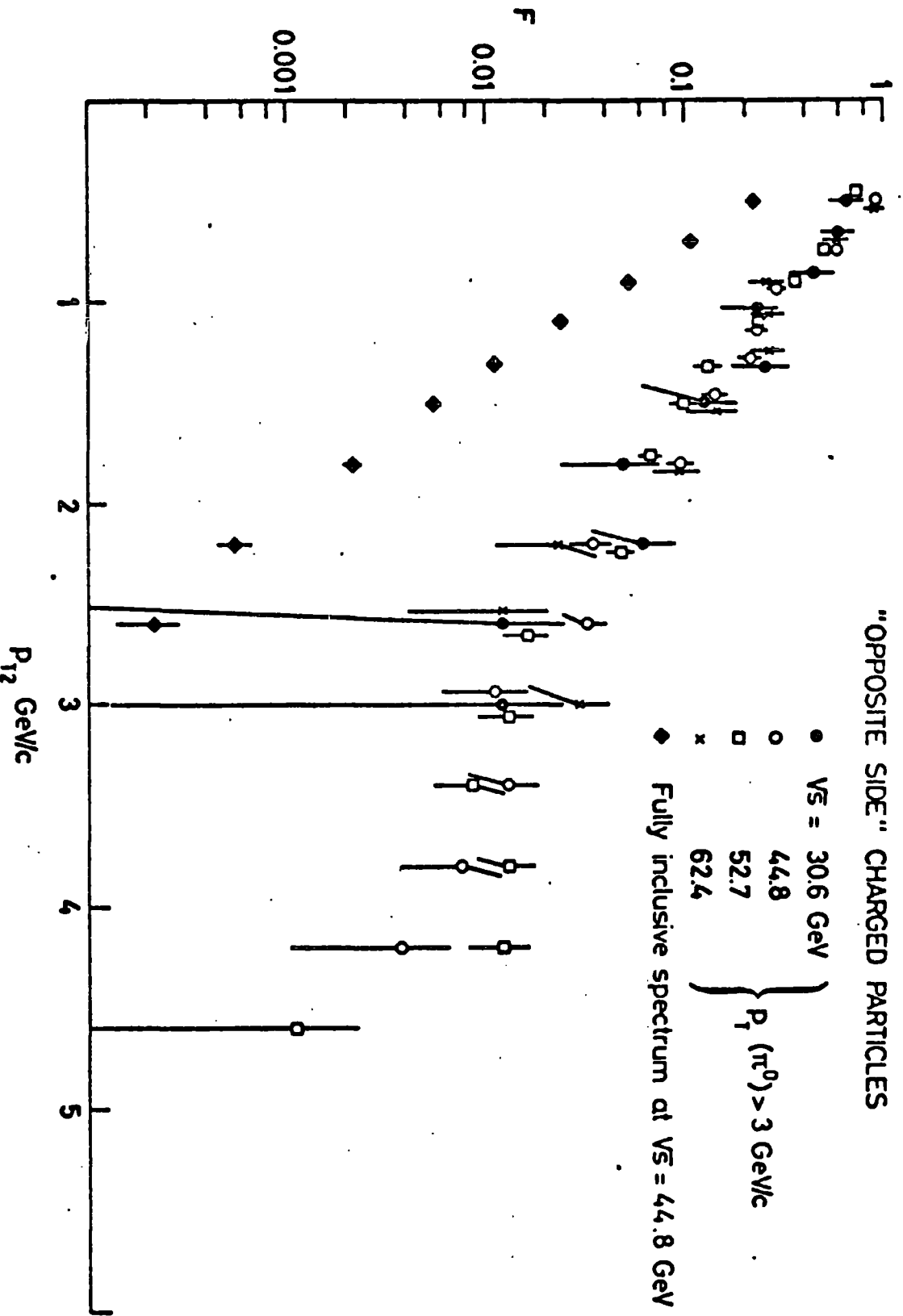


Figure 30

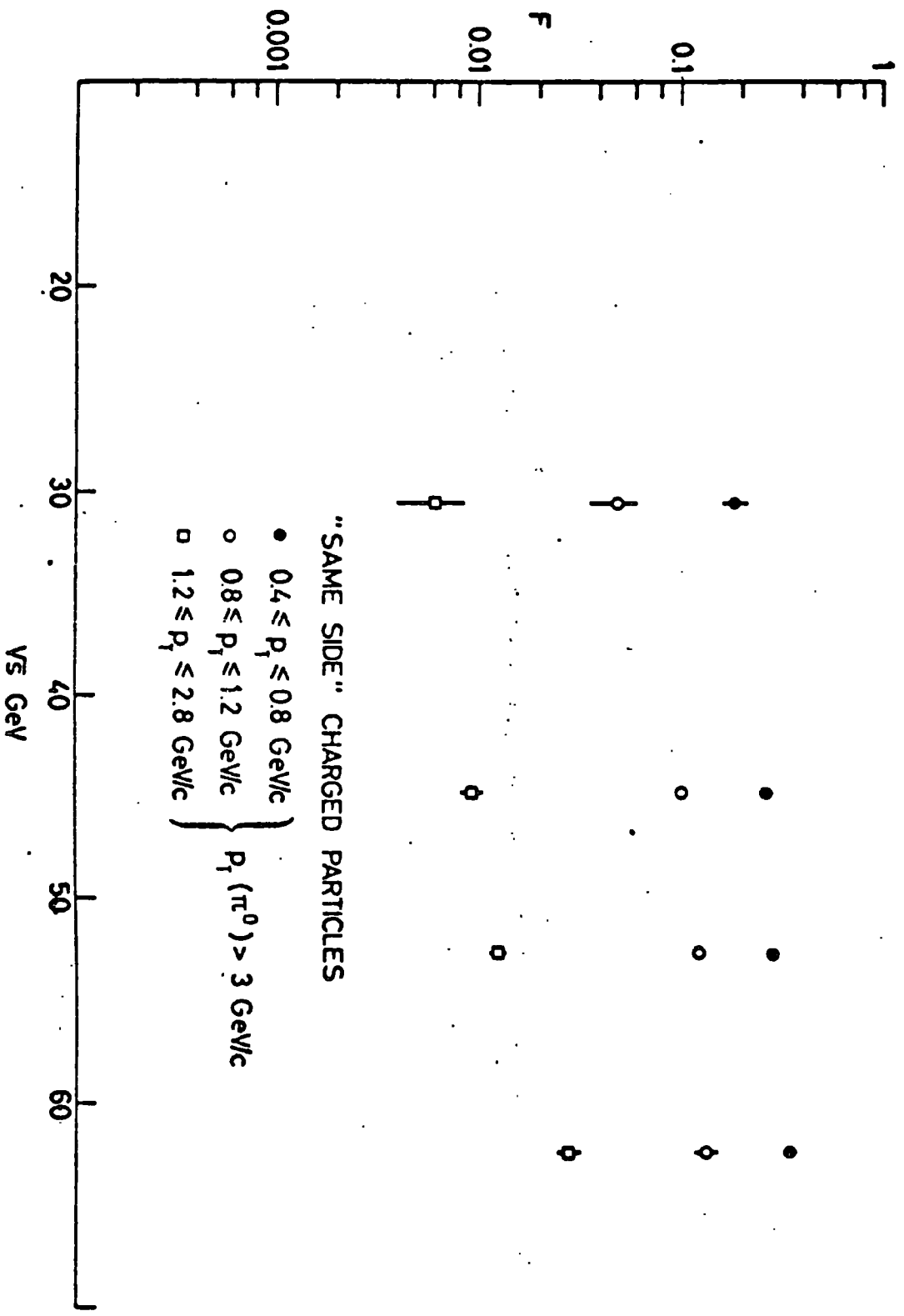


Figure 31

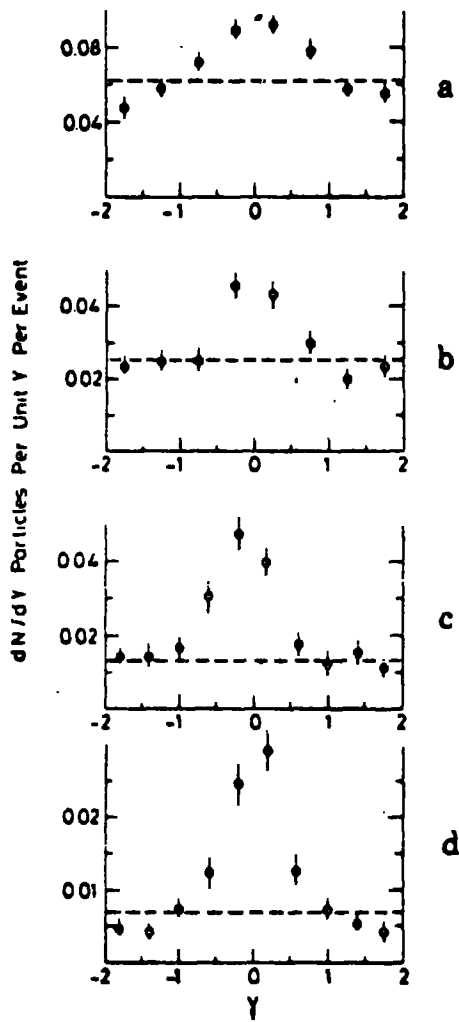


Figure 32

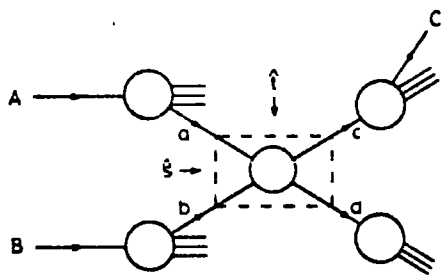


Figure 33

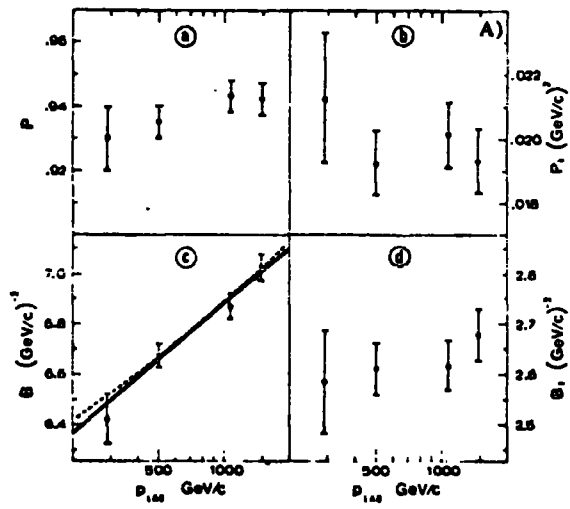


Figure 34

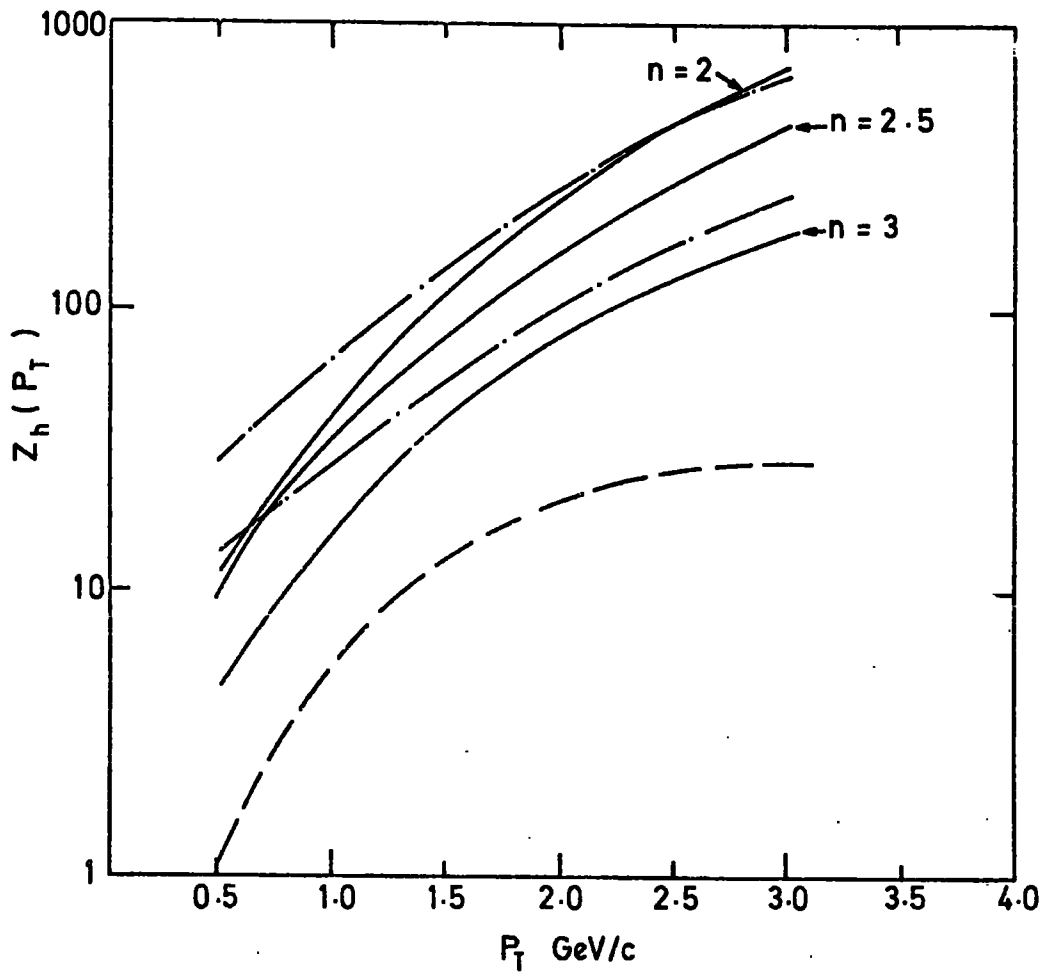


Figure 35

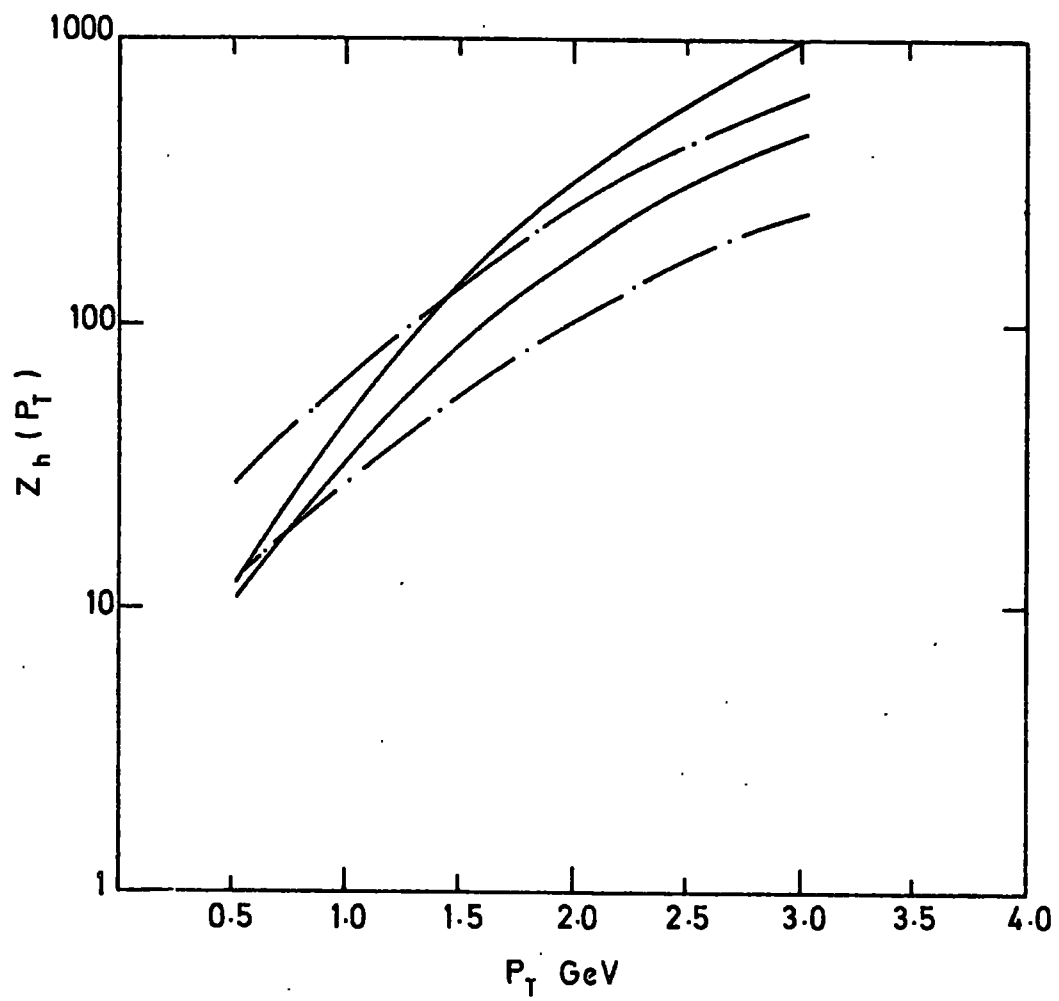


Figure 36

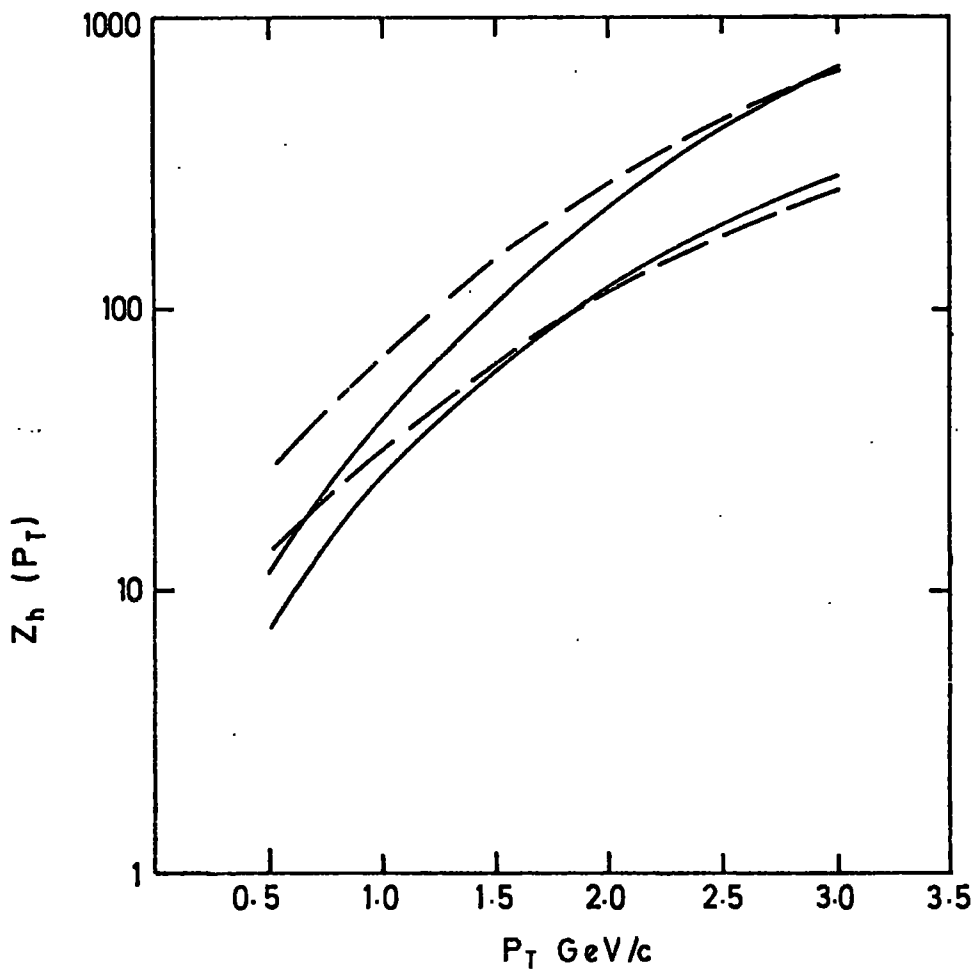


Figure 37

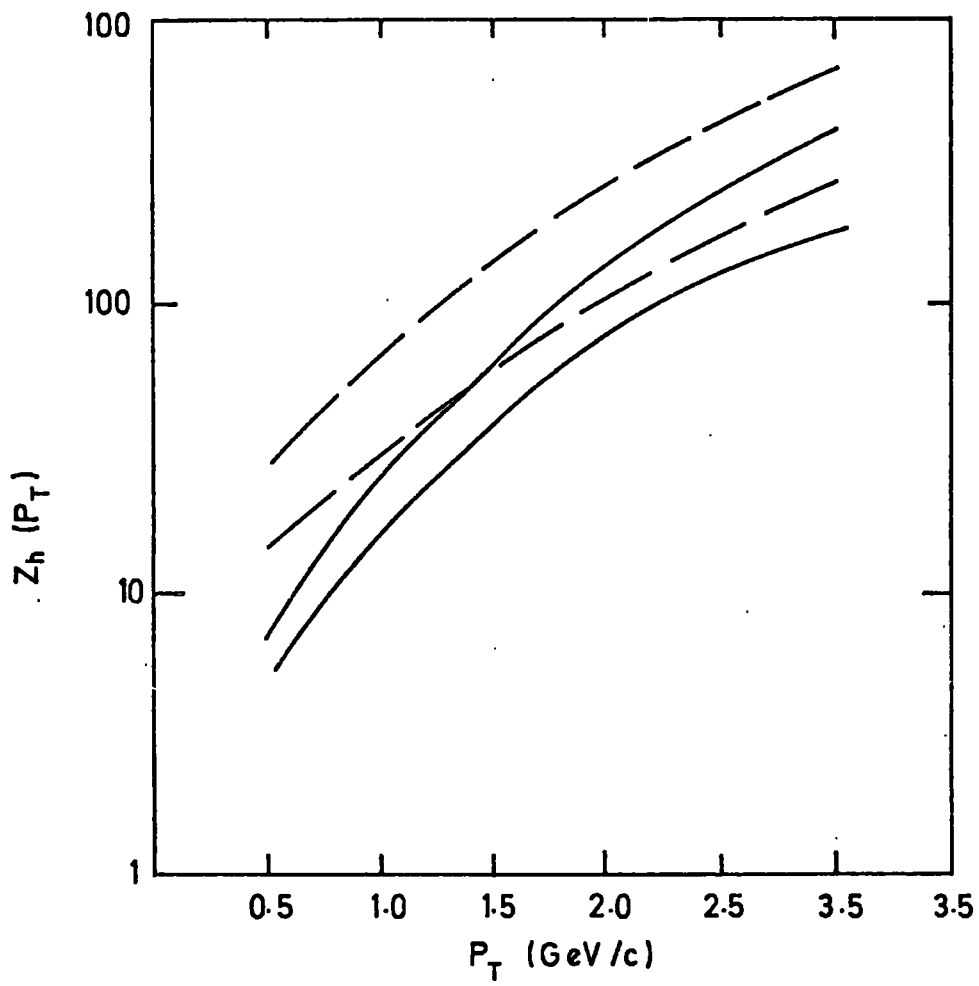


Figure 38

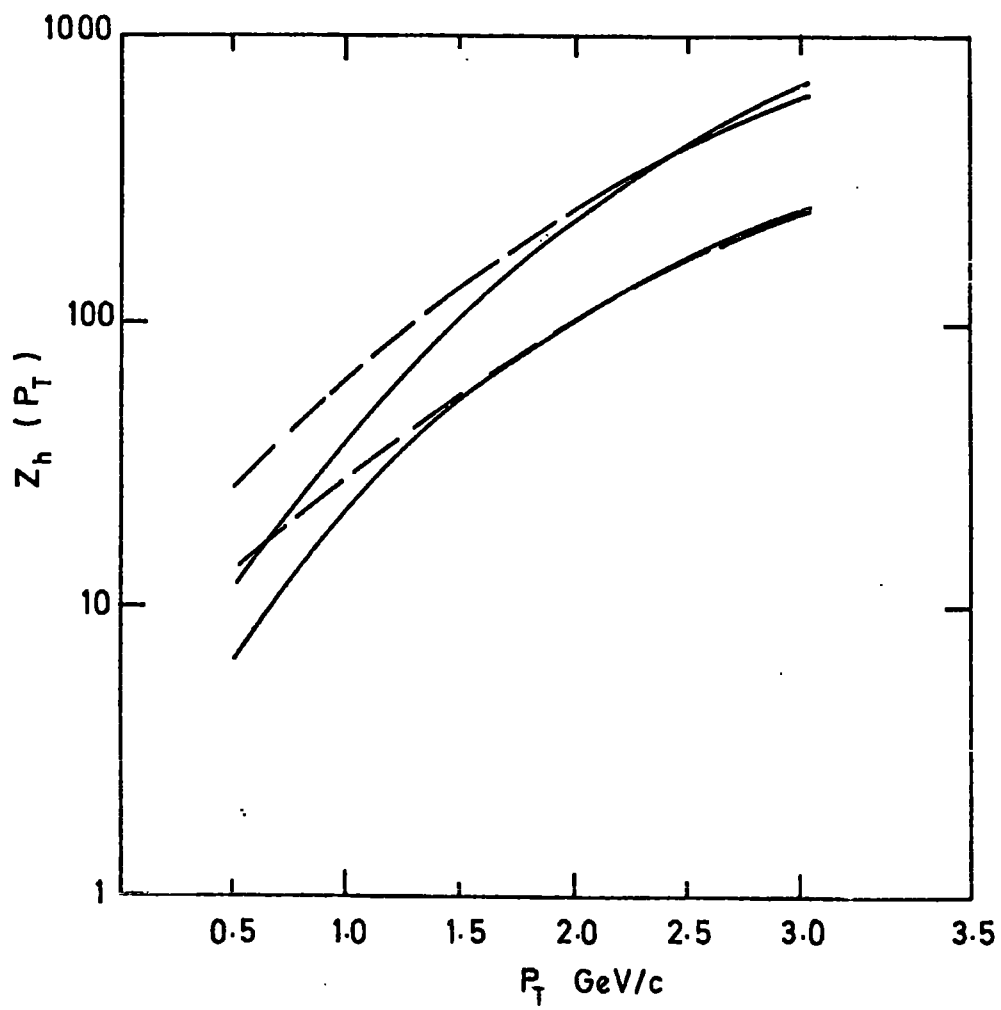


Figure 39

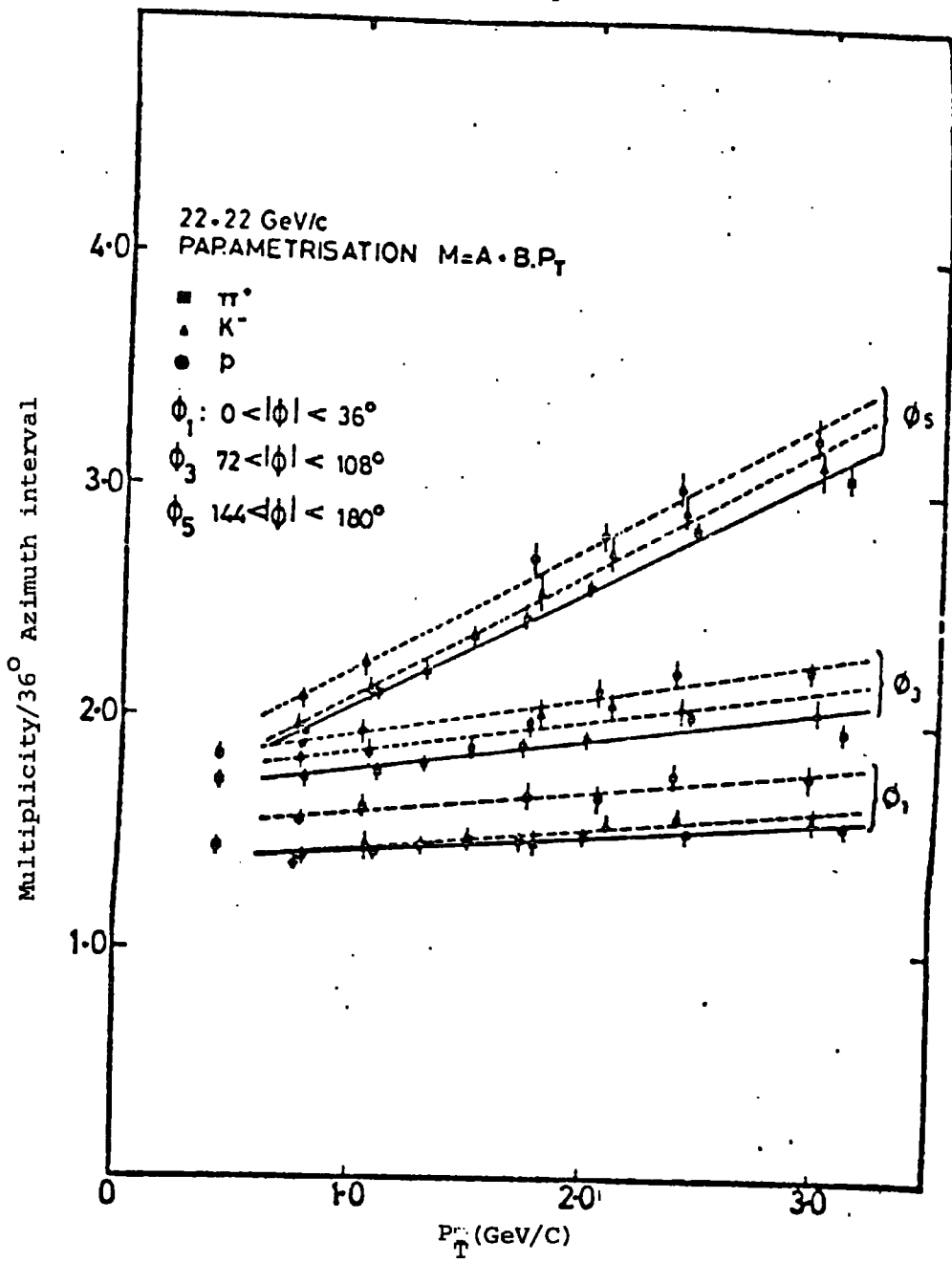


Figure 40

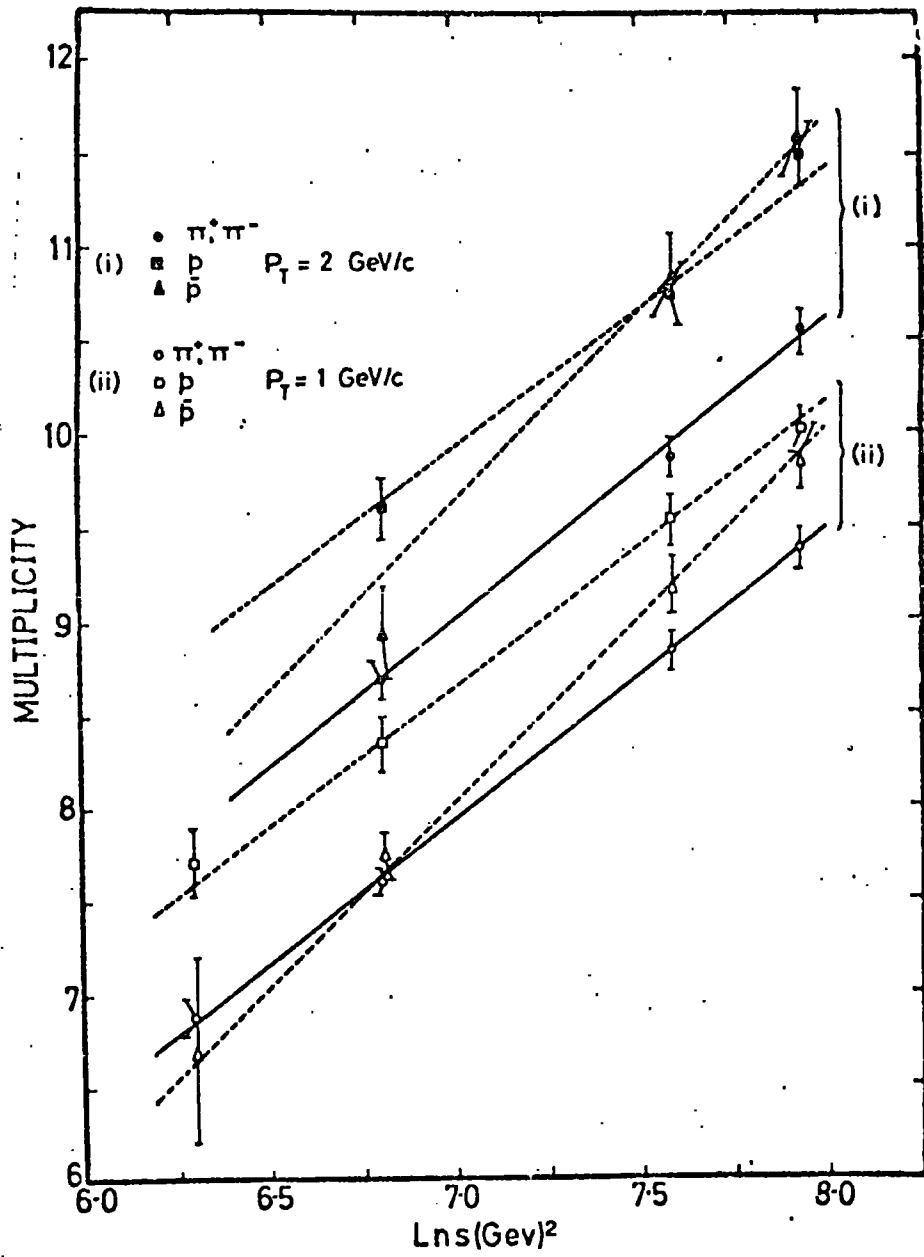


Figure 41

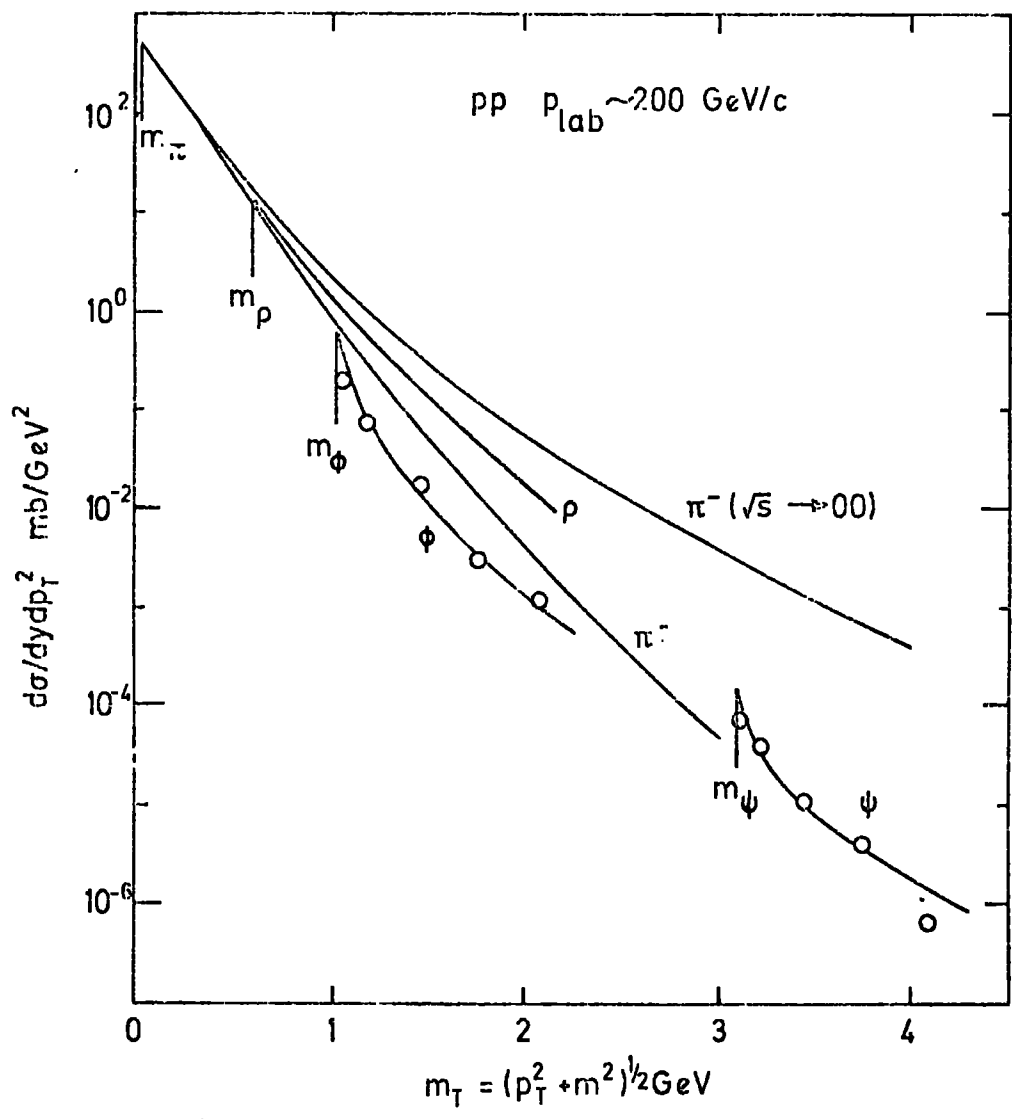


Figure 42

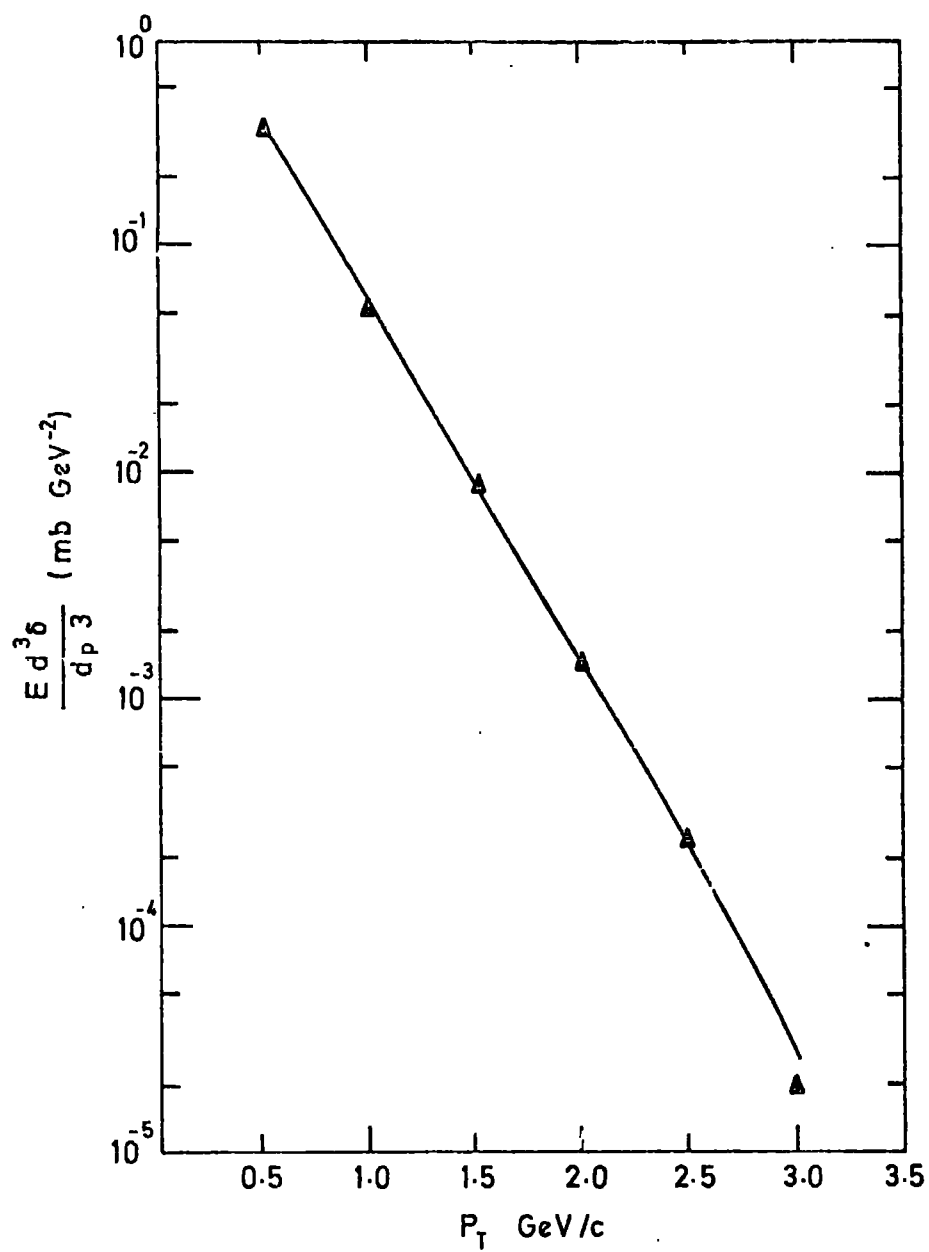


Figure 43

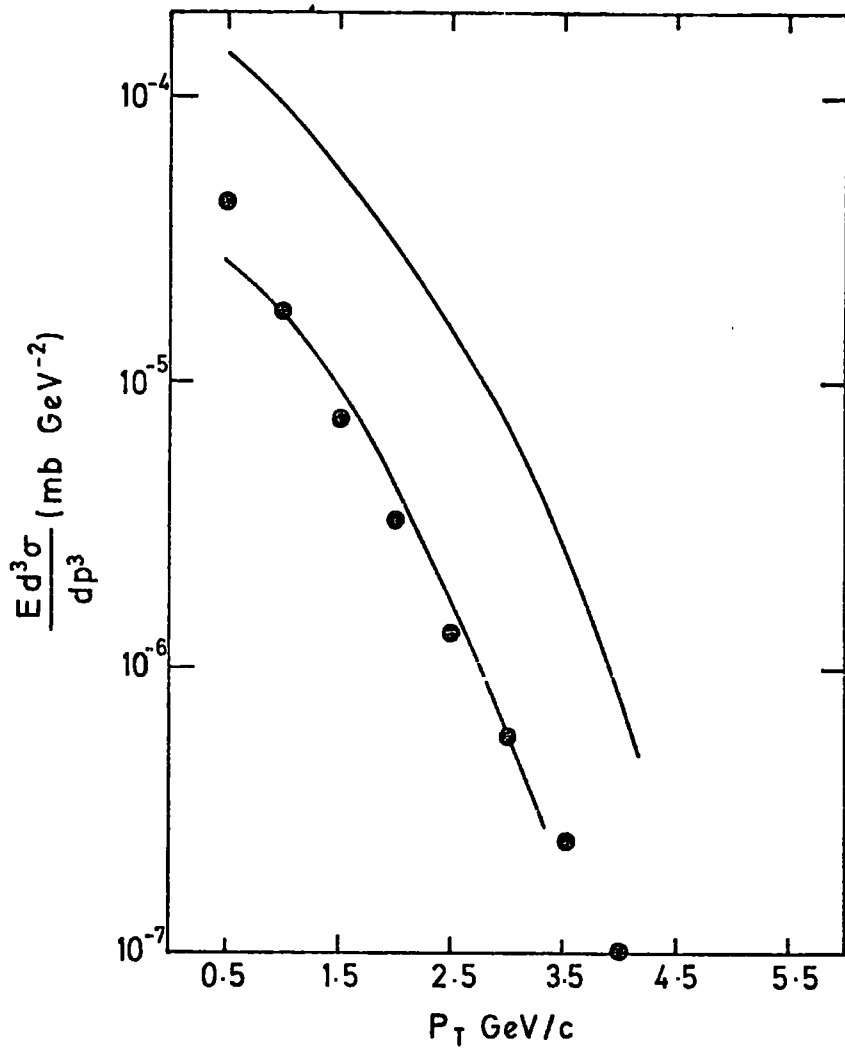


Figure 44

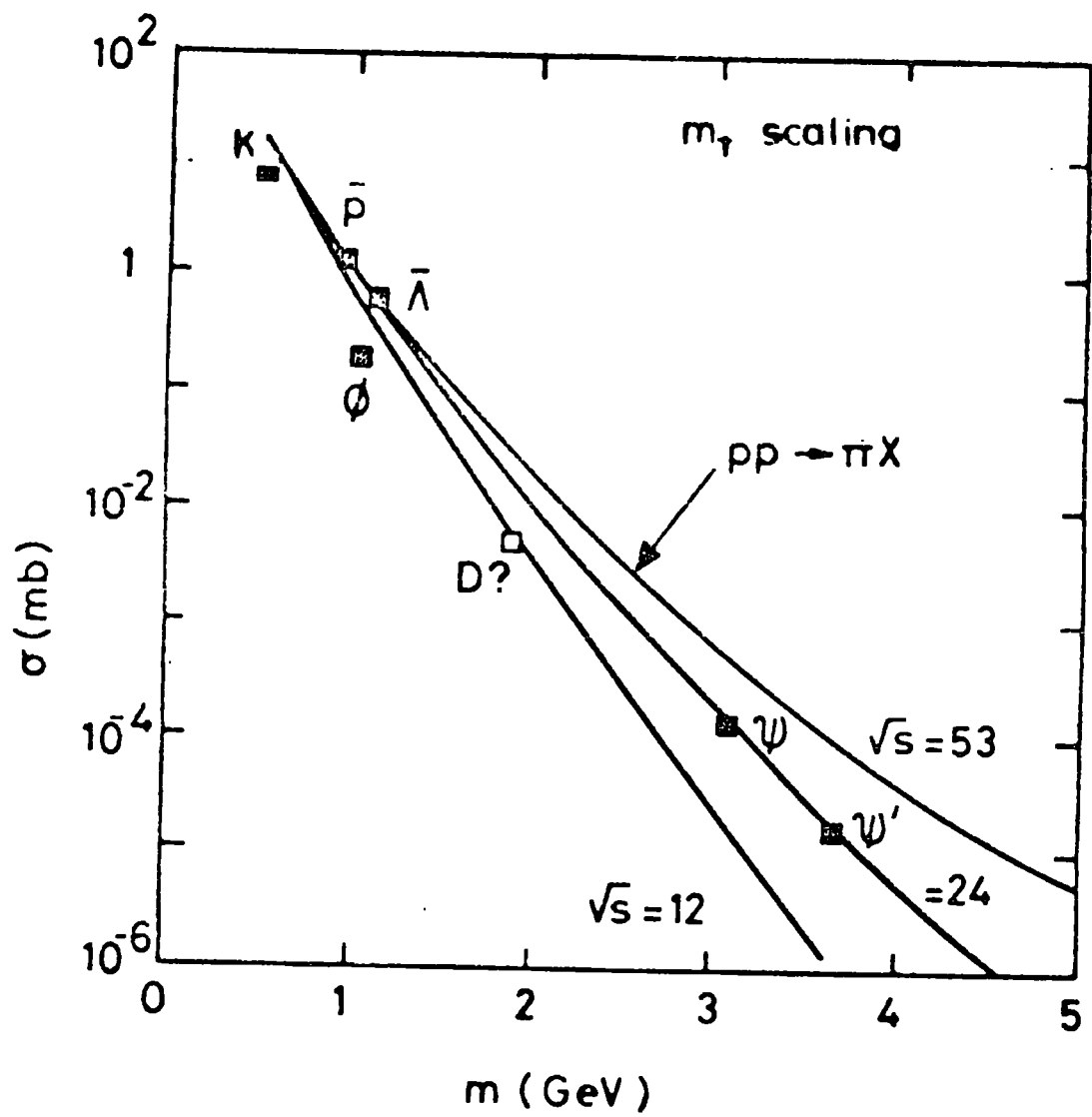


Figure 45

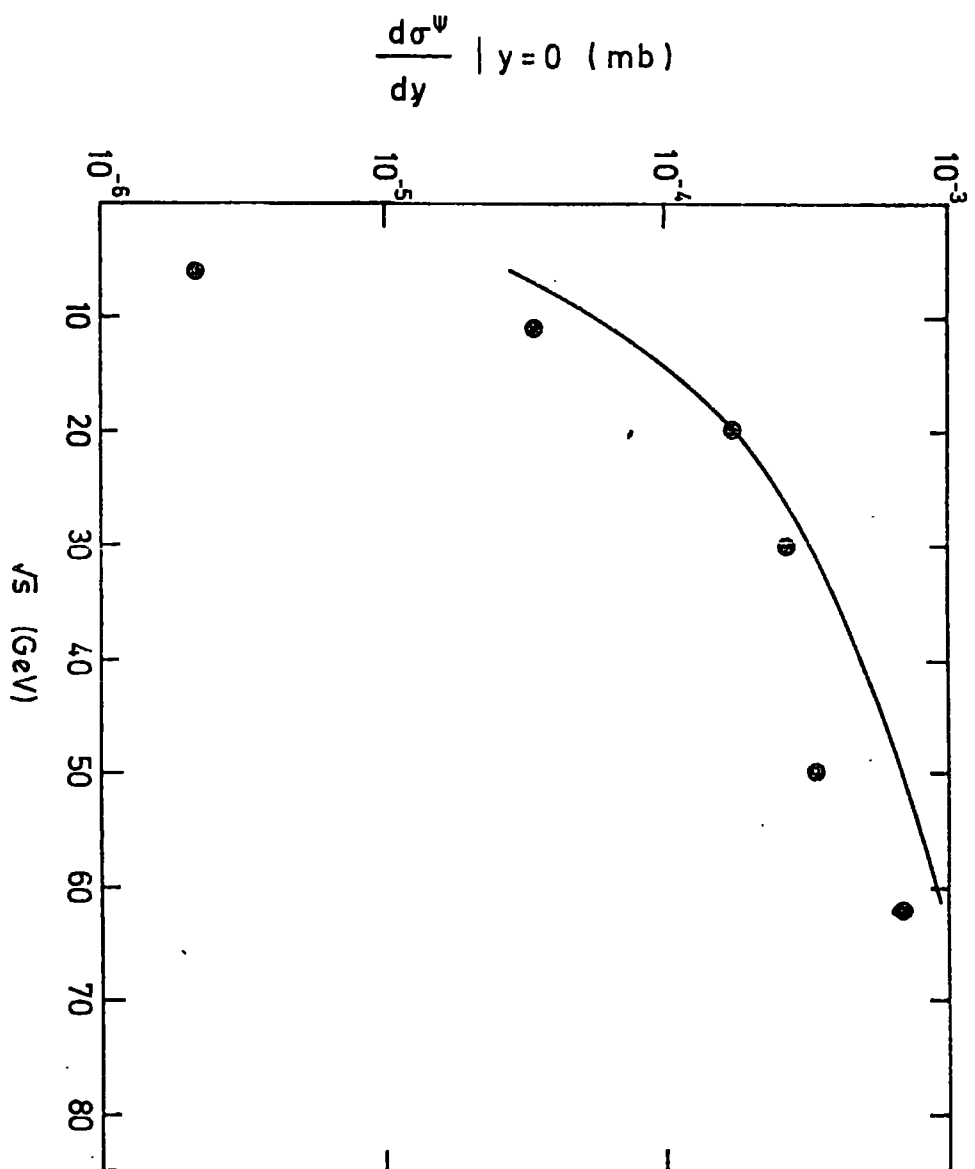


Figure 46

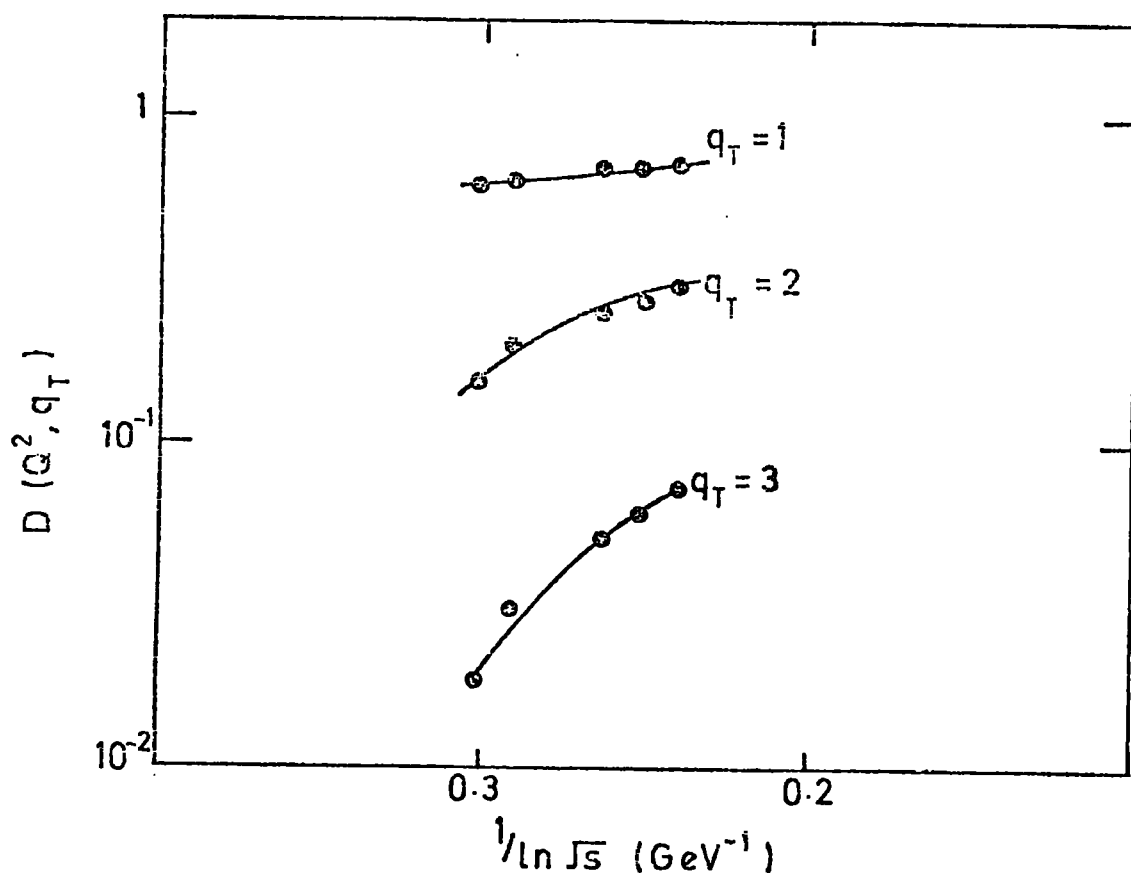


Figure 47

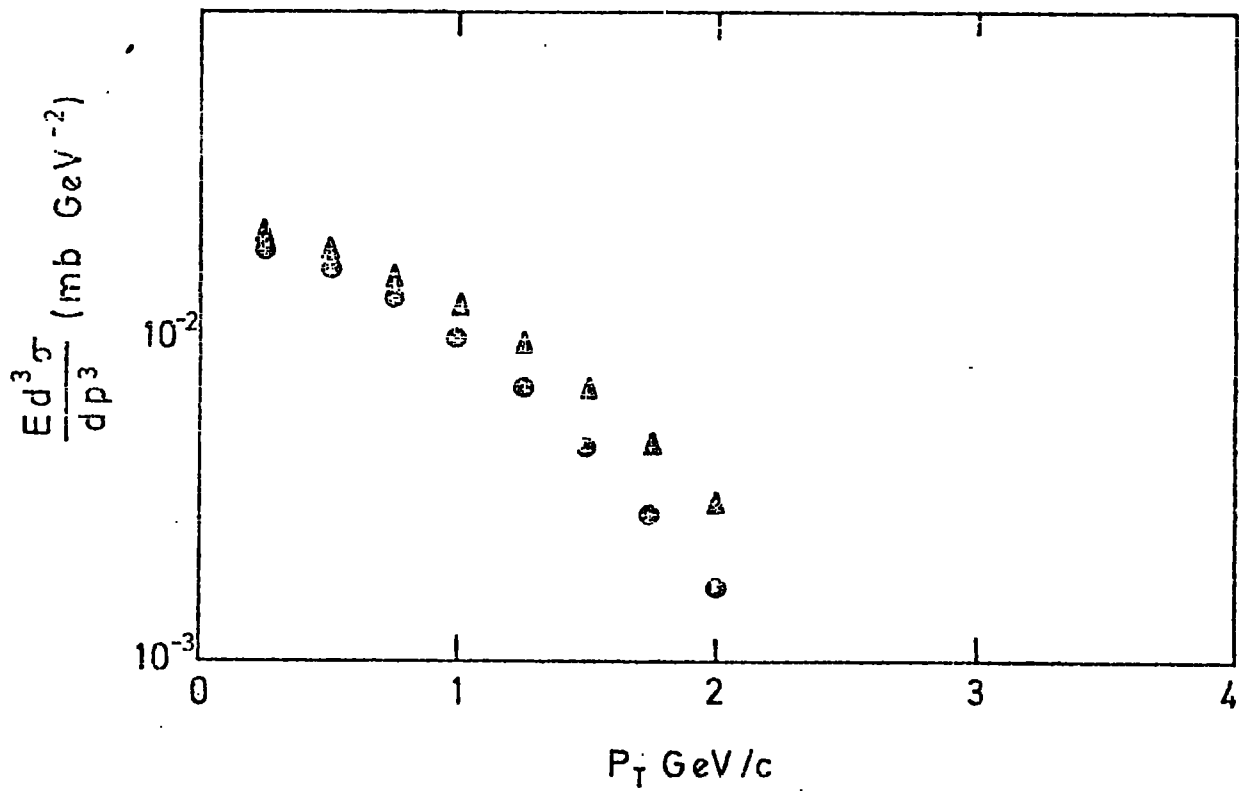


Figure 48

SEP 1971
REVISION
LIBRARY